Geometry-based Radio Channel Characterization and Modeling: Parameterization, Implementation and Validation

Zhu, Meifang

2014

Geometry-based Radio Channel Characterization and Modeling: Parameterization, Implementation and Validation

Doctoral Dissertation

Meifang Zhu

Lund, Sweden
August 2014

博学之，审问之，慎思之，明辨之，笃行之。
To this attainment there are requisite the extensive study of what is good, accurate inquiry about it, careful reflection on it, the clear discrimination of it, and the earnest practice of it.

《礼记·中庸》
The Doctrine of the Mean

Abstract

The propagation channel determines the fundamental basis of wireless communications, as well as the actual performance of practical systems. Therefore, having good channel models is a prerequisite for developing the next generation wireless systems. This thesis first investigates one of the main channel model building blocks, namely clusters. To understand the concept of clusters and channel characterization precisely, a measurement based ray launching tool has been implemented (Paper I). Clusters and their physical interpretation are studied by using the implemented ray launching tool (Paper II). Also, this thesis studies the COST 2100 channel model, which is a geometry-based channel model using the concept of clusters. A complete parameter set for the outdoor sub-urban scenario is extracted and validated for the COST 2100 channel model (Paper III). This thesis offers valuable insights on multi-link channel modeling, where it will be widely used in the next generation wireless systems (Paper IV and Paper V). In addition, positioning and localization by using the phase information of multi-path components, which are estimated and tracked from the radio channels, are investigated in this thesis (Paper VI).

Clusters are extensively used in geometry-based stochastic channel models, such as the COST 2100 and WINNER II channel models. In order to gain a better understanding of the properties of clusters, thus the characteristics of wireless channels, a measurement based ray launching tool has been implemented for outdoor scenarios in Paper I. With this ray launching tool, we visualize the most likely propagation paths together with the measured channel and a detail floor plan of the measured environment. The measurement based ray launching tool offers valuable insights of the interacting physical scatterers of the propagation paths and provides a good interpretation of propagation paths. It shows significant advantages for further channel analysis and modeling, e.g., multi-link channel modeling.

The properties of clusters depend on how clusters are identified. Generally speaking, there are two kinds of clusters: parameter based clusters are characterized with the parameters of the associated multi-path components;

physical clusters are determined based on the interacting physical scatterers of the multi-path components. It is still an open issue on how the physical clusters behave compared to the parameter based clusters and therefore we analyze this in more detail in Paper II. In addition, based on the concept of physical clusters, we extract modeling parameters for the COST 2100 channel model with sub-urban and urban micro-cell measurements. Further, we validate these parameters with the current COST 2100 channel model MATLAB implementation.

The COST 2100 channel model is one of the best candidates for the next generation wireless systems. Researchers have made efforts to extract the parameters in an indoor scenario, but the parameterization of outdoor scenarios is missing. Paper III fills this blank, where, first, cluster parameters and cluster time-variant properties are obtained from the 300 MHz measurements by using a joint clustering and tracking algorithm. Parameterization of the COST 2100 channel model for single-link outdoor MIMO communication at 300 MHz is conducted in Paper III. In addition, validation of the channel model is performed for the considered scenario by comparing simulated and measured delay spreads, spatial correlations, singular value distributions and antenna correlations.

Channel modeling for multi-link MIMO systems plays an important role for the developing of the next generation wireless systems. In general, it is essential to capture the correlations between multi-link as well as their correlation statistics. In Paper IV, correlation between large-scale parameters for a macro cell scenario at 2.6 GHz has been analyzed. It has been found that the parameters of different links can be correlated even if the base stations are far away from each other. When both base stations were in the same direction compared to the movement, the large-scale parameters of the different links had a tendency to be positively correlated, but slightly negatively correlated when the base stations were located in different directions compared to the movement of the mobile terminal. Paper IV focuses more on multi-site investigations, and paper V gives valuable insights for multi-user scenarios. In the COST 2100 channel model, common clusters are proposed for multi-link channel modeling. Therefore, shared scatterers among the different links are investigated in paper V, which reflects the physical existence of common clusters. We observe that, as the MS separation distance is increasing, the number of common clusters is decreasing and the cross-correlation between multiple links is decreasing as well. Multi-link MIMO simulations are also performed using the COST 2100 channel model and the parameters of the extracted common clusters are detailed in paper V. It has been demonstrated that the common clusters can represent multi-link properties well with respect to inter-link correlation and sum rate capacity.

Positioning has attracted a lot of attention both in the industry and academia during the past decades. In Paper VI, positioning with accuracy down to centimeters has been demonstrated, where the phase information of multi-path components from the measured channels is used. First of all, an extended Kalman filter is implemented to process the channel data, and the phases of a number of MPCs are tracked. The tracked phases are converted into relative distance measures. Position estimates are obtained with a method based on so called structure-of-motion. In Paper VI, circular movements have been successfully tracked with a root-mean-square error around 4 cm when using a bandwidth of 40 MHz. It has been demonstrated that phase based positioning is a promising technique for positioning with accuracy down to centimeters when using a standard cellular bandwidth.

In summary, this thesis has made efforts for the implementation of the COST 2100 channel model, including providing model parameters and validating such parameters, investigating multi-link channel properties, and suggesting implementations of the channel model. The thesis also has made contributions to the tools and algorithms that can be used for general channel characterizations, i.e., clustering algorithm, ray launching tool, EKF algorithm. In addition, this thesis work is the first to propose a practical positioning method by utilizing the distance estimated from the phases of the tracked multi-path components and showed a preliminary and promising result.

Preface

This thesis represents a culmination of the work and learning of my Ph.D. study that has taken place over a period of almost five years (2009-2014) and consists of two parts. The first part gives an introduction of the research field in which I have been working on during my Ph.D. study and also a summary of my contributions to the field. The second part includes six research papers that present my working results and achievements during my Ph.D. study. The included six papers are:

I. M. Zhu, A. Singh, and F. Tufvesson, "Measurement based ray launching for analysis of outdoor propagation," in *Proc. 6th European Conference on Antennas and Propagation (EUCAP)*, Prague, Czech Republic, pp. 3332-3336, Mar. 2012.

II. M. Zhu, K. Haneda, V.-M. Kolmonen, and F. Tufvesson "Parameter based clusters, physical clusters and cluster based channel modeling in sub-urban and urban scenarios," submitted to *IEEE Transactions on wireless communications*, Jun. 2014.

III. M. Zhu, G. Eriksson, and F. Tufvesson, "The COST 2100 Channel Model: Parameterization and validation based on outdoor MIMO measurements at 300 MHz," *IEEE Transactions on wireless communications*, vol. 12, no. 2, pp. 888-897, Feb. 2013.

IV. M. Zhu, F. Tufvesson, and J. Medbo, "Correlation properties of large scale parameters for 2.66 GHz multi-site macro cell measurements," in *Proc. IEEE 73rd Vehicular Technology Conference (VTC2011-Spring)* , Budapest, Hungary, pp. 1-5, May 2011.

V. M. Zhu, and F. Tufvesson, "Virtual multi-link propagation investigation of an outdoor scenario at 300 MHz," in *Proc. 7th European Conference on Antennas and Propagation (EUCAP)*, Gothenburg, Sweden, pp. 687-691, Apr. 2013.

VI. M. Zhu, J. Vieira, Y. Kuang, A. F. Molisch, and F. Tufvesson, "Positioning using phase information from measured radio channels," to be submitted to *IEEE Wireless Communications Letters*.

During my Ph.D. study, I have also contributed to the following publications that are not included in the thesis:

VII. C. Zhang, L. Liu, Y. Wang, M. Zhu, O. Edfors, and V. Öwall, "A highly parallelized MIMO detector for vector-based reconfigurable architectures," in *Proc. IEEE Wireless Communications and Networking Conference (WCNC)*, Shanghai, China, pp. 3844-3849, Apr. 2013.

VIII. V. Plicanic, M. Zhu, and B. K. Lau, "Diversity mechanisms and MIMO throughput performance of a compact six-port dielectric resonator antenna array," in *Proc. International Workshop on Antenna Technology (IWAT)*, Lisbon, Portugal, pp. 1-4, Mar. 2010.

During my Ph.D. study, I have also been involved in the European Cooperation in Science and Technology (COST) actions COST2100 and IC1004, where my contributions are given as temporary documents (TDs):

IX. M. Zhu, K. Haneda, V.-M. Kolmonen, and F. Tufvesson, "A study on parameter based clusters and physical clusters," in *9th IC1004 Management Committee Meeting*, Ferrara, Italy, TD(14)09062, Feb. 2014.

X. G. Dahman, F. Rusek, M. Zhu, and F. Tufvesson, "On the probability of non-shared clusters in cellular networks," in *9th IC1004 Management Committee Meeting*, Ferrara, Italy, TD(14)09055, Feb. 2014.

XI. M. Zhu, and F. Tufvesson, "A study on the relation between parameter based clusters and physical clusters," in *5th IC1004 Management Committee Meeting*, Bristol, UK, TD(12)05066, Sept. 2012.

XII. M. Zhu, A. Singh, and F. Tufvesson, "Measurement based ray launching for analysis of outdoor propagation," in *3th IC1004 Management Committee Meeting*, Barcelona, Spain, TD(12)03022, Feb. 2011.

XIII. M. Zhu, F. Tufvesson, and G. Eriksson, "Validation of 300 MHz MIMO measurements in suburban environments for the COST 2100 MIMO channel model", in *11th COST2100 Management Committee Meeting*, Bologna, Italy, TD(10)12048, Nov. 2010.

XIV. W. Jiang, L. Liu, M. Zhu, and F. Tufvesson, "Implementation of the COST2100 multi-link MIMO channel model in C++/IT++", in *11th COST2100 Management Committee Meeting*, Bologna, Italy, TD(10)12092, Nov. 2010.

XV. M. Zhu, F. Tufvesson, G. Eriksson, S. Wyne, and A. F. Molisch, "Parameterization of 300 MHz MIMO measurements in suburban environments for the COST 2100 MIMO channel model", in *10th COST2100 Management Committee Meeting*, Aalborg, Danmark, TD(10)11071, Jun. 2010.

XVI. V. Plicanic, M. Zhu, and B. K. Lau, "Diversity mechanisms of a compact dielectric resonator antenna array for high MIMO throughput performance", in *9th COST2100 Management Committee Meeting*, Vienna, Austria, TD(09)969, Sept. 2009.

Acknowledgements

I am filled with emotions now that my 22 years of education have arrived at this curtain call on the stage of my pending graduation. Seven years ago, I came alone to this unfamiliar place far from home with only a luggage bag and an unknown future, but excited to begin my new journey. Seven years ago, with the youthful exuberance of a 22-year-old, I chose to focus on the world of mathematics, electronics, and English. Seven years ago, I had little money and no time for romance, but with soaring aspirations and dreams of hope, I maintained a strong love of life. Over the last seven years, I have matured. Over the last seven years, I got married and even became a mother. Now seven years later, I look back on the time that I spent studying at Lund University as the most significant investment of my life.

In this time that I spent on my Ph.D. education, I have been humbled by failures, but thanks to those who gave me their support. I have also experienced the joys of success and even shared laughter along the way. Without you, my supporters, the journey that I began seven years ago would not have been so rich.

First and foremost, I would like to express my deepest gratitude to my supervisor, Prof. Fredrik Tufvesson, for giving me the opportunity to pursuit a Ph.D. under his guidance. I am grateful for his strong support, insightful discussions, frequent encouragement and critical suggestions during my Ph.D. study. I am extremely fortunate to have a supervisor who cares so much about my work and promptly responds to my questions with such insight. His extensive knowledge, creative spirit and mentoring personality make him one of my most influential teachers. He has been invaluable to me in the research field and helped me to mature. He, as a supervisor, cared about me as a father and made me feel at home while studying at Lund University, which has been important to me as a foreigner starting this journey without any family nearby.

I am also grateful to Dr. Tommy Hult, my co-supervisor during the first half of my Ph.D. study, for his fruitful dialogs, help in understanding the rudiments of multi-link channel modeling. I am also thankful to Dr. Ghassan Dahman,

my co-supervisor during the second half of my Ph.D. study, for his support in measurements, his discussions and critical feedback. I am also grateful to Prof. Buon Kiong Lau for his coordination during the Ph.D. study and encouragement. I am grateful to Prof. Ove Edfors for teaching me the knowledge of radio systems. I am thankful to Prof. Fredrik Rusek for his helpful discussions in communication theories.

I would like to express my gratitude to Prof. Katsuyuki Haneda and Dr. Veli-Matti Kolmonen in Finland. Prof. Katsuyuki Haneda is always supporting me and providing valuable feedback. Dr. Veli-Matti Kolmonen explained detailed measurements setup and data analysis to me. I found your cooperation very beneficial.

I am especially grateful to my colleagues in the communication engineering group. Thanks to my office-mates Nafiseh and Saeedeh for the accompaniment, Taimoor for technical discussions, Rohit for providing practical information, Carl for practicing Chinese, Xiang for sharing memories of Chengdu, Pepe for parental discussions, and Joao for Portuguese humor. Also thanks to Anders, Atif, Muris and Dimitrios for being around to helping out.

Thanks to all the administrative and technical staff in the department. I am especially grateful to Pia for your endless support. Whenever I need help, you always save me. Also thanks for Lars, Josef, and Robert for technical support. I also want to acknowledge Vetenskapsrådet for sponsoring my Ph.D. study.

I am especially grateful to my dear friends, Maomao, Dangdang, and Tutu. Thanks for sharing all the happiness and sadness. I feel so lucky to have you three in my life.

Thanks to my parents. My father's desire and thirst for knowledge deeply influenced me. He had to give up his education when he was 15 years old, so he has put all his effort into making sure that I received a good education. This legacy has always energized my pursuit of a Ph.D. degree. It is my strong desire to make you proud of me. I especially appreciate my mother's accompaniment during the past two years. You are always the one I can rely on. I would like to express my appreciation to my parent-in-laws for taking care of our little daughter while I was working at the office and always backing us. Special thanks go to my husband, Tao, for your partnership in this journey. My gratitude to you is beyond words. Last but not least, I would like to thank to my daughter, Qianmo. When mum is tired, you smile at me sweetly. You give mum more than usual.

Meifang Zhu
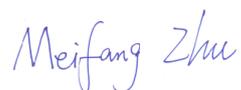
Lund, August 2014

List of Acronyms and Abbreviations

3D 3-dimensional

AAD angle of arrival difference

AOA angle-of-arrival

AOD angle-of-departure

BS base station

COST Co-operation in Science and Technology

DMC diffuse multi-path component

EKF extended Kalman filter

GNSS global navigation satellite system

GPS global positioning system

GSCM geometry-based stochastic channel model

GUI graphical user interface

IEEE Institute of Electrical and Electronics Engineers

LOS line-of-sight

LTE long-term evolution

MIMO multiple-input multiple-output

MISO multiple-input single-output

MPC multi-path component

MS mobile station

NLOS non line-of-sight

PDP power delay profile

RMSE root-mean-square error

RSSI received signal strength indication

RANSAC Random sample consensus

RX receiver

SAGE space-alternating generalized expectation maximization

SNR signal-to-noise ratio

SV Saleh-Valenzuela

TOA time of arrival

TDOA time difference of arrival

TX transmitter

UWB ultra-wideband

VR visibility region

WINNER Wireless World Initiative New Radio

WSS wide sense stationary

Contents

Part I

Overview of the Research Field

Chapter 1

Introduction

The evolution of wireless communication in the last decades has been accelerating at an extraordinary pace to fulfill the modern lifestyle requirements, such as smart-phones, tablets, sensor networks, smart grid schemes, etc. To keep pace with this ever-increasing demand, new wireless communication standards such as long-term evolution (LTE), and LTE-advanced [1], target a downlink peak data rate of 1 Gbit/s. Multi-input multi-output (MIMO), distributed MIMO, massive MIMO and millimeter wave systems are among the main core technologies that are adopted or probably will be adopted in order to increase the data rate and maximize the utilization of the limited spectrum by exploiting the spatial domain. The performance of these technologies is highly affected by the wireless channels between the different communication terminals. Therefore, understanding the behavior of wireless channels in time and space is crucial in order to fully exploit the benefits of these core technologies.

Several approaches have been used in order to characterize different aspects of wireless channels, for example, channel measurements and ray tracing simulations. Channel measurements are usually used to capture the temporal and spatial behavior of wireless channels. However, performing channel measurements is a complicated process that requires huge data storage, significant financial resources, and manpower efforts. On the other hand, ray tracing provides an alternative option in modeling wireless channels. However, among other factors, the accuracy of ray tracing depends on the accurate and detailed description of the physical properties of the propagation environment. Such detailed information is not available in most of the environments of interest, and even if they are available, they result in huge computational complexity. Stochastic channel models provide a balance between cost (computational as well as financial) and accuracy in modeling the different channel parame-

ters. Stochastic channel models utilize both propagation measurements and ray tracing simulations in order to understand the behavior of wireless channels and capture their characteristics. Consequently, the extracted parameters are utilized to model wireless channels in ways that statistically reflect realistic propagation conditions. However, more research is needed in order to develop sophisticated models that are able to accurately model wireless channels in complicated environments, and different scenarios, e.g., with large number of users, large number of base stations (BSs), various mobility models, wide possible arrangements of transmit and received antennas, and so on. There have been well-established stochastic channel models, e.g., the Kronecker model [2], COST 207 [3], WINNER II [4], and COST 2100 [5]. Studying and understanding these models is an essential step toward improving current channel models, or introducing new channel models that are in a position to fulfill the design and planning requirements for next generation wireless systems.

In this chapter, first, a short introduction of MIMO technology is given. Secondly, an example of MIMO channel measurements is given. Then, ray tracing is discussed. Later, stochastic MIMO channel models together with their advantages and limitations are discussed. Lastly, an overview of the thesis wraps up this chapter.

1.1   MIMO Communications

MIMO systems have been an increasingly popular research area in the wireless communications community during the last 15 to 20 years. It exploits the space dimension in order to improve capacity, range and reliability of wireless communication systems. These improvements are achieved by using multiple antenna elements at the transmitter (Tx) and/or the receiver (Rx) sides. MIMO technology is becoming mature, and is already incorporated into emerging wireless broadband standards. For example, LTE-advanced [1] allows up to eight antennas for the downlink and up to four antennas for the uplink. To fully exploit the space dimension of wireless channels, technologies like distributed MIMO and massive MIMO have been investigated. Recently, very-large MIMO systems, also known as massive MIMO or large-scale antenna systems, have become a new research field in the wireless area [6]. It has been shown in theory that, with simple signal processing schemes, massive MIMO has the potential to remarkably improve performance in terms of link reliability and data rate [6, 7].

MIMO radio channels represent a major part of MIMO systems that should be considered when evaluating system performance. They are typically described by multi-path components (MPCs) that originate from different obsta-

cles due to the reflection, diffraction or scattering mechanisms. These MPCs reach the receive antennas with different delays and compose the MIMO impulse response. Usually, we use $h_{i,j}(t,\tau)$ to represent the impulse response between the jth transmit antenna and the ith receive antenna at delay τ. Thus, a MIMO channel with N_{Rx} receive antennas and N_{Tx} transmit antennas can be described by the matrix:

$$\mathbf{H}(t,\tau) = \begin{bmatrix} h_{1,1}(t,\tau) & h_{1,2}(t,\tau) & \cdots & h_{1,N_{\text{Tx}}}(t,\tau) \\ h_{2,1}(t,\tau) & h_{2,2}(t,\tau) & \cdots & h_{2,N_{\text{Tx}}}(t,\tau) \\ \vdots & \vdots & \ddots & \vdots \\ h_{N_{\text{Rx}},1}(t,\tau) & h_{N_{\text{Rx}},2}(t,\tau) & \cdots & h_{N_{\text{Rx}},N_{\text{Tx}}}(t,\tau) \end{bmatrix}. \quad (1.1)$$

Then the relation between the input and output for a MIMO channel can be expressed as:

$$\mathbf{y} = \mathbf{H} * \mathbf{s} + \mathbf{n}, \quad (1.2)$$

where $\mathbf{s}$ is the signal vector, $*$ is the convolution operator and $\mathbf{n}$ is the noise vector.

It can be noted that the MIMO channel determines the received signal, thus the link and the system level performance. Therefore, it is essential to have a good understanding of the behavior of MIMO channels, and take their influence into account when planning and evaluating MIMO systems.

1.2 MIMO Channel Measurements

The most straightforward way to capture and, consequently, characterize MIMO channel properties is to perform channel measurements, which is also called channel sounding [8]. The basic idea of channel sounding is that a transmitter sends out a known signal, while the receiver observes and stores the received version of the transmitted signal. Consequently, the channel impulse responses are derived by comparing the known transmitted signal and its corresponding received version for each Tx-Rx antenna pair. For MIMO measurements, it is sometimes difficult to process and/or record the data that are received at all Rx antennas at the same time. Thus, each Tx-Rx antenna pair is measured separately [9,10]. A fast switch between Tx and Rx antenna elements is used where each Tx-Rx antenna pair is visited. The MIMO channel has to be static during the time required to visit all the Tx-Rx antenna pair combinations. Fig. 1.1 shows an example of a measured channel impulse response at the center frequency of 5.3 GHz using dual antennas at the Tx and Rx sides. It can be noted that describing a single channel sample needs a large
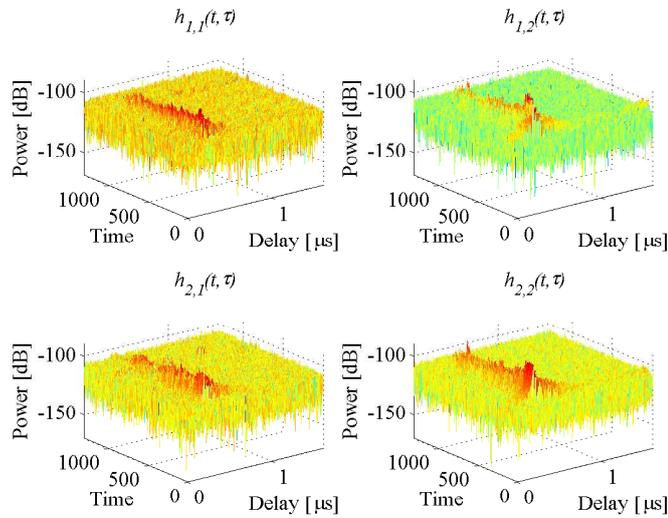
Figure 1.1: Measured channel impulse responses for a 2-by-2 MIMO wireless channel.

amount of information. Therefore, to measure a complete set of channels over a certain time and space is extremely costly.

1.3   Ray Tracing

As mentioned earlier, performing MIMO channel measurements is a complex process that requires significant effort and financial resources. As an alternative, channel models are widely used in order to generate MIMO channel realizations that can be used for different purposes such as system evaluation. Physical models aim at explicitly characterizing the effect of the physical environment on the wireless channels. One of the most widely used physical modeling methods is ray tracing [11]. Ray tracing aims to visualize propagation paths in the simulated environment and it provides channel realizations with high accuracy, especially when the transmitting antenna is positioned in moderately low heights, e.g., small micro-cells, and pico-cells [12, 13]. There are different approaches for the implementation of ray tracing techniques, but the rudimentary idea is to predict the most likely propagating paths based on the detailed description of the concerned environment. First, rays are launched from one communication terminal. When a ray interacts with an obstacle, it
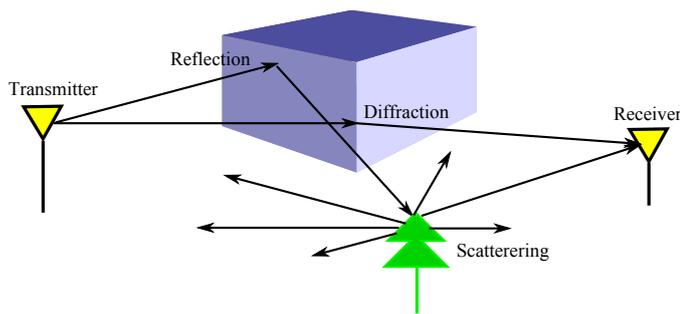
Figure 1.2: Rays propagation example.

gets reflected, diffracted or scattered in different directions, depending on the properties of the obstacle, see Fig. 1.2. The obstacles may be buildings, trees, windows, etc. In general, obstacles are described by simple models that characterize the interacting behavior of rays, e.g., be reflected from a wall with a specific power loss due to the wall material. After interacting with an obstacle, a ray may split into numerous rays, e.g., during scattering at a rough wall. The ray splitting process continues until the other terminal is reached, or until the ray power falls under a certain threshold. As long as a ray interacts with the different obstacles, the total number of rays increases exponentially, which requires large calculation time and memory. Even though the ray tracing is a highly computationally complex method, it is able to provide deterministic channel models that are very similar to the real physical channels.

1.4 Stochastic Channel Models

As the channel measurements and ray tracing techniques are of high complexity, stochastic channel models are widely used. The stochastic channel models are characterized by the statistics of their parameters, such as their correlation properties, path-loss, the ratio between the strongest MPC and the others, etc. Stochastic channel models have the advantage of describing wireless channels using simpler approaches compared to channel measurements and ray tracing techniques. However, they might compromise accuracy, as they do not aim for a complete description of the propagation processes. E.g., the correlative models [14] only characterize the correlation experienced at the Tx and Rx sides. As a consequence, channel models that have a balanced performance between the complexity and accuracy have attracted attention in the research field, e.g., WINNER II [4] and COST2100 channel models [5]. A brief overview

with respect to these channel models is given in the following.

1.4.1 Correlative Models

Correlative models try to simplify the wireless MIMO channel modeling effort by modeling only the correlation properties of the channel. In correlative models, wireless channels are represented as a white Gaussian channel with specific correlation properties at the two communication terminals, namely transmitter and receiver. These models are used extensively due to their simplicity, especially the Kronecker model [2] and the somewhat more advanced Weichselberger model [15].

Kronecker Model

The Kronecker model is one of the most popular, but simple MIMO channel models. It has been extensively used for the wireless system level verifications. The narrowband Kronecker channel model is simply described by a correlation matrix at the Tx and Rx sides and a Gaussian channel between them. It is assumed that there is no coupling between the scatterers located at the Tx and the Rx sides. Mathematically, the Kronecker model represents a simple form describing the channel matrix as:

$$\mathbf{H}_{\mathrm{Kron}} = \mathbf{R}_{\mathrm{Rx}}^{1/2} \mathbf{H}_{\mathrm{w}} \mathbf{R}_{\mathrm{Tx}}^{1/2}, \tag{1.3}$$

where $\mathbf{H}_{\mathrm{w}}$ represents the Gaussian channel with $E\{\mathbf{H}_{\mathrm{w}}\mathbf{H}_{\mathrm{w}}^{H}\} = \mathbf{I}$.

For the use of this model, only the correlation matrices at the Tx and Rx sides are needed. Usually the correlation matrices are estimated from the channel matrix with $\mathbf{R}_{\mathrm{Rx}} = E\{\mathbf{H}\mathbf{H}^{H}\}$ and $\mathbf{R}_{\mathrm{Tx}} = E\{\mathbf{H}^{H}\mathbf{H}\}^{T}$, where H is the Hermitian conjugate and T is the transpose. So the parameterization of the Kronecker model is simple and straightforward.

The Kronecker model can also be applied to wideband MIMO channels, where the wideband channel is treated as a collection of uncorrelated narrowband channels. Often the wideband Kronecker model is described as:

$$\mathbf{H}_{\mathrm{Kron}}[n] = \mathbf{R}_{\mathrm{Rx}}^{1/2}[n]\mathbf{H}_{\mathrm{w}}[n]\mathbf{R}_{\mathrm{Tx}}^{1/2}[n], \tag{1.4}$$

where n indicates each independent narrowband channel. Therefore, parameterization for each independent narrowband channel is needed for the use of the wideband model.

The Kronecker model is widely used due to its simplicity. However, measurements have suggested that the Kronecker model is not accurate enough and sometimes it fails to represent the real physical channel [16]. This lack

of accurately representing physical channels has raised the question: to which level, the Kronecker model can be trusted? With respect to the uncorrelated assumption in the Kronecker model, the model usually has a good performance when the number of antennas is small. As the number of antennas increases, e.g., as in massive MIMO, the space resolution of the system increases and the performance of the Kronecker model is highly degraded.

Weichselberger Model

In order to include the coupling between the scatterers at the Tx side and the ones at the Rx side, Weichselberger has developed a correlative model that has a more accurate description of the properties in the spatial domain [15]. Besides requiring the link end correlation matrices, as in the Kronecker case, the Weichselberger model also requires the additional knowledge of a coupling matrix between the Tx and Rx. The model is defined as

$$\mathbf{H}_{\text{Weichsel}} = \mathbf{U}_{\text{Rx}}(\widetilde{\Omega}_{\text{Weichsel}} \odot \mathbf{H}_{\text{w}})\mathbf{U}_{\text{Tx}}, \tag{1.5}$$

where $\mathbf{U}_{\text{Rx}}$ and $\mathbf{U}_{\text{Tx}}$ are the eigen bases resulting from the eigenvalue decomposition of the link end correlation matrices $\mathbf{R}_{\text{Rx}}$ and $\mathbf{R}_{\text{Tx}}$, respectively. The $\widetilde{\Omega}_{\text{Weichsel}}$ is the element-wise square root of the coupling matrix Ω. The $\odot$ represents the element-wise multiplication, and the $\sim$ operator indicates an element-wise square-root. The parameters for this model are the eigenbasis of the receive and the transmit correlation matrices and a coupling matrix. Same as the Kronecker model, the correlation matrices are estimated from the channel matrix while the coupling matrix is given by

$$\Omega = E\{(\mathbf{U}_{\text{Rx}}^{H}\mathbf{H}\mathbf{U}_{\text{Tx}}^{*}) \odot (\mathbf{U}_{\text{Rx}}^{T}\mathbf{H}\mathbf{U}_{\text{Tx}})\}. \tag{1.6}$$

Parameterization for Weichselberger model is still with reasonable complexity, where only the coupling matrix is added compared to the Kronecker model. The Weichselberger channel model has been validated by measurement data in [17]. It has been demonstrated that the model gives a reasonable approximation of the system performance, especially for the channel capacity and spatial properties. Still with complexity, it has been widely used especially for the narrowband channel applications.

Structured Model

The Weichselberger model focuses primarily on narrowband channels, where the correlations over different bands are not considered. The structured model is an extension of the Weichselberger model to the wideband MIMO channel,
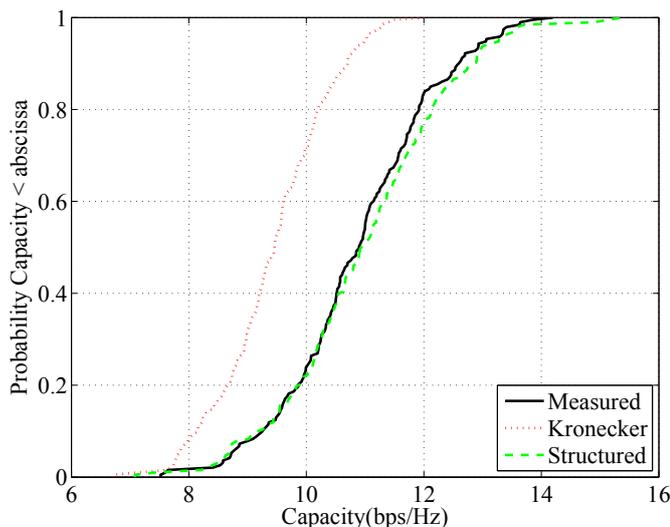
Figure 1.3: Modeled versus measured capacity for a wideband 4-by-4 MIMO measurement.

that includes the wideband correlation over receiver-transmitter-delay space and is defined as [18]:

$$\mathbf{H}_{\text{struct}} = \Gamma \times_1 \mathbf{U}_{\text{Rx}} \times_2 \mathbf{U}_{\text{Tx}} \times_3 \mathbf{U}_{\text{del}}. \tag{1.7}$$

$\mathbf{U}_{\text{Rx}}$, $\mathbf{U}_{\text{Tx}}$ and $\mathbf{U}_{\text{del}}$ are the orthogonal eigen bases for the correlation matrix over receiver, transmitter and delay space, respectively. Γ is the wideband channel matrix with weighted complex-Gaussian random variables. The weighted factors, depending on the wideband coupling coefficients, are defined as

$$\omega_{ijk} = (\mathbf{u}_{\text{del},k} \otimes \mathbf{u}_{\text{Tx},j} \otimes \mathbf{u}_{\text{Rx},i})^H \mathbf{R}_{\text{WB,H}} (\mathbf{u}_{\text{del},k} \otimes \mathbf{u}_{\text{Tx},j} \otimes \mathbf{u}_{\text{Rx},i}), \tag{1.8}$$

where $\mathbf{u}_{\text{Rx},i}, \mathbf{u}_{\text{Tx},j}$, and $\mathbf{u}_{\text{del},k}$ are the one-sided eigenvectors, and $\mathbf{R}_{\text{WB,H}}$ is the wideband correlation matrix. The $\otimes$ represent the Kronecker product.

For the parameterization of the structured model, the full wideband matrix and the correlation matrix over each dimension have to be estimated. Compared to the wideband Kronecker model, the performance is improved due to the inclusion of the full correlation over different bands. Fig. 1.3 shows the capacities from the Kronecker and the structured model based on a wideband 4-by-4 MIMO measurement at a signal-to-noise ratio (SNR) of 10 dB. As expected, the Kronecker model underestimates the channel capacity while
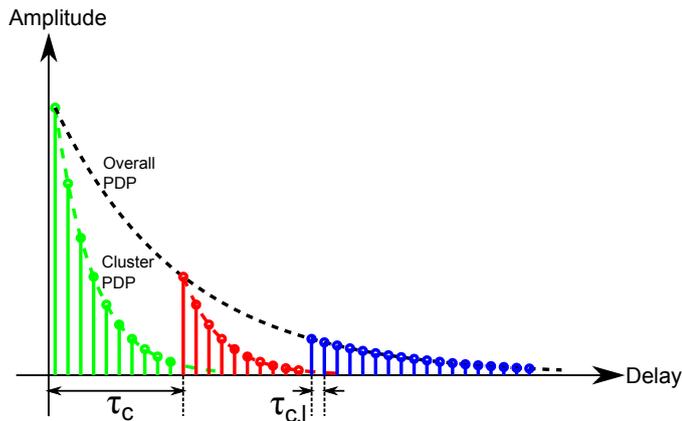
Figure 1.4: The Saleh-Valenzuela model, schematic description of the PDP.

the structured model gives more accurate capacity estimates for a wideband MIMO channel.

1.4.2 Cluster-based Channel Models

Cluster based models bridge the gap between correlative channel models and ray tracing models, and provide a balanced performance between modeling accuracy and complexity. The first well-known cluster based model is the Saleh-Valenzuela (SV) model [19], which describes channels with time invariant properties. It focuses on modeling the channel with respect to both power and delay [19]. SV model is one of the first channel models that include the clustering of MPCs. It divides the channel impulse response into several clusters, each of which is consisting of a number of MPCs. The power delay profile (PDP) of each cluster is modeled with an exponentially decaying profile, with its own arrival time and decay factor, see Fig. 1.4. The overall PDP is also modeled with exponential decay; however, with slower decay factor. The modeled channel impulse response is given as

$$h(\tau) = \sum_{c=0}^{\infty} \sum_{l=0}^{\infty} a_{c,l} e^{j\phi_{c,l}} \delta(\tau - \tau_c - \tau_{c,l}) \qquad (1.9)$$

where τ_c is the cluster arrival time, and $\tau_{c,l}$ is the arrival time of the lth MPC inside cluster c. The parameters $a_{c,l}$ and $\phi_{c,l}$ are the gain and phase of the lth
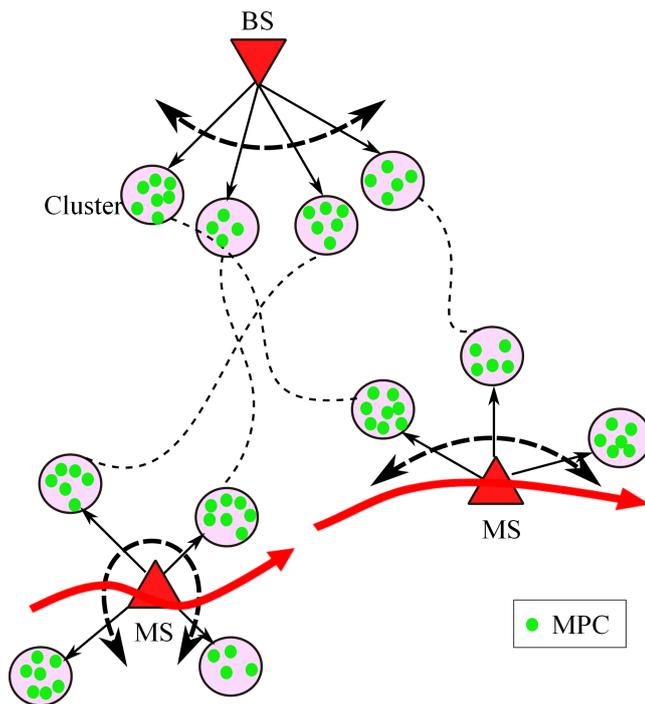
Figure 1.5: Cluster concept in WINNER II channel model.

MPC in cluster c. It can be noted that the parameters of the SV model are limited. Thus, the model can be implemented with low complexity. However, usually the SV model works well only for the indoor scenario and lacks the time invariant description of the real channel. The SV model is simple and easy to use, but more sophisticated channel models are needed to give a more detailed characterization of the wireless channel.

1.4.3 Geometry-based Channel Models

The fundamental basis of geometry-based channel models is also clusters, together with geometrical descriptions, such as directional information. There are well-established geometry-based channel models, e.g., COST 273 [20], WINNER II [4], COST 2100 [5] etc. These models are with reasonable complexity and high accuracy, which makes the geometry-based channel models significantly attractive. In this section, WINNER II and the COST 2100 channel

models are discussed in more detail.

WINNER II Channel Model

In the WINNER II channel model, multi-path clusters are used in order to develop a realistic description of the wireless channels. Fig. 1.5 shows the modeling concept for a single link MIMO channel. Each large black circle represents a multi-path cluster that is associated with a group of MPCs (represented as tiny solid green circles). As the mobile stations (MSs) move, different clusters will contribute to the communication links.

The WINNER II channel model covers a wide range of propagation scenarios, including an indoor office, indoor hall, urban micro-cell, outdoor to indoor and so on [4]. For each scenario, different sets of parameters are extracted from measurements, e.g., delay spread, angle spread, shadow fading and cross-polarization ratio. There are two groups of parameters used in the WINNER II channel models: large scale parameters and support parameters. The model parameters are summarized in [4] and are all included in the open MATLAB WINNER II implementation. To generate channel snapshots using the WINNER II channel model, parameters for each snapshot are calculated from the global parameters and parameter distributions, which means the channel parameters vary over time. However, the concept of channel segments has been introduced to keep the channel stationary, i.e., to make sure that the large scale parameters do not change, over such intervals.

The WINNER II channel model has significant advantages, e.g., it covers many scenarios, and it is scalable with multi-link modeling. However, it is affected by a major shortcoming, that is, the clusters are of the same size. This is not true when considering the physical properties of different propagation environments. Therefore, the model accuracy degrades, especially in indoor scenarios, where clusters have significantly different sizes. In addition, the model has a rigid structure such that when new large scale parameters are introduced, the entire initialization of the propagation environment must be redefined, which hinders the development or extension of the model itself [21].

The COST 2100 Channel Model

The COST 2100 channel model is an extension of, and have inherited several concepts from, the previous COST 273 MIMO channel model [5]. The COST 2100 channel model describes the physical radio propagation in various scenarios including the macro-, micro- and pico-cells with a generic and flexible structure that shows good compatibility with other scenarios. It also supports
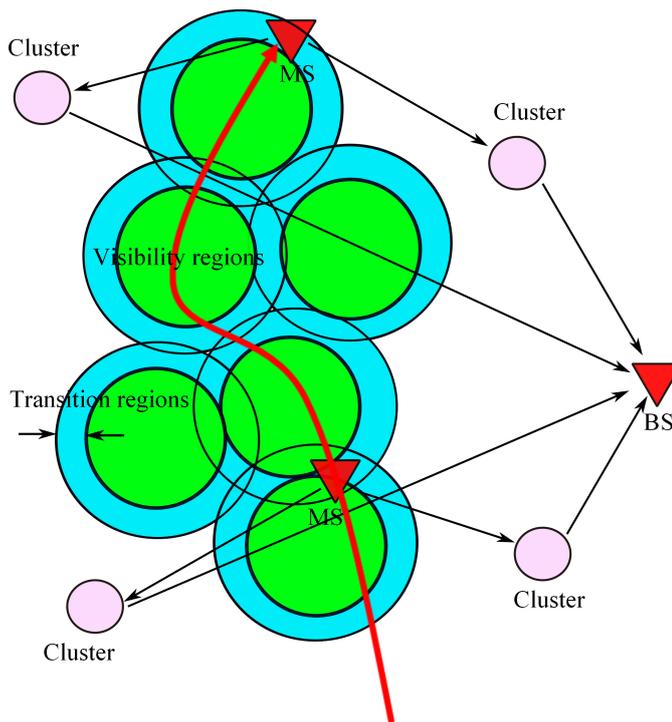
Figure 1.6: The COST 2100 channel model, an example of clusters, visibility regions and transition regions.

both single- and multiple-link MIMO channel access.

The basic modeling methodology of the COST 2100 channel model is based on multi-path clusters and their corresponding visibility regions. Basically, clusters are assumed to be uniformly distributed in the communication area, and each cluster is associated with a visibility region. When a user is inside a visibility region, the corresponding cluster is active, thus having contributions to the channel. Generally, a cluster can have more than one visibility region, but each visibility region can only be assigned to one cluster. Users can exist within several visibility regions at the same time, e.g., in the overlapping area of several visibility regions. As a user is moving, the clusters that can be seen by the user are changing. Even along the duration in which the cluster is being active, its power contribution changes as the position of the MS changes. This change takes place within what is called a transition region. The transition regions are defined within the visibility regions and their role is to smoothly

allow the user to enter or leave the visibility region of interest. Fig. 1.6 shows an example of the relations between clusters, visibility regions and transition regions.

To simulate channels using the COST 2100 model, parameters for the considered scenarios have to be provided. Typically, the COST 2100 channel model includes indoor and outdoor scenarios, where some of the scenarios have the complete set of parameters, but a subset of the modeling parameters of some scenarios is missing.

The COST 2100 channel model has significant importance for the development of the next generation wireless system. Its cluster-level structure provides an efficient and a realistic solution for incorporating diverse channel properties into the channel description. Hence, it promises a solution to model different aspects in multi-link and cooperative communication systems. The COST 2100 model covers different communication scenarios, includes new channel characteristics, e.g., diffuse multi-path components (DMCs), and is suitable for system level simulations. A more thorough discussion of the COST 2100 channel models is given in Chapter 3.

1.5   Overview of the Thesis

MIMO channel models are important for the development of wireless systems. There is a wide amount of literature on channel modeling. However, sophisticated channel models need more efforts targeting different environments, parameterization, implementation and validation, which are the primary objectives of the thesis.

First, to be able to understand the basis of geometry-based channel models, clusters are studied in Chapter 2, including their spatial and physical properties. Then, one of the geometry-based channel models using the concept of clusters, the COST 2100 channel model, is studied, analyzed, and implemented in Chapter 3, including the discussions on multi-link extension of channel models. Recently, high accuracy indoor positioning attracted high attention both in industry and academia. In Chapter 4, the possibility for positioning using phase information of MPCs from the radio channels is investigated. The contributions and conclusions of the thesis are presented in Chapter 5, together with discussions of future work.

Chapter 2

What is a Cluster?

As a general term, a cluster is defined as a collection of objects that are similar to each other in some agreed-upon sense [22]. In radio channels analysis, a multi-path cluster is defined as a group of MPCs that have similar delay and angular parameters. Identifying clusters in radio channels has attracted a lot of research attention due to the fact that clusters represent the basis for popular channel models [19, 23–37]. In 1987, Saleh and Valenzuela were the first to propose using the concept of clusters for channel modeling [19]. They focused on defining clusters in the delay domain. Later on, other domains, including azimuth angle of departure and arrival as well as delay, were suggested to be considered when identifying clusters, such as the COST 259 model [23, 24]. Significant research effort has been made in order to study clusters and obtain a better understanding of their behavior based on measurement data [25–37].

The procedure of identifying clusters is called clustering, and there are two widely used methods for clustering. The first one is the parameter based clustering method, where clustering is performed based on the parameter space of the MPCs. The corresponding extracted clusters are therefore called parameter based clusters [25–35]. The second is the physical clustering method where ray tracing or ray launching techniques are used to identify the different groups of scattering objects and their associated MPCs [36, 37]. Usually, compared to the parameter based clusters, physical clusters can easily be interpreted and linked to the different physical scatterers in the environment. However, physical clusters are often linked to a more complicated extraction methodology.

In this chapter, we start by reviewing the parameter based clusters, including their extraction using the joint clustering and tracking algorithm, and some of their properties such as cluster positions, spreads, and movements. Then we discuss the physical clusters, with respect to their extraction using a

measurement based ray launching extraction method, and some of their properties such as cluster's lifetimes and spreads. At the end of this chapter, the physical interpretation of the parameter based clusters is discussed.

2.1 Parameter Based Clusters

Clustering algorithms focusing on the parameter space of MPCs, such as KPowerMeans, Hierarchical, and Gaussian mixture, have been discussed and widely used in cluster related channel analysis [26, 28–31]. The extracted clusters from such clustering algorithms are called parameter based clusters. A parameter based cluster is usually characterized by its lifetime, angular spreads, delay spread, shadowing factor and so on, see e.g., [28, 31]. Usually, clustering algorithms concentrate on determining clusters in each snapshot and do not take into account characterizing the evolution of clusters' properties among consecutive snapshots. However, from a modeling perspective, cluster time variant properties have to be considered to give a better description of the channels. Therefore, cluster tracking algorithms that are able to obtain the different time variant properties of clusters [38, 39] have been developed. At an early stage, algorithms were introduced such that they first extract clusters, and then track them, e.g., see [38]. Later, a so called joint clustering and tracking algorithm, which extracts and tracks clusters at the same time, has attracted researchers' interests [39]. In this section, the joint clustering and tracking algorithm is reviewed as well as the properties of the extracted clusters.

2.1.1 Joint Clustering and Tracking Algorithm

The idea of joint clustering and tracking allows identifying clusters and tracking their time variant properties concurrently. To achieve this goal, the following steps are performed. First, a Kalman filter is used to predict the position parameters of the clusters for the next snapshot and, then, a KPowerMean clustering algorithm is used to identify different clusters from the measurement data based on these predictions. The tracking algorithm determines how clusters of different snapshots are related to each other. Depending on their properties, clusters from a new snapshot can be associated with the clusters from the previous snapshot or treated as newborn clusters. Similarly, clusters in the previous snapshot are seen as dead if they cannot be related to any cluster in the next snapshot. This algorithm has been tested in several measurement environments, both for indoor and outdoor scenarios, and demonstrated significant improvement in tracking clusters [39]. The main parts of the joint clustering and tracking algorithm, i.e., KPowerMean and Kalman filtering, are

discussed in the following.

KPowerMean Clustering

The KPowerMean clustering algorithm is based on the power weighted K-means algorithm [29, 30]. First, K initial cluster centroid positions are chosen, and then the MPCs, characterized by delay, angle-of-arrival (AOA), angle-of-departure (AOD) and power, are associated to the cluster centroids $\boldsymbol{\mu}_c$ according to the distance function, which is defined as:

$$D(i) = \sum_{l=1}^{L} P_l \text{MCD}(\text{x}_l, \boldsymbol{\mu}_c) \tag{2.1}$$

Each MPC x_l is associated with the cluster centroid which has the minimum distance $D(i)$. After assigning all the MPCs to their corresponding centroids, the centroids of the different clusters are re-calculated based on their associated MPCs as

$$\boldsymbol{\mu}_c = \begin{bmatrix} \frac{1}{\sum^{l \in \boldsymbol{\mu}_c} P_l} \sum^{l \in \boldsymbol{\mu}_c} P_l \tau_l \\ \text{angle}(\sum^{l \in \boldsymbol{\mu}_c} P_l \exp(j\phi_{\text{Rx},l})) \\ \text{angle}(\sum^{l \in \boldsymbol{\mu}_c} P_l \exp(j\phi_{\text{Tx},l})) \end{bmatrix} \tag{2.2}$$

where P_l, τ_l, $\phi_{\text{Rx},l}$ and $\phi_{\text{Tx},l}$ are the power, delay, AOA and AOD of the lth MPC, respectively. A comparison between the newly observed cluster centroids and the previous centroids is performed. Only when all the cluster centroids are not changed, the algorithm will stop assigning MPCs to clusters. Otherwise the MPCs will continue to be assigned to the new centroids. In order to make a more efficient algorithm, usually a maximum iteration number is needed [26]. When the KPowerMean clustering algorithm is performed based on the three considered domains, i.e., AOA, AOD, and delay, any of these three properties might dominate the clustering performance. For example, clusters with significantly different delays but with similar properties in other domains can be grouped into one cluster. Therefore, in [39], a weighting factor of the delay component was introduced to give a trade-off between the delay and angular domain.

Kalman Filter Tracking

Kalman filtering, which is also known as linear quadratic estimation [40], is an algorithm that uses a series of measurements observed over time, containing noise (random variations) and other inaccuracies. Also it allows tracking, and produces estimates of unknown variables that tend to be more precise than those based on a single measurement alone. Basically it contains two parts for

the channel parameter tracking, Kalman prediction and Kalman update. Both are focusing on cluster centroids. Based on the assumption of having linear movements of clusters in delay and angle domains, the state-space model is defined by using the cluster tracking parameters $\boldsymbol{\theta}$, which consists of cluster centroid position and centroid speed [30],

$$\boldsymbol{\theta}^n = \Phi\boldsymbol{\theta}^{n-1} + \mathbf{w}^n \tag{2.3}$$

where $\mathbf{w}^n$ is the state noise at the nth stage and Φ is the state-transition matrix and is given by

$$\Phi = \mathbf{I}_3 \otimes \begin{bmatrix} 1 & 1 \\ 0 & 1 \end{bmatrix}, \tag{2.4}$$

where $\mathbf{I}_3$ is the identity matrix and $\otimes$ denotes the Kronecker product.

The derived Kalman filter tracking equations include prediction and update steps: [30]

Prediction

$$\boldsymbol{\theta}^{n|n-1} = \Phi\boldsymbol{\theta}^{n-1|n-1} \tag{2.5}$$

$$\mathbf{M}^{n|n-1} = \Phi\mathbf{M}^{n-1|n-1}\Phi^{\mathrm{T}} + \mathbf{Q} \tag{2.6}$$

Update

$$K^{n|n} = \mathbf{M}^{n|n-1}\mathbf{O}^T(\mathbf{O}\mathbf{M}^{n|n-1}\mathbf{O}^T + \mathbf{R})^{-1} \tag{2.7}$$

$$\boldsymbol{\theta}^{n|n} = \boldsymbol{\theta}^{n|n-1} + K^{n|n}(\boldsymbol{\mu}_c - \mathbf{O}\boldsymbol{\theta}^{n|n-1}) \tag{2.8}$$

$$\mathbf{M}^{n|n} = (\mathbf{I} - K^{n|n}\mathbf{O})\mathbf{M}^{n|n-1} \tag{2.9}$$

where $\mathbf{O}$ is the transition matrix for the cluster centroid position. The parameters $\mathbf{Q}$, $\mathbf{M}$ and $\mathbf{R}$ are initialized as identity matrices.

The Kalman filter both tracks the clusters' centroids over time and predicts their centroids for the next snapshot. By using the Kalman filter, the time variant properties of clusters can be obtained. Also, the prediction of the centroids of the new clusters helps the clustering algorithm to converge quickly.

(a) Snapshot 1

(b) Snapshot 2

(c) Snapshot 3

(d) Snapshot 4
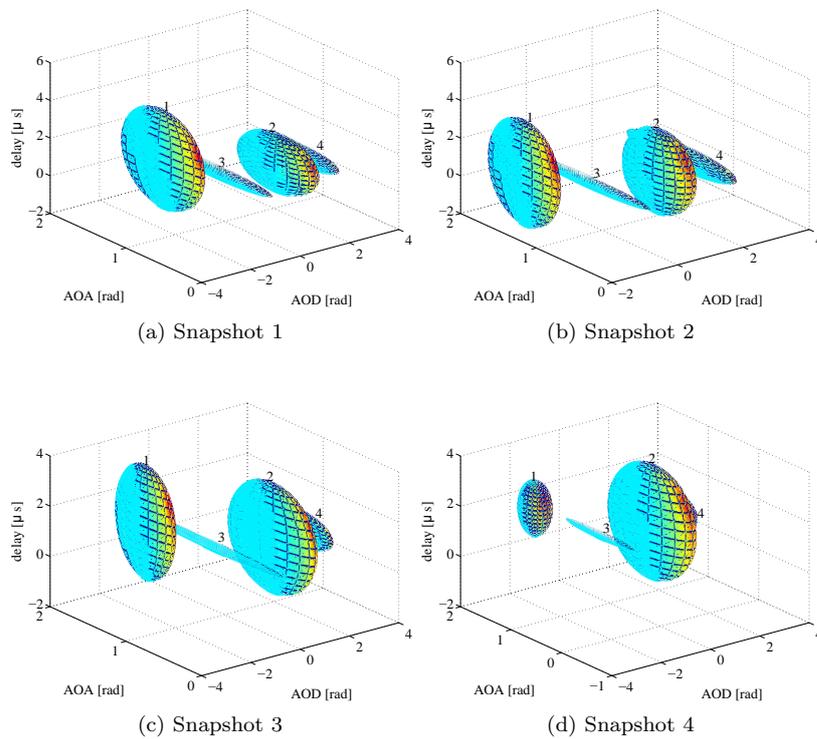
Figure 2.1: Examples of tracked clusters over time.

2.1.2   Cluster Properties

By using the joint clustering and tracking algorithm, a cluster is characterized not only by its position and spreads, but also by its lifetime, and movements with respect to its position and spreads, power etc. In [30,39], cluster properties have been investigated for both indoor and outdoor scenarios, where it has been found that clusters have significant movements in the different parameter domains, which can be attributed to the changing of propagation conditions. To have a deep understanding of the cluster properties, cluster position, spreads, movements and lifetime are discussed more in detail in the following.

(a) Cluster delay movements   (b) Cluster angular movements
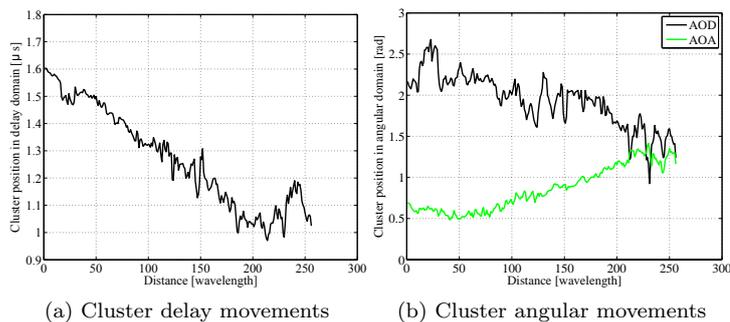
Figure 2.2: Examples of movements of parameter based clusters in the delay and angular domains: a) cluster delay movements, b) cluster angular movements.

Cluster Position and Cluster Spreads

A cluster position is determined by the cluster's centroid, including delay, AOD and AOA, while the cluster's spreads determine the size of the cluster. The determined clusters have an ellipsoidal shape. Fig. 2.1 shows examples of the position and the size of a cluster in a sub-urban scenario, where the propagation environment is changing slowly. It can be noted that clusters are separated well in delay, AOA and AOD. Inside each cluster, the cluster spreads are within a reasonable range thus the cluster sizes are limited with small values. The used algorithm is able to separate clusters and identify their associated MPCs.

Cluster Movements

Movements of the clusters include the movements of their positions and the changes of their sizes. The tracking algorithm provides the possibility to capture the variations of the cluster properties over time. Usually the movement of clusters highly depends on the propagation scenarios [30]. For the cluster delay, it shows a steady variation in indoor scenarios while it changes fast in outdoor scenarios [34], such as sub-urban. Usually the BS is static thus the change of parameters in the cluster AOD (assuming the BS as the transmitter) domain keeps a similar pattern for all scenarios. However, the movement at the receiver side highly relies on the scatterers around the Rx. A local scatterer usually leads to large variations in the angular properties of the clusters [35]. In general, the movements of clusters describe the changes of the propagation conditions. An example of movements in the delay and angular domains is
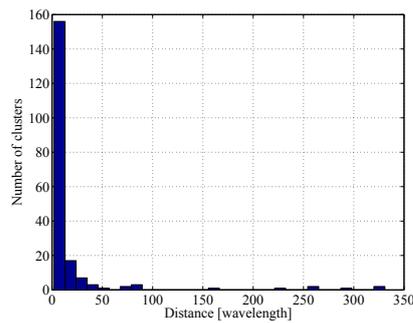
Figure 2.3: Statistics of the lifetime of a parameter based cluster.

shown in Fig. 2.2. In this particular sub-urban scenario, the cluster has slow variations in both delay and angular domains, because the dominant scatterers keep contributing to the channel over a long time.

Cluster Lifetime

The lifetime of a cluster shows its active time span and hence relates to its visibility region, which is an important property for cluster based models. When a cluster is active, it contributes to the channel response. Over the active time span of a cluster, the contributions from this cluster to the channel response have slow variations over the time. However, clusters can also vanish fast, e.g., due to a shadowing object between the Tx and Rx. Therefore, clusters may be blocked and die [34]. Fig. 2.3 shows an example of a lifetime of a cluster in a sub-urban scenario. Most of the clusters have lifetimes less than 10 wavelengths. There are, however, a number of clusters with longer lifetimes that reflect the dominant scatterers in the environment.

2.2 Physical Clusters

Physical clusters, as the name indicates, are identified based on the physical interpretation of propagation paths. Therefore, the measurement ray launching tool is discussed in this section due to its capability to link MPCs with physical environment, and thus can be used for the purpose of physical clustering. Then the physical cluster extraction and properties are given as well.
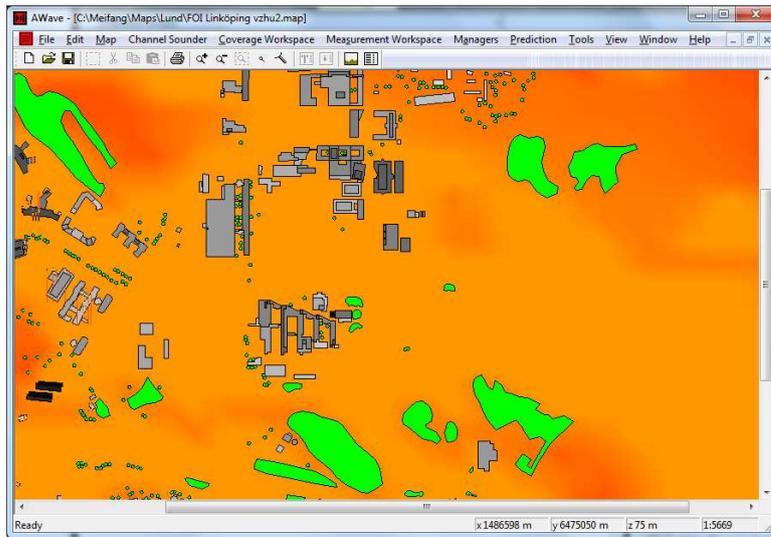
Figure 2.4: GUI of the measurement based ray launching tool for outdoor scenarios. From [43].

2.2.1   Measurement Based Ray Launching Tool

Ray tracing and ray launching are promising candidates to help understanding the channel behavior and link it to the physical propagation environment. These techniques have high computational complexity and have no *direct* connection to measurements; therefore, a measurement based ray launching technique is introduced where the information from measurements is used in order to link the channel measurements to the physical environment. Besides providing a connection between measurements and the physical environment, it has the advantage of requiring lower complexity compared to conventional ray launching approaches as rays are launched only in the directions of the estimated MPCs.

The first use of the measurement based ray launching technique was for a low complexity indoor propagation scenario where there were two inputs for the developed indoor measurement based ray-tracer: (i) high resolution channel parameter estimates and (ii) physical structure of the propagation environment [41]. With the tool, it was possible to identify the dominant propagation phenomena and relate them with the scatterers of the physical environment. The developed indoor measurement based ray-tracer did not have the capability to simulate outdoor scenario due to the complicated outdoor propagation phe-
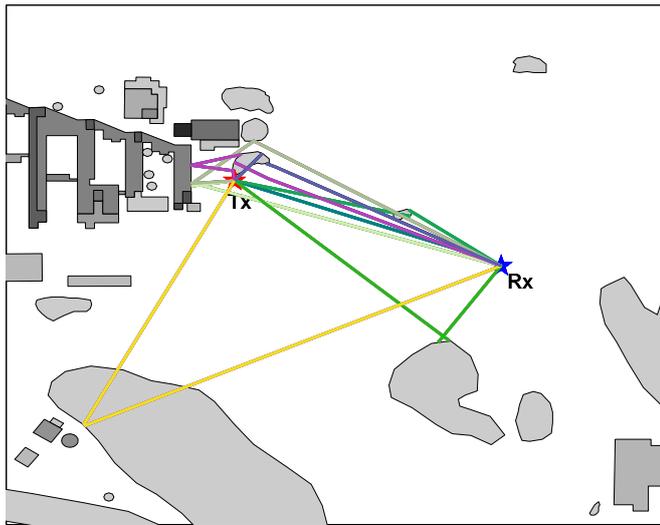
Figure 2.5: Examples of ray launching performance. From [43].

nomena. Therefore, in [42, 43], efforts have been made to develop a measurement based ray launching tool for outdoor scenarios. First, a simple outdoor measurement based ray launching structure was built based on the C++ application by E. Olsson [42] and A. Stranne, where only specular ray reflections from scatterers are considered. Later on, the application was made more sophisticated and capable to simulate diffraction and scattering as well [43], see Fig. 2.4. Similar to the indoor measurement based ray-tracer, a detailed floor plan of the measured area has to be provided, including the different interacting scatterers such as buildings, trees etc. If 3D ray tracing is aimed for, elevation information has to be included as well. Secondly, the measured channel is estimated with a high resolution algorithm, e.g., SAGE [44], or EKF [45, 46], to extract the MPC parameters. Consequently, the developed tool uses the delay, AOA, AOD and power of the extracted MPCs in order to visualize the most likely propagation paths on top of the environment map. Propagation processes of each MPC can be easily linked to the different physical scatterers. Fig. 2.5 shows examples of the visualized propagation paths together with their interacting scatterers.

Measurement based ray launching is an efficient way to understand the propagation mechanisms, especially to have a physical interpretation of the propagation channel. It offers valuable insights for channel modeling. However, there are some challenges for improving the efficiency and accuracy of this

tool. For instance, it is difficult to obtain detailed 3D floor plans for every environment of interest, and propagation models for different scatterers in the environment need to be improved as well.

2.2.2   Physical Clustering

Physical clustering has been evaluated in indoor scenarios by Poutanen et al. [36,41], which relies on the assumption that there exists a unique physical scattering object (or a group of scatterers in the case of multiple bounce clusters) that can be identified in the measurement environment for each extracted cluster. In order to determine the interacting scatterers in the environment, an extended Kalman filter has been used to extract MPCs with AOA, AOD and delay [45,46]. An indoor measurement based ray tracer has been used to plot rays on top of a floor plan of the measurement environment according to the measured parameter estimates [41]. It thus shows the physical propagation paths, enabling the clusters to be explicitly mapped to physical scatterers in the environment. Using this approach, a cluster is defined as a group of MPCs originating via similar scattering processes, e.g. via a reflection from the same wall. Therefore, the extracted clusters are called physical clusters.

Physical clustering in an outdoor scenario has been carried out in [37]. For outdoor scenarios, it is often possible to identify dominant scatterers from a map. These dominant scatterers contribute to the channel impulse response over a long time and determine the main properties of the channel, i.e., over many separate channel snapshots. The scatterer based physical clusters can be related to a single scatterer or a group of scatterers. Furthermore, a scatterer can contribute to more than one physical cluster. In [37], physical clustering based on the distance between scatterers was suggested, where the distance between scatterers should be sufficiently close, so that the Tx/Rx cannot distinguish them. The term "close" is defined as when the distance between scatterers is much smaller than the distance to the Tx/Rx, more specifically one third of the distance between the Tx and Rx.

2.2.3   Properties of Physical Clusters

Physical clusters have been studied in [36] for the indoor environment. There, the number of clusters, cluster lifetime, and cluster visibility region have been investigated. It was shown that, the number of active clusters was 2.2 in non line-of-sight (NLOS) and 3.7 in line-of-sight (LOS) on the average. Also the cluster visibility region is suggested as 1 m in NLOS and 3.8 m in LOS in [36]. Recently, the study of physical clusters for outdoor scenarios has been carried out in [37], where both the sub-urban and urban scenarios are considered. The
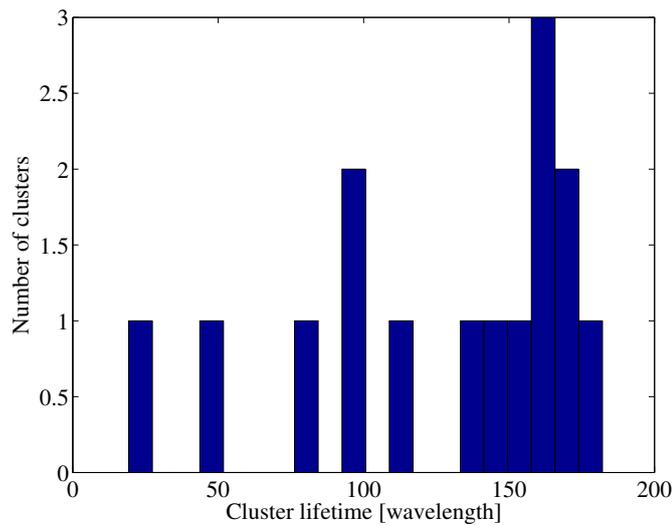
Figure 2.6: Statistics of the lifetime of one physical cluster.

discussions of properties of physical clusters are limited due to the lack of a refined physical clustering method. The properties of physical clusters with respect to cluster lifetime and cluster spreads are discussed more in detail in the following.

Cluster Lifetime

The time during which a physical cluster can be seen is called as the cluster lifetime, which is a fundamental basis for cluster visibility regions. When the terminal is moving, a physical cluster can be visible for a while, but also be blocked or shadowed by scatterers. Therefore, Fig. 2.6 shows an example of the cluster lifetime in units of wavelengths in the same sub-urban scenario as for the parameter based clusters. It can be noted that the extracted cluster lifetime in average is much longer than the ones for the parameter based clusters; more than 50% of the clusters have a lifetime larger than 100 wavelengths. This fact is well reflected in outdoor sub-urban environments where a physical object usually can give contributions to the channel over a longer time duration.

Cluster Spreads

The cluster spreads for physical clusters have been investigated in [37], including delay spread and angular spread. It has been seen that the delay spread and angular spreads have in general small values in the sub-urban and urban scenarios, e.g., 10 degree in AOA spread and 0.05 μs delay spread, which in turn reflects that the physical clustering results in a limited delay spread and angular spread of the associated MPCs. Therefore, the size of clusters is limited in a reasonable range.

2.3   Physical Interpretation of Parameter Based Clusters

Clusters that are extracted using the parameter based method capture the channel variations in position, size, and lifetime. However, finding a physical interpretation for these clusters is still an open topic which needs more investigations. In order to understand and determine the physical interpretation of clusters, the MPCs of each cluster need to be related to the physical environment.

With the developed measurement based ray launching tool, it is possible to investigate the behavior of the parameter based clusters and their interactions with the different physical scatterers in the environment. This investigation was performed for the first time in [37], where the clusters and their associated MPCs are analyzed so that they can be visualized together with the measured environment map. It was found that if the parameter based cluster is characterized as single-bounce then it has tight connections with the physical environment. Otherwise, it is difficult to relate the clusters with the physical environment. In general, the associated MPCs of a cluster have tight connections with the physical environment in the angular domain but not the case in the delay domain. Typically, a parameter based cluster is not interacting with a single physical scatterer but rather with several scatterers. Generally speaking, the investigation in [37] has shown that it is not straightforward to interpret the connections between the parameter based clusters and the physical environment.

Chapter 3

The COST 2100 Channel Model: Parameterization, Implementation, and Validation

The COST 2100 channel model is a well-established wireless channel model that can be integrated to evaluate current and next generation wireless systems. It provides statistical descriptions of wireless channels both for indoor and outdoor scenarios. However, the COST 2100 channel model implementation is still under development and needs more efforts, such as parameterization for some typical scenarios, especially when two or more wireless terminals are introduced. Also, there is a lack of studies validating the COST 2100 channel model due to the absence of a general methodology to validate channel models. Moreover, the validation processes are also dependent on available measurement data and the nature and use of the particular channel model. One of the most important characters of the COST 2100 channel model is the multi-link extension, where simulations with multiple BSs and MSs are supported. Analyses of the multi-link extension are rare due to a lack of multi-link measurements.

In this chapter, parametrization and validation of the COST 2100 channel model are discussed in detail. And then, the multi-link channel properties and its extension in the COST 2100 channel model are discussed.

3.1   Parametrization for the COST 2100 Channel Model

Parametrization is an essential step for the implementation of channel models. The first effort for the COST 2100 channel model parametrization was carried out by Poutanen et al. in [47], where only a single indoor link was considered. There, inter-cluster parameters, such as number of clusters, radius of the visibility regions, cluster decay factors, as well as the intra-cluster parameters (e.g., number of MPCs in a cluster, angular spreads, polarizations), were given, including both LOS and NLOS scenarios. More recently, in [31], parametrization for sub-urban scenarios has been carried out, where a complete set of parameters for outdoor scenarios is provided. In this section, details of the parametrization methodology and the corresponding results are reviewed.

3.1.1   Visibility Region

The visibility region is one of the most important concepts, because the size and number of visibility regions, etc, are parameters for the COST 2100 channel model. It was first introduced in the COST 259 channel model, where the visibility region is defined as the duration of the cluster in which it can be seen by the MSs [23]. In [47], the visibility region has been discussed and extracted similarly as in [23] for indoor scenarios. More recently, in [31], the visibility region has been derived from a modified extraction method. The main motivation for the modified method is that the MS does not always go through the center of the cluster visibility region and the visibility region of each cluster cannot simply be equal to the so called cluster lifetime distance, which is the multiplication of cluster lifetime and moving speed. Therefore, in [31], a relation between the visibility region and cluster lifetime is proposed. There, it has been assumed that the cluster visibility region is a circle, and the radius of the circular visibility region r is deterministic. It is further assumed that the measured route traverses the circular visibility regions at a random (uniformly distributed) distance d from the respective centers of the cluster visibility regions. Given this geometry, the length of an intersection between a measured route and a cluster visibility region is

$$L = \begin{cases} 2\sqrt{r^2 - d^2} & 0 \le d \le r, \\ 0 & \text{otherwise.} \end{cases} \tag{3.1}$$

Now, the average cluster lifetime distance is

$$\Lambda \triangleq E\left[L\right] = \int_0^r 2\sqrt{r^2 - x^2}\, f_d(x)\,\mathrm{d}x, \tag{3.2}$$

where $E[\cdot]$ denotes statistical expectation and $f_d(x)$ is the probability density function for d. By solving the integral in (3.2) for a uniformly distributed r, $0 \leq d < r$, it can be obtained as

$$\Lambda = \frac{\pi}{2}r, \tag{3.3}$$

where the factor $\frac{\pi}{2}$ is defined as a compensation factor between the cluster visibility region radius r and the average cluster life distance Λ. In the COST 2100 channel model, the visibility region for indoor scenarios is suggested as 2.8 m and 3.8 m for LOS and NLOS respectively [5]. For outdoor scenarios, 32.8 m and 24.5 m are recommended for LOS and NLOS, respectively [31], based on the related channel measurement analysis. In indoor scenarios, scatterers are usually within a small scale and also the properties of each scatterer vary from one to another so that clusters vanish more frequently, thus the corresponding visibility region is in a scale of meters. However, in outdoor scenarios, objects can be larger, e.g., high buildings, and large walls, so clusters are visible for a longer time and cluster visibility regions are thus larger.

3.1.2 Cluster Power Decay Factor

The power carried by each cluster is modeled as a function of the cluster delay; basically, the longer the cluster delay, the weaker the cluster power is. In the COST 2100 channel model, cluster power is characterized with cluster decay factor, which describes how rapidly the power of the clusters decays as a function of the increasing delay. The factor gives control of the channel power in total and is thus crucial to the channel model as well. In general, a linear regression in dB domain between the power and delay can be done to extract the decay factor [31]. An example of extracting the decay factor is given in Fig. 3.1, where all the extracted clusters over the time and space are used. In this extraction process, it is crucial to consider the selection of noise level and maximum excess delay, which can give significantly different estimates of the decay factor [48]. In [47], a cluster power decay factor was estimated for each cluster and then an average process over all the cluster power decay factors has been applied to give a single cluster power decay factor. It has been seen that the cluster power decay factor for each cluster fluctuates in the indoor scenario, ranging from 30 dB/μs to 80 dB/μs, and a mean value 54 dB/μs is suggested [47]. The crucial problem with this method is that the estimated power decay factor for each cluster lacks sufficient statistics because some of the data may be missing [48] while the clusters vanish frequently.
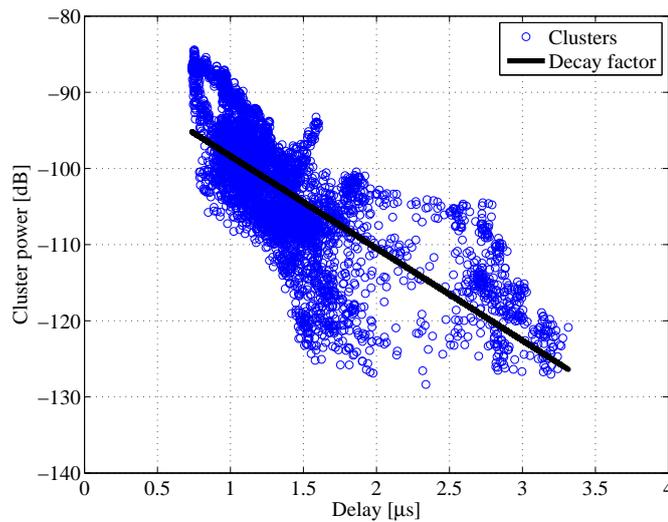
Figure 3.1: Cluster power decay factor. The scatter plot shows the cluster power vs. the cluster delay.

3.1.3   Single- and Multiple-bounce Clusters

Clusters are characterized as single- and multiple-bounce clusters depending on the number of interactions along the propagation path and are implemented with different geometry models. The ratio between them, the so called cluster selection factor, is another critical parameter for the COST 2100 channel model. To be able to differentiate between single- and multiple-bounce clusters, usually a physical interpretation of the propagation properties is needed, where the interaction properties of each path have to be observed. In [47], the cluster selection factor has been extracted for the physical clusters together with a measurement based ray launching tool. It has been suggested that the cluster selection factor could be set to zero in indoor NLOS scenarios. While for the indoor LOS scenarios, around 70% of the clusters are multiple-bounce clusters. It can be argued that in indoor scenarios, the BS and MS are usually surrounded with more scatterers, which leads to more multiple-bounce clusters. The number of interactions with physical objects for parameter based clusters in an outdoor scenario is studied in [31], where the geometry properties of the centroid of each cluster are used. It is initially checked whether a ray from the BS in the AOD direction of each cluster and a ray from the MS in the AOA direction of the same cluster can meet each other or not. If there is no valid

intersecting point between the two rays, a multiple-bounce cluster is assumed.
With a valid intersecting point, the total travel time is employed as an addi-
tional check. When the travel time corresponds to the geometrical distance for
a single interaction, a single-bounce cluster is determined. Around 90% and
80% multiple-bounce clusters has been observed for the LOS and NLOS sce-
narios, respectively. Later on, in [37], the single- and multiple-bounce clusters
are determined for the extracted physical clusters together with a measurement
ray launching tool, which is similar as the method in [47]. There it has been
found that physical scatterers can be single- and multiple-bounce clusters at
the same time [37], and 33% and 20% single-bounce clusters has been founded
for the considered sub-urban and urban scenarios, respectively.

3.1.4   Cluster Spreads

Cluster spreads, including delay spread, AOA spread, and AOD spread, deter-
mine the size of the cluster, and thus have significant effects on the channel
properties. The spreads are usually defined as [5]:

$$DS_{\mathrm{c}} = \sqrt{\frac{\sum_{i}^{N_{\mathrm{c}}} P_i (\tau_i - \bar{\tau})^2}{\sum_{i}^{N_{\mathrm{c}}} P_i}}, \tag{3.4}$$

$$AS_{\mathrm{c}} = \sqrt{\frac{\sum_{i}^{N_{\mathrm{c}}} P_i (\mathrm{angle}(\exp(j(\varphi_i - \bar{\varphi}))))^2}{\sum_{i}^{N_{\mathrm{c}}} P_i}} \tag{3.5}$$

where DS_{c} is cluster delay spread, AS_{c} is cluster angular spread, N_{c} is number
of MPCs associated each cluster and j is the imaginary unit. Furthermore, P_i
is the power for the ith MPC, $\bar{\varphi}$ and $\bar{\tau}$ are power weighted means calculated as

$$\bar{\tau} = \frac{1}{\sum_{i}^{N_{\mathrm{c}}} P_i} \sum_{i}^{N_{\mathrm{c}}} P_i \tau_i \tag{3.6}$$

$$\bar{\varphi} = \mathrm{angle}(\sum_{i}^{N_{\mathrm{c}}} P_i \exp(j\varphi_i)), \tag{3.7}$$

where τ_i is the delay and φ_i is the AOD/AOA of the ith MPC. The cluster
spreads are studied in [31, 37, 47]. A delay spread of 2 ns is suggested in [47],
and angular spreads are relatively small, specifically, less than 5 degrees in the

indoor scenario. It has been pointed out that the angular spread at the MS side is larger than the one at BS side and angular spreads in elevation do not have significant differences compared to the ones in azimuth. In [31], the delay spread is in the scale of μs, where a large measurement area is included in the considered outdoor scenario. There, only the azimuth angles are analyzed due to the limitation of the measurement setup. The angular spreads show reasonably small values as well and thus can limit the size of the clusters. Also in [37], investigations of the cluster spread properties are carried out for both sub-urban and urban scenarios, where smaller cluster spreads were observed compared to the values in [31]. This observation is mainly due to the consideration of physical clusters, which have tight connections to the physical environment.

3.1.5   Cluster Cross-polarization Discrimination

The cluster cross-polarization discrimination (XPD) characterizes the power ratio between one polarization to another. To be able to characterize the XPD for a cluster, XPD ratios of each MPC belonging to the cluster are determined as [5]:

$$\mathrm{XPD}_\mathrm{V} = \frac{P_\mathrm{VV}}{P_\mathrm{VH}} \tag{3.8}$$

and

$$\mathrm{XPD}_\mathrm{H} = \frac{P_\mathrm{HH}}{P_\mathrm{HV}}. \tag{3.9}$$

The MPC XPD ratios are modeled as log-normally distributed over different clusters, with a mean μ_XPD and standard deviation σ_XPD for a cluster. Thus the cluster cross-polarizations are also log-normally distributed, with parameters $(m_{\mu_\mathrm{XPD}}, S_{\mu_\mathrm{XPD}})$ and $(m_{\sigma_\mathrm{XPD}}, S_{\sigma_\mathrm{XPD}})$. In [37, 47], XPD parameters for indoor and outdoor scenarios have been discussed. In the indoor scenario, XPD_V and XPD_H are very close to each other and the mean and standard deviation being approximately 15 dB and 10 dB. In the outdoor scenario, mean values around 4 dB and 6 dB are observed for XPD_V and XPD_H, together with standard deviation of approximately 4 dB and 3 dB. Note that, there is a lack of studies of the XPD parameters in some common scenarios, which is mainly due to the fact that the full polarization measurements for such scenarios are not available.

3.1.6   Other Parameters

Usually, clusters are classified as local clusters and far clusters. Local clusters are located around MS or BS, and far clusters are located away from both the BS and MS sides. The number of local clusters and far clusters is extracted

separately. Usually, a local cluster is observed at the MS side in an outdoor
scenario [31].

The number of far clusters, in general, is between 2 to 6 [31,37,47]. Regarding the number of MPCs in each cluster, in [47] the DMCs have been removed and less than 5 MPCs in each cluster is observed. The number of MPCs in each cluster in [31] is around 25 that is mainly due to the fact that the DMCs are taken into account and are treated as specular MPCs.

There is also a group of additional parameters when the LOS condition is fulfilled, which are so called LOS parameters. In [31,47], LOS parameters, including LOS power, visibility region of LOS, LOS cutoff distance, are extracted for the considered scenarios.

There are also some other important parameters in the COST 2100 channel model, e.g., transition region, cross-correlation between large scale parameters. Further detailed values are summarized in [31,37,47] for different scenarios.

3.2   Validation of the COST 2100 Channel Model

Validation is one of the most important steps for channel model development, where the extracted parameters from measurements are applied for channel simulations. Then the validation is performed by comparing the stochastic properties of the simulated channel and the measured channel that the parameters are drawn from.

The first attempt at validating the COST 2100 channel model has been carried out by Haneda et al. in [49] for an indoor scenario, where the angular and delay spreads were chosen due to their influences on the system metric, e.g., eigenvalue and capacity distribution. It was found that an acceptable level of agreement in terms of the angular and delay spreads is observed between practical channel simulations and measurements. Also the work has stated that the COST 2100 channel model is a reliable tool for realistic and dynamic MIMO channel simulations. Recently, in [31], the validation of the COST 2100 channel model has been performed with respect to delay spreads, spatial correlations, singular value distributions and antenna correlations in a sub-urban scenario, where it was concluded that the model has potential for modeling 300 MHz channels in outdoor environments. Although some modifications are needed for the distribution of cluster delay spreads and the size of the cluster visibility regions. Later, the validation of the delay spread and singular value distribution for an urban scenario was carried out in [37] together with the extracted parameters based on the concept of physical clusters. It was concluded that the physical clusters give better control of the delay spread; also, the COST 2100 channel model can well represent the channel characteristics with respect

to system capacity.

3.3   Multi-link Extension of the COST 2100 Channel Model

Multi-link channel modeling is one of the major challenges for the next generation wireless channel models, where multiple BSs and MSs are introduced. In general, the key idea of multi-link channel modeling is to capture the cross-correlation properties between the considered links. Often, it is assumed that there is no correlation between two links if the two links are far away from each other [50]. However, it has been shown that cross-correlation of large scale parameters between multi-links indeed exists and also has significant effects on the channel properties [51–53] and the system level performance [54, 55]. Thus, modeling of large scale parameters between multi-links can give valuable improvements for multi-link system models. From a geometry-based modeling point of view, the cross-correlation between multi-links is due to the shared interacting scatterers along the propagation paths. Therefore, common clusters which describe the commonality between multi-links are introduced in [56], and are used in the COST 2100 multi-link channel model [57].

To have a thorough understanding of the multi-link channel modeling, cross-correlation of large scale parameters between links is discussed in the following. Later, common clusters, which describe the cross-correlation properties in the COST 2100 channel model, are discussed in detail as well.

3.3.1   Cross-correlation of large scale Parameters between Links

The large scale parameters, i.e., shadow fading, delay spread, AOA spread and AOD spread, are usually modeled as a function related to the distance in each link, such as an exponential decay with increasing distances [58]. When it comes to multi-link configurations, the distance and angle separations between multiple links become significantly important. The discussions on cross-correlation properties of large scale parameters are given in the following.

Shadow Fading

Shadow fading describes the long-term variations in the received power, which is usually assumed to be the results of shadowing by objects in the propagation paths [59, 60]. The averaged received power level in dB domain is usually

modeled as

$$P(d) = P_0 - n \log_{10}(\frac{d}{d_0}) + SF(d),$$ (3.10)

where d is the distance, n is the path-loss exponent and P_0 is a reference value
at the distance d_0. To extract the shadow fading component, a linear regression
in dB domain of the received power versus distance is required.

Gudmundson has proposed that the auto-correlation of shadow fading in
a single link follows an exponential decay as the distance is increasing [58],
and many measurements have been carried out to validate this model [60–63].
When it comes to multiple links, cross-correlation of the shadow fading has
also shown a significant importance for the system level performance. The
early studies focused on the effects of the angle of arrival difference (AAD) at
the mobile sites. A correlation coefficient of around 0.7 was obtained from the
measurements when the AAD is small [64]. In addition, a table look up model
of correlation coefficients versus AAD was proposed in [64]. Later on, Mawria
proposed a simple formula for the approximation of the link correlation versus
the angle θ in degree seen from the MS to the two considered BSs [62]:

$$\rho(\theta) = 0.9 - \frac{|\theta|}{200}$$ (3.11)

This simple approximation has not taken the positions of the BSs and MSs into
account. In [65], a position dependent correlation function is introduced and a
new simple model was proposed including position dependence.

After that, Perahia et al. in [66] has shown that the cross-correlation of
shadow fading between BSs ranged from -0.34 to +0.43 for different environ-
ments and angular separations. Jaldén et al. in [51] has studied the influence of
the distance between two BSs. It has been emphasized that the shadow fading
has a high correlation when the two BSs are close. Recently, in [52], another
measurement has been analyzed, where it was found that the cross-correlation
between links can have a large value even when the two links are far away from
each other. The shadow fading has shown negative cross-correlation between
different links when the MS is moving towards one BS but away from the other
BS. On the other hand, when MS is moving towards both BSs, the shadow
fading is positively correlated.

Note that most of the work mentioned above is for outdoor-to-outdoor sce-
narios. Therefore, Jaldén et al. in [67] have put lots of efforts into investigating
the indoor multi-link cross-correlation properties. There, a correlation coeffi-
cient of 0.5 was found for shadow fading in some measurement areas. Also, the
correlation coefficient versus distance was studied in [67], where, generally, the
cross-correlation increase with the decreasing distance. It has to be noted that,
besides some specific measurement areas, the shadow fading cross-correlation is

generally low in most of the indoor scenarios, and can thus be treated as independent of each other. More recently, indoor multi-link correlation with respect to shadow fading has been investigated in [53], where a strong correlation was found even when the terminals are highly separated.

Delay Spread

Delay spread is the normalized second-order central moment of the power delay profile, and it shows the frequency selectivity of the channel. In [61], it has been suggested that the delay spread can be modeled as a log-normal distribution and the auto-correlation in each link can be modeled as an exponential decay with increasing distance. Nonetheless, due to the lack of multi-link measurements, the cross-correlation of the delay spread has rarely been studied. In [63], it was found that higher BS antenna arrays resulted in higher cross-correlation with respect to delay spread. Recently, in [52], a study of the cross-correlation of delay spread between multiple BSs in an outdoor scenario was carried out. It was seen that when the MS is moving towards one BS but away from the other BS, the delay spread had negative cross-correlation. On the other hand, when MS was moving towards both BSs, the delay spread was positively correlated, which is a similar trend as for the cross-correlation of shadow fading between links.

Angular Spread

The angular spread reflects the geometry of the local scatterers, so it is generally different at the transmitter and receiver sides. The cross-correlation of angular spread is related to the probability of the shared local scatterers between links. However, the study for angular spread concentrates on single link auto-correlation, e.g., in [61]. It has been seen that the angular spread has an exponential decay, negatively correlated with the shadow fading in each link. Recently, the cross-correlation of angular spread between multiple links has been analyzed in [51], where the BS and MS angular spread is introduced. However, both the two angular spreads show low cross-correlation, so that the authors suggest giving a lower priority to include cross-correlation of angular spreads into future wireless channel models.

3.3.2   Common Clusters

There have been a few studies on the cross-correlation between links, and results have shown that cross-correlation is an important property that should be well described in channel models. The COST 2100 channel model is a geometry-based stochastic channel model using the concept of clusters. To be compatible
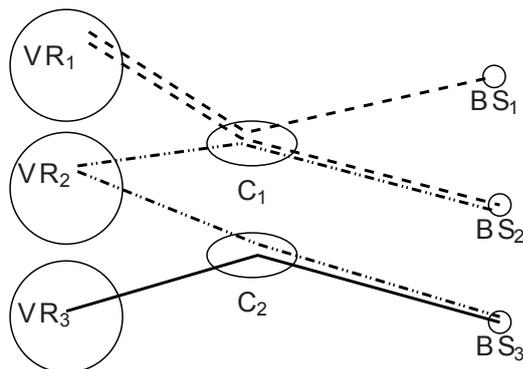
Figure 3.2: An example of common clusters and their link connections with 3 static BSs and 3 VRs. The lines describe different link connections from each VR. From [5].

with the single-link COST 2100 channel model, the concept of common clusters is introduced [5] to describe the multi-link cross-correlation.

The concept of common clusters is introduced based on the assumption that the propagation paths between two links have a shared part and can interact with the same physical scatterers [68,69]. The shared common physical scatterers are modeled as common clusters. Same as for the conventional clusters, visibility regions have to be assigned to common clusters, but now the visibility region has to be extended to maintain both the single-link and multiple-link channel model characteristics. Two concepts for the common clusters have been adopted in the COST 2100 channel model. One is BS-common clusters and the other is visibility region (VR) groups [5]. Fig. 3.2 gives an example of common clusters, where BS1 and BS2 have C1 as a BS-common cluster, VR2 and VR3 are in a VR group due to the common seen cluster C2. To give a thorough understanding of common clusters, common cluster identification, significance of common cluster, and validity of common cluster are discussed in the following.

3.3.3 Common Cluster Identification

Generally, common clusters behave like conventional clusters, and at the same time they represent the shared part of the radio channel between multiple links. The common cluster ratio, defined as the ratio between the common clusters and total clusters, is introduced to characterize the amount of common clusters in the COST 2100 channel model. In order to observe the common cluster ra-

tio, we first have to identify the physical propagation paths for multi-links and associate them to clusters. An indoor measurement based ray launching tool has been used by Poutanen et al. in [70]. It plots the propagation paths on top of the map and shows the interactions between the MPCs and scatterers. Therefore, the shared physical scatterers between multiple links were determined based on two conditions. One is the distance between scatterers and the links. The other is the angular separation of scatterers seen from the MS sides. The thresholds for these values differ from environment to environment. In the indoor scenario, a distance of 5 meters and an angle of 45 degrees is suggested [56]. Similarly, common clusters for an outdoor scenario are analyzed together with an outdoor measurement based ray launching tool, where more complicated propagation phenomena are considered, e.g., diffraction, scattering [43]. For outdoor scenarios, to be able to determine a common cluster, a ratio between the distance of two cluster centroids and the larger distance from the two cluster centroids to the BS is introduced in [71]. A value of 0.2 for the ratio is recommended.

3.3.4   Significance of Common Clusters

The significance of common clusters was first introduced to characterize the ratio between the power carried by common and all the clusters by Poutanen et al. [56]. It was defined there as

$$S_{\text{common}}^i = \frac{P_{\text{common}}^i}{P_{\text{tot}}^i},$$ (3.12)

where P_{common}^i is the power for a common cluster in link i, and Pi_{tot} is the sum of powers of link i. It was found that the total significance varied from 40% to 95% in indoor scenarios [56], while it varied from 10% to 40% for outdoor scenarios [71]. For the indoor analysis, the dominant power is usually coming from nearby walls or objects; in those cases, the common cluster becomes more significant. However, in the outdoor scenarios, where users typically are more separated, other scatterers can provide equivalent or even higher power and diminish the dominance of the common clusters.

3.3.5   Validation of Common Clusters

A validation of multi-link modeling using common clusters has been carried out for an indoor scenario with respect to sum rate capacity [56]. It has been seen that the common cluster can well predict the capacity if their significance is high, specifically, around 85%. For the clusters with low significance, such as 10%, the model usually underestimates the link capacity due to the effects

of the locations of the clusters. Later, a validation of the COST 2100 model
for multi-link modeling using common clusters in an outdoor scenario was car-
ried out in [71]. It was shown that as the distance between links increases,
the number of common clusters as well as the multi-link cross-correlation de-
creases [71]. This property is also validated with the COST 2100 channel model
multi-link simulations. Results show that the simulated cross-correlation de-
creases in a similar manner as the common cluster ratios. The simulated and
measured sum-rate capacities show a decreasing tendency as the link distance
decreases. This indicates that the common clusters can capture the multi-link
characteristics and reflect the system level performance.

3.4   Summary

The COST 2100 channel model is a well-established MIMO channel model,
which supports both single- and multi-link MIMO simulations. Parametriza-
tion and validation are essential steps in order to ensure that the channel model
can simulate the desired properties of the real channel. Researches have been
performed to provide complete sets of parameters for some scenarios, e.g., in-
door office, outdoor urban scenario. The multi-link extension of the COST
2100 channel model is implemented so that it can be used for next genera-
tion wireless system evaluations. However, analysis with respect to multi-link
properties needs more efforts, especially for multi-link outdoor scenarios, where
there is a lack of multi-link measurements.

Chapter 4

Phase Based Positioning

Radio based positioning and tracking is a research area that has attracted a lot of attention during the past decades. The technology is often seen as a key enabler for new cellular services. Global Navigation Satellite System (GNSS) such as the Global Positioning Systems (GPS) is one of the most frequently used positioning system that provides location information around the globe through a constellation of at least 24 satellites [72, 73]. However, the accuracy of GPS is usually limited and it can lose its performance in shadowed areas, such as in indoor environments, and beside tall buildings. Therefore, there are extensive research efforts targeting developing new positioning techniques that can work with high accuracy in shadowed scenarios. Recent proposals for indoor positioning systems usually rely on distinct signaling methods and/or perform joint processing of radio channel parameters, e.g., received signal strength indication (RSSI), AOA, time of arrival (TOA) and time difference of arrival (TDOA), which brings new opportunities to achieve a centimeter-level positioning accuracy. One of the proposals is to introduce ultra-wideband (UWB) indoor positioning systems [74], where the TOA can be estimated more precisely using the ultra wide bandwidth. However, when considering current cellular systems that have a bandwidth around 40 MHz, achieving the same accuracy as the UWB systems represents a real challenge.

In this chapter, a positioning technique, called phase based positioning, using phase information of MPCs of the radio channels and aiming for positioning accuracy down to centimeters using a standard cellular system bandwidth, is discussed.

4.1 Examples of Phase Based Positioning Systems

Phase disciplined positioning has been already used in several positioning systems. For example, there is a phase based positioning approach aiming for a centimeter-level of accuracy using GNSS, which is called Real Time Kinematics (RTK) [75]. The RTK technique is based on the measurements of the phase of the signal carrier. The carrier phase measurement, which is a measure of the range between a satellite and a GPS receiver expressed in units of cycles of the carrier frequency, can be made with very high precision. Note that, the whole number of cycles between the satellite and the GPS receiver is not measurable, which is also a major challenge of carrier phase based positioning and is referred to the integer ambiguity. For RTK technique, two receivers, simultaneously observing the same satellites, are required to measure carrier phase differences and solve the integer ambiguity [75]. There is also another technique used for phase based Radio Frequency Identification (RFID) positioning. At the early stage of RFID positioning, RSSI is used [76], e.g., LANDMARC [77]. Later on, phase information from the RFID tags has attracted attention [78], where the phase of the dominant LOS component from the RFID tags is tracked and used for positioning or tracking purposes. It has improved location estimation performance even in complicated propagation environment [79]. However, it cannot be applied in cellular systems since the LOS condition is not always fulfilled.

In this thesis, we use the scatterers, where the MPCs are stemming from, as virtual, but coherent, transmitters located at unknown positions for positioning and tracking purposes. By tracking the phase of MPCs, relative distances between the user and virtual transmitters are observed. The user position can then be estimated and tracked using a structure-of-motion approach.

4.2 Positioning Based on the Phases of MPCs

MPCs in wireless channels carry distance information in terms of delay and phase. As long as the multi-paths propagate in the space, the delay and phase are varying. Delay estimates, which are used in UWB systems to estimates distances, are usually limited by the bandwidth and SNR. However, the phases of MPCs, which also carries the distance information, are not dependent on the bandwidth. Therefore, it becomes attractive to utilize phase information in cellular systems for distance estimation and thus positioning.

In the following sections, positioning using phase information of MPCs from radio channels is discussed. First, a synthetic multi-input single-output (MISO)
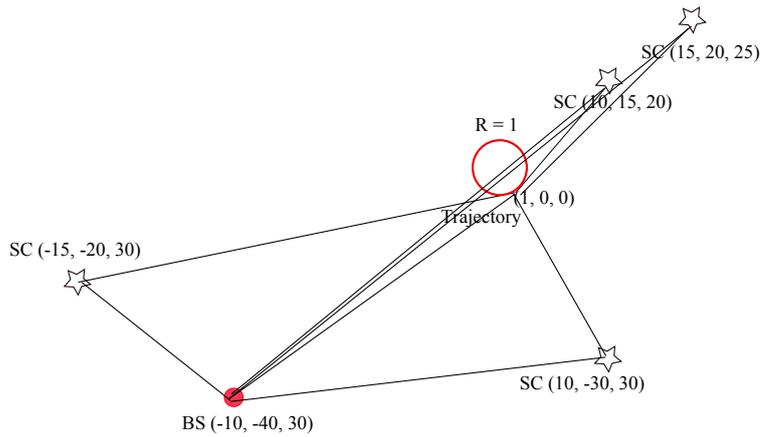
Figure 4.1: Synthetic scenario.

channel with a large number of antenna elements is utilized to get an initial idea of the phase based positioning technique. Secondly, an experimental investigation is also conducted to show the performance of phase based positioning in a real environment.

4.2.1 Synthetic Study

As positioning using phase information of MPCs is quite a new topic, a synthetic data study is first carried out to give a brief discussion of the state-of-the-art of phase based positioning.

Synthetic Channel

First, a synthetic scenario with four geometrically separated scatterers contributing to the synthetic channel responses is assumed. Further, the link from the MS to the BS is assumed to have only a single reflection and be with NLOS condition. Thus the four scatterers give rise to four MPCs, each of which is initialized with a different magnitude and phase. The MS, equipped with a single omni-directional antenna, is moving along a circle with a radius of 1 meter. An antenna array with 128 ports at the BS side is utilized to reconstruct channel responses. Together with a measured antenna array radiation pattern, 128-by-1 channel responses under an SNR of 20 dB are generated as the MS moves. In total, 721 channel samples are collected over the circular trajectory. The geometrical relations of the scatterers, MS and BS are shown in Fig. 4.1

together with their coordinates. Note that, the figure is a 2D projection of the 3D environment.

Phase Estimation and Tracking

Parameter estimation or tracking from multi-dimensional MIMO channel sounding measurements is a well-established research topic. In traditional approaches, parameters, e.g., delay, AOA, AOD, phase, and magnitude, describing specular propagation paths, are estimated in a per-snapshot fashion. Since channel snapshots are assumed to be i.i.d., algorithms such as SAGE [44], RIMAX [80], are applied for the single snapshots, and later a tracking algorithm is applied to obtain the time variant behavior [39]. Recently, based on a state-space model, a few methods have been developed that can perform direct sequential estimation and tracking of propagation parameters at the same time, e.g., extended Kalman filter (EKF) [45] and particle filter [81]. These methods bring numerous advantages to the propagation path parameter tracking. For example, the parameters describing the individual paths are automatically paired and tracked across measurements, the estimation error is reduced due to the filtering, and the computational complexity is also reduced. Among the different state-space estimation and tracking algorithms, the EKF algorithm is the one with low complexity but good enough parameter estimation and tracking performance. Thus it is used in this thesis.

There are two main steps in the EKF approach. First, the EKF gives a prediction of the parameters based on the previous state and the dynamic model. Secondly, the filter corrects the estimation errors based on the recently observed samples. The generalized channel samples are the input of the EKF approach. It then estimates and tracks the parameters of the MPCs based on the designed dynamic model and the observations.

The phases of the 4 synthetic MPCs are estimated and tracked, see Fig. 4.2a. It can be noted that the tracked phases show a sinusoidal variation pattern, which is perfectly corresponding to the circular trajectory. From the propagation properties, we know that a 2π change in phase is corresponding to a movement of a wavelength. Therefore, with the tracked phases, we can simply get the relative distance changes of each MPC over the channel samples as follows:

$$\Delta d = \frac{\Delta \phi}{2\pi} \lambda, \tag{4.1}$$

where λ is the wavelength and $\Delta \phi$ is the phase differences between the current position and a reference position.
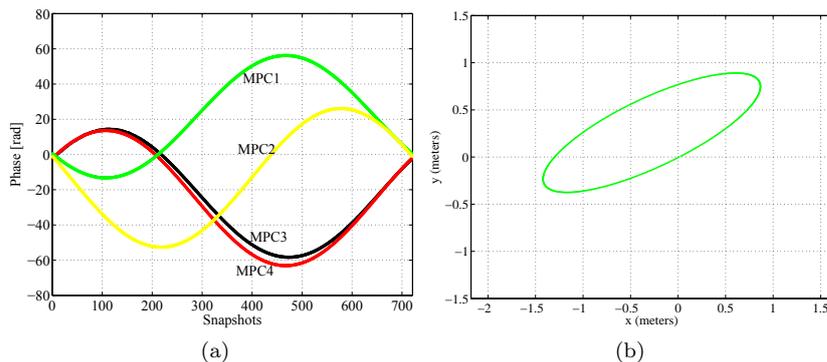
Figure 4.2: (a) Tracked phases of the MPCS from the synthetic channel. (b) Tracking performance of the synthetic circular movement.

Structure-of-Motion Positioning

There are a few approaches that use the wireless channel characteristics to estimate the position of a transmitter or a receiver [82]. Usually, for a single source network, in order to estimate the required positions, the floor-plan of the environments is needed [83]. The authors in [84] suggested an anchor free positioning method for a system with a single transmitter and a single moving receiver. There, the scatterers, where the MPCs are stemming from and being planar surfaces or a smaller reflecting objects, give rise to virtual transmitters at positions s_j. Given measurements of distance estimates $d_{i,j}$, the positioning problem becomes determining both transmitter positions s_j and receiver positions r_i such that

$$d_{i,j} = |r_i - s_j| \tag{4.2}$$

is fulfilled. A factorization-based approach followed by a non-linear least squares optimization is suggested and a good positioning performance has been achieved using this method in [84].

As stated before, the relative distance can be estimated from phase information, so that the 4 MPCs give rise to 4 different distance equations as in (4.2). By solving these equations, the relative movement can be observed. Fig 4.2b shows the positioning results of the predefined circular movement by using the positioning method in [84]. It can be seen that the relative moving pattern can be perfectly located. The only concern here is that the movement is in 2D, but the plane of movement is different from the plane of virtual transmitters.
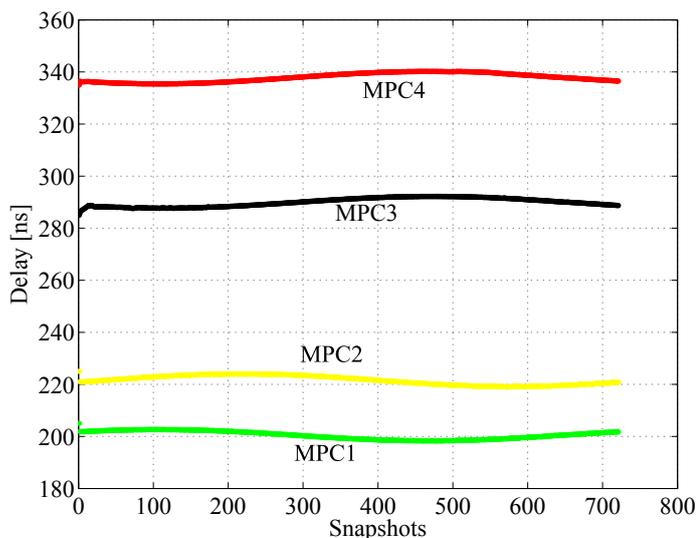
Figure 4.3: Tracking delays of MPCs for the synthetic scenario.

Therefore the positioning algorithm gives a projection of the circle, which in terms gives us an ellipse. The projection issues will be analyzed more in detail in future work.

4.2.2   Discussions on Absolute Positioning

Phase based positioning shows good tracking capability of relative movements, but not the absolute position. To observe the absolute position, a known reference position is needed. To be able to estimate a reference position, accurate delay estimations are needed for each MPC. Fig. 4.3 shows the corresponding delay tracking of the 4 MPCs. It can be seen that at the beginning, the delay traces jitter frequently and later start to converge to more stable traces. If the reference position is chosen as the first position, and is directly estimated from the beginning of the delay traces, it will give a bias. Phase, which also contains information about distance thus delay, can serve to give a better estimation of the reference position. The relation between the phase and delay is defined as:

$$\tau_k = \tau_{ref} + \frac{1}{2\pi f_c} \sum_{i=1}^{k} \Delta\phi(i), \tag{4.3}$$

Table 4.1: Reference delay estimates from EKF and from averaging after removing phase contributions.

Number of MPC	True delay [ns]	EKF delay [ns]	Ave. delay[ns]
MPC 1	200.2	205	201.7
MPC 2	219.1	225	220.8
MPC 3	286.5	285	288.7
MPC 4	333.8	335	336.4

where τ_{ref} is the reference delay, and f_c is the center frequency. By removing the phase contribution, we can estimate τ_{ref} over the entire data set. By averaging the τ_0 over the entire 721 samples, better statistics can be obtained. Table 4.1 shows the comparison between the true delay, EKF estimated delay and the averaged delay with subtracting the phase contributions. It can be noted that the averaging processes can help to obtain more accurate delay estimates. However, if the delay estimates of the EKF algorithm are not good enough, the averaged results cannot remove the estimation bias, e.g., for MPC4. With the delay estimates of the reference position and the geometry of the virtual transmitters, the absolute position of the movements can be observed. However, it has to be mentioned that bias in delay estimates of reference position can lead to significant offsets in the estimation of reference position, which is a part of the major challenge of the phase based positioning technique.

4.2.3   Experimental Study

An experimental investigation for positioning using phase information of MPCs of measured radio channels is carried out in this section to give a deep understanding of the phase based positioning technique in a real environment.

First, channel measurements were conducted in a large open hall, using the LUND RUSK channel sounder, with a 40 MHz bandwidth at a center frequency of 2.6 GHz (161 frequency points) [85]. An omni-directional antenna was used to represent a single-antenna user. The antenna was mounted on a tripod with wheels 1.7 m above the ground. During the measurements, the antenna was moved manually along a circle with radius 0.6 m. To minimize the influence of the persons moving the station, they were staying very close to the floor such that body reflections are kept to a minimum, and ground reflections were not blocked. The cylindrical Rx array was mounted on top of the received sounder
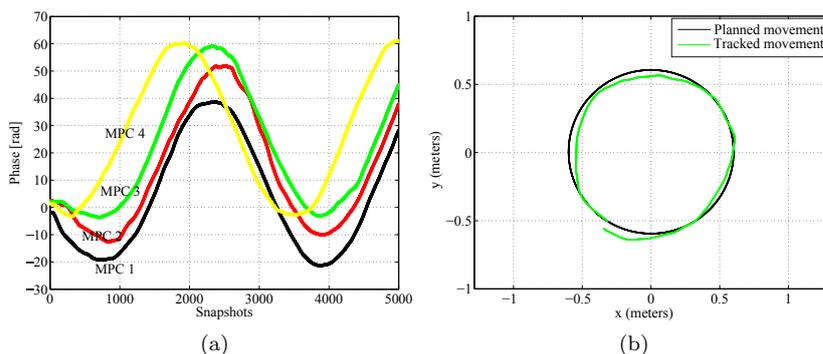
Figure 4.4: (a) Tracked phases for a number of MPCs. (b) Positioning performance.

and acted as a static BS. The center of the cylindrical array was about 2.07 m above the ground. Over the moving trajectory, 5000 channel samples were collected and each sample is with a size of 128-by-161. The measurement is conducted under line-of-sight (LOS) condition.

Similar to what has been done in the synthetic case, the EKF algorithm was used for phase estimation and tracking. Phases are expected to have sinusoidal shapes due to the circular movement. Fig. 4.4a shows clear sinusoids for the tracked phases of a number of MPCs estimated from the measured channel. It can be noted the four MPCs start with different phases and the maximum phase differences is around 62 rad. This maximum phase difference corresponds to a maximum distance change of approximately 1.2 m, which is the diameter of the circle.

The resulting estimated user movements are shown in Fig. 4.4b [85]. It can be noted that the offset between the planned movements and tracked positions in maximum is 5 centimeters, and more than 50% locations are within 2 centimeter offset. The standard deviation of the errors is approximately 4.0 cm. Phase based positioning shows promising results, where the estimation and tracking of the phase information of MPCs give valuable contributions to the positioning accuracy.

Chapter 5

Contributions, Conclusions and Future Work

This thesis focuses on geometry-based channel modeling with an emphasis on multi-link modeling. It includes an extensive analysis of clusters, and implementation of analytical algorithms and tools, e.g., joint clustering and tracking algorithm, and ray launching tool. The thesis has made contributions to parameterization, validation and implementation of the COST 2100 channel model as well as its multi-link extension. In addition, this thesis introduces a new phase based positioning technique, which can provide positioning accuracy down to centimeters.

Contributions of the six included papers, are summarized and presented in detail in this chapter. A brief overview is given together with my contributions to the research field. Also, conclusions of this thesis are presented. Finally, a discussion of future work in the related field wraps up this chapter.

5.1 Contributions

5.1.1 Paper I: A Ray Launching Tool for Channel Analysis

Cluster is a key concept in existing MIMO channel models, such as the COST 2100 model. Parameter based clusters have been well studied and extensively used. Nonetheless, how parameter based clusters relate to the physical environment is not clearly understood yet. In order to understand the relation between parameter based clusters and the physical environment, and to get a

more accurate channel characterization, a measurement based ray launching tool is implemented, where measurements can provide additional information such as AOA, AOD, delay and power of MPCs and help identifying the most likely propagation paths and reduce the complexity of calculations.

In this work, we have developed a measurement based ray launching tool for outdoor scenarios, using a 3D map including buildings and trees. Ray reflection, diffraction, and scattering are described in the tool. We analyzed outdoor 300 MHz measurement data by using the ray launching tool. Based on the delay and angular properties of the MPCs from measurements, the ray launching tool provides a meaningful interpretation of propagation paths and shows the interacting physical scatterers along the propagation paths. We notice that when the MS moves, some physical scatterers continue to contribute to the channel response while others disappear and sometimes also later re-appear. These physical interacting processes well interpret the properties of clusters with respect to cluster lifetime and common clusters.

I am the main author of the paper. I implemented the channel analysis tool as an extension of a previous master thesis work, which the other two authors were involved in. I carried out data analysis together with the implemented tool and summarized the results. The other authors contributed to the discussion, gave insights to the models and contributed to the paper writing.

5.1.2 Paper II: Channel Modeling Basis: Cluster Analysis

Conventionally, a cluster is defined as a group of MPCs that have similar delay, AOA and AOD. This is commonly referred to as a parameter based cluster. There are however two kinds of clusters: 1) parameter based clusters are characterized with the parameters of MPCs; 2) physical clusters, which are determined based on the interaction properties with physical scatterers of MPCs. It is an open issue how the physical clusters relate the parameter based clusters and therefore we analyze this in more detail in this paper.

First, the parameter based clusters are investigated with the developed ray launching tool for the considered sub-urban and urban scenarios. It has been seen that single-bounce parameter based clusters can well be reflected in the physical environment, but this is not necessarily the case for multiple-bounce clusters, which have more complicated behavior. In this paper, a simple geographical clustering method is proposed and we observed the corresponding physical clusters and their properties. A physical cluster can be seen for a relatively long time. The frequent cluster deaths observed for the parameter based clusters are not observed for physical clusters, which hence have longer cluster visibility regions. Also, the physical clusters can be single- and multiple-bounce

clusters at the same time, which is not the case for parameter based clusters. To our best knowledge, no such comparison has been made before. Based on the definition of the physical clusters, we extract model parameters for the COST 2100 channel model for sub-urban and urban micro-cell scenarios. As such parameters are lacking in the literature, we also fill this gap of knowledge, which is a second important contribution of this paper. In addition, we also validate these parameters with the current COST 2100 channel model MAT-LAB implementation. The validation results show that the physical clusters give better control of delay spread and the singular value distribution. They also give good agreement between simulations and measurements.

This work is done together with Aalto University, where I was a guest for a week. I am the main author of the paper. I did the background studies, as well as the data processing. I implemented the used analysis tool and algorithm. Simulations, together with the related analysis, were performed by me. The second and third authors contributed to the measurements and data processing. The second author was involved in some of the data analysis. I wrote the majority of the paper, and the other three authors contributed to the discussions and gave valuable comments on the paper.

5.1.3 Paper III: Parameterization and Validation of the COST 2100 Channel Model

The COST 2100 channel model is a geometry-based stochastic channel model for MIMO simulations. The parameterization of this generic model from measurements is not yet complete and only a few environments have been analyzed. Furthermore, there is a lack of studies validating the COST 2100 channel model. This paper presents a parameterization and validation of the channel model for peer-to-peer communication in the 300 MHz band.

The main contributions of this paper are: Cluster parameters and cluster time-variant properties are obtained from the 300 MHz measurements by using a joint clustering and tracking algorithm. Parameterization of the channel model for single-link outdoor MIMO communication at 300 MHz is conducted. Validation of the channel model is performed for the considered scenario by comparing simulated and measured delay spreads, spatial correlations, singular value distributions and antenna correlations. Our findings suggest that the model has potential for modeling 300 MHz channels in outdoor environments, although some modifications are needed for the distribution of cluster delay spreads and the size of cluster visibility regions.

I am the main author of the paper. I did the background studies, implemented the algorithm for analysis, carried out simulations, analyzed the measurement and simulation data, and summarized the conclusions, while the

other authors contributed to the channel measurements, data processing, and some valuable discussions, e.g., methodologies, and mathematical insights.

5.1.4   Paper IV: Cross-correlation of Large Scale Parameters in Multi-link Channels

In order to make realistic wireless channel models, extensive measurements are required so that parameters for channel models can be extracted. Among these parameters, there are so called large scale parameters describing the main characteristics of the environment, such as shadow fading, angular spread and delay spread. There has been extensive studies focusing on large scale parameters, but only a few on cross-correlation properties of large scale parameters between multiple links due to the fact that there is a lack of multi-link measurements. Therefore, further analysis of multi-links properties is desirable.

In this paper, multi-site measurements with three BSs are analyzed where the three BSs are far away from each other. We first estimate the wide sense stationary (WSS) time by using the local scattering function. Together with a map of the measured environment, we defined WSS regions for further correlation property studies. The correlation properties of large scale parameters, e.g., shadow fading and delay spread, are investigated both for each link and between different links in an urban macro scenario based on small WSS subsets. We concluded that the cross-correlation of the large scale parameters between multiple links do exist, even when the two links are far away from each other, with high or low correlation coefficients. The shadow fading has been observed as negative cross-correlation between different links when the MS is moving towards one BS but away from the other BS. On the other hand, when MS is moving towards both BSs, the shadow fading is positively correlated. Similar behavior was observed for cross-correlations of delay spread. To our best knowledge, the observations are notable contributions for current channel model developing, such as WINNER II channel model, where the cross-correlation between two links for large scale parameters is modeled as zero.

I am the main author of the paper. I performed the analysis of the measurements which were carried out by the third author. I did the data processing, analyzed the measured data and summarized the conclusions. I wrote the paper mainly with the second author, who had the original idea of the work and gave valuable insights into the fundamental principle of the work.

5.1.5   Paper V: Virtual Multi-link Propagation Investigation

The COST 2100 channel model supports multi-link simulation by dropping multiple MSs and BSs in the simulation area. When multiple MSs/BSs are utilized, cross-correlations between links, so called inter-link correlations, can have significant effects on the system level performance. Hence, modeling of inter-link correlations is required. To be compatible with previous geometry-based stochastic channel models, common clusters are introduced in the COST 2100 channel model to model inter-link correlations. Recently, the indoor multi-link measurements have been analyzed and common clusters and their properties have been extracted. However, for the outdoor scenario, there is still a lack of analyses and investigations.

In this paper, it has been found that in a multi-link outdoor propagation scenario there are shared scatterers among different links, which reflects the physical existence of common clusters. The identification of common clusters in the measured outdoor scenario is discussed according to the shared scatterers and distances between the scatterers and MSs. We observe that, as the MS distance separation increases, the number of common clusters decreases and the inter-link correlation decreases as well. Multi-link MIMO simulations are also performed using the COST 2100 channel model with extracted common cluster parameters. It has been demonstrated that the common clusters can represent multi-link properties well with respect to inter-link correlations and sum rate capacity. This work makes an important contribution to the COST 2100 multi-link channel model implementation, where the outdoor common cluster ratios for different link distance separations are suggested.

I am the main author of the paper. I did the data processing, analyzed the measured data, and summarized the conclusions. The other author gave critical comments on the work and contributed to the paper writing.

5.1.6   Paper VI: Positioning Using Phase Information from MPCs

Radio based positioning has attracted a lot of attention in the research field during the past decades. GPS works well for most outdoor scenarios, but it can lose its performance in shadowed areas, such as inside buildings, or beside tall buildings. Therefore, indoor positioning with extraordinary accuracy grows as a crucial issue in the field.

In this paper, we proposed a positioning technique using phase information of MPCs from measured channels, so called phase based positioning. To our best knowledge, no such method has been presented before. First, indoor MISO

measurements have been conducted. In order to observe the phase changes of the MPCs, an extended Kalman filter has been implemented to identify and track the parameters of MPCs from the measured channel matrices. With the tracked phases of the MPCs, the corresponding relative propagation distances of each MPC are determined. Position estimates are obtained with a structure-of-motion approach to determine the relative movement. Circular movement has been tracked with root-mean-square error of 4.0 cm, using a bandwidth of 40 MHz. The results represent a significant improvement compared to current indoor positioning methods. The phase based positioning approach gives valuable and promising results for further work on indoor positioning.

I am the main author of the paper. I did the theoretical study and carried out the measurements together with colleagues. I partly contributed to the implementation of the used algorithm. I performed data processing, estimated parameters from the measured data, analyzed the estimation results and summarized the conclusions. The other authors contributed to the algorithms, which are used in the paper. The last author had the original idea of the work and was involved in all parts of the work.

5.2   Conclusions

During this thesis work, lots of efforts were devoted to implementing and extending one of the geometry-based channel models, the COST 2100 channel model, including providing parameters for the model, validating the model, investigating multi-link properties. After years of maintaining and implementing the COST 2100 channel model framework, now it has a complete parameter set for the outdoor single-link MIMO scenario. Also multi-link modeling parameters, i.e. common cluster ratio, are proposed in this thesis. In the meantime, tools and algorithms for fundamental channel modeling analysis have been implemented or extended by the author, like the outdoor measurement ray launching tool, which can be used for further multi-link channel characterizations; the joint clustering and tracking algorithm, which can be applied for general cluster identifications; and EKF algorithm, which highly improved the tracking performance by visualizing and tracking MPCs jointly. These tools and algorithms can cope with any additional measurements with a few setups and data processing. With these tools and algorithms, the basis of the COST 2100 channel model, clusters, is further investigated in detail in this thesis. The author found that physical clusters, which are scatterers or groups of scatterers, can improve modeling performance and can better reflect the multi-link channel characteristics than the parameter based clusters, which are grouped based on the parameter space of MPCs. In addition, in this thesis

we have presented some initial research of phase based positioning. Both the synthetic study and experimental investigations have shown promising results of the introduced phase based positioning technique.

5.3   Future Work

First of all, this thesis has presented extensive work on the COST 2100 channel model. The model has some limitations when controlling the delay spread in outdoor scenarios. In the model, the radii of clusters are modeled as a log-normal distribution which sometimes can give extremely large delay spreads. It has been suggested that a truncated log-normal distribution of the radii of clusters and has also verified with a considered outdoor scenario. More investigations can be carried out for this aspect to give a better description of the radii of clusters. Also this thesis has shown that the model for visibility regions cannot be well connected to the physical environment, where the distribution of visibility regions is recommended to be included in the model. To our best knowledge, there is a lack of investigations for such distribution. Looking at the implementation of the COST 2100 channel model, there are some aspects that can be improved. First of all, in the current model, the geometrical relation between the cluster centroid and the center of visibility region is characterized by a parameter that has not been thoroughly investigated. How to select this value and what are the impact on the channel model performance is still an open issue. DMCs have been well modeled in the COST 2100 channel model. Further work on extracting the DMCs and their related parameterization for the model are needed. More recently, the polarization modeling has been implemented. Related parameters exist for some scenarios but further validation of this implementation and parameters should be done in the future.

Secondly, as one of the most important features of the COST 2100 channel model, multi-link simulation still needs further work. Practically, it is difficult to perform multi-link measurements, especially for outdoor scenarios. Therefore, analysis for multi-link channel models is advantageous, including providing multi-link channel model parameters and validating the parameters etc. Here, as stated in this thesis, physical clusters have to be considered and more sophisticated physical clustering methods are needed as well.

Thirdly, as one of the most important contribution of this thesis, the measurement based ray launching tool has been used frequently in this thesis and also can be used for future channel characterization. The current ray launching tool visualizes MPCs based on the AOA, AOD and delay, where the power is not taken into account. Angles and delay can determine the most likely MPCs with a good enough accuracy, if together with a competent power model, visualized

paths can be made even more realistic. It is difficult to have power models for some propagation scenarios, e.g., diffraction across the edge of buildings, and scattering through vegetation. Therefore, more efforts are needed in order to give better power model for ray launching tool. In addition, during developing the ray launching tool, it has been noted that for outdoor scenarios, besides buildings and vegetation, lamps and street signs can be significant scatterers, which have not been included in the map for now. Therefore, 3D maps or floor plan with more detailed descriptions are needed.

Lastly, phase based positioning has been discussed in this thesis and has shown promising results. However, further analysis is required. First of all, the utilized EKF algorithm can usually track a smooth change but not a sharp variation, i.e., turning to the other direction at the corner. Therefore, the EKF algorithm needs to be strengthened to have capabilities to handle all realistic variations. Due to the multi-path environment, the positioning algorithm has to decide the best candidate paths. A random sample consensus (RANSAC) algorithm has been tried, which highly relies on the true positions. For now, the MPCs with good tracked phases are selected as the best candidates for positioning purpose. However, studies should be carried out to give a better understanding of selecting the best candidate paths for positioning. One of the most valuable advantages of the proposed positioning method in this thesis is that a 40 MHz bandwidth can still give accuracy comparable to ultra wide-band positioning. When a massive MIMO system is used, even with a single frequency, comparable level of positioning accuracy can be achieved. However, more investigations are needed in order to achieve this goal. Until now, we have shown a promising result for movement tracking. An initial position or any exact position is needed as a reference position for a precise localization. We have tried to estimate the first or the last absolute positions by using the tracked phases and delays, where it was found that the reference position is sensitive and highly dependent on the accuracy of the delay estimates. Hence, accurate delay estimation needs more efforts in the future. As this thesis presents preliminary work for this topic, only LOS measurements have been studied. NLOS scenarios, which are more common in real life, should also be studied.

References

[1] E. Dahlman , S. Parkvall, and J. Skold, *4G: LTE/LTE-Advanced for Mobile Broadband*, 1st ed., Oxford, U.K.: Academic Press, 2011.

[2] D. Chizhik et al., "Multiple-input multiple-output measurements and modelling in Manhattan," *IEEE Journal on Selected Areas in Communications*, vol. 21, no. 3, pp. 321-332, Apr. 2003.

[3] Commission of the European Communities, *COST 207: Digital land mobile radio communications*, Office for Official Publications of the European Communities, Luxembourg, 1989.

[4] IST-4-027756 WINNER II D1.1.2 V1.2. (2008). *WINNER II Channel Models*. [Online]. Available: http://www.ist-winner.org.

[5] R. Verdone and A. Zanella, "Radio channel modeling for 4G networks," in *Pervasive mobile and ambient wireless communications: COST Action 2100 (signals and communication technology)*, 1st ed., London: Springer, 2012, pp. 67-148.

[6] F. Rusek et al., "Scaling up MIMO: opportunities and challenges with very large arrays," *IEEE Signal Processing Magazine*, vol. 30, no. 1, pp. 40-60, Jan. 2013.

[7] T. L. Marzetta, "Noncooperative cellular wireless with unlimited numbers of base station antennas," *IEEE Transactions on Wireless Communications*, vol. 9, no. 11, pp. 3590–3600, Nov. 2010.

[8] A. F. Molisch, *Wireless Communications*, 2nd ed., Chichester, West Sussex, U.K.: Wiley, 2005.

[9] R. S. Thomä, D. Hampicke, A. Richter, G. Sommerkorn and U. Trautwein, "MIMO vector channel sounder measurement for smart antenna system

evaluation," *European Transactions on Telecommunications*, vol. 12, no. 5, pp. 427-438, Sept./Oct. 2001.

[10] RUSK channel sounder – Measurement principle. [Online]. Available: http://www.channelsounder.de/ruskchannelsounder.html.

[11] C. A. Balanis, *Advanced Engineering Electromagnetics*. New York: Wiley, 1989.

[12] D. Shiu, G. J. Foschini, M. J. Gans, and J. M. Kahn, "Fading correlation and its effect on the capacity of multielement antenna systems," *IEEE Transactions on Communications*, vol. 48, no. 3, pp. 502-513, Mar. 2000.

[13] M. F. Catedra, J. Perez, F. Saez de Adana, and O. Gutierrez, "Efficient ray-tracing techniques for three-dimensional analyses of propagation in mobile communications: application to picocell and microcell scenarios," *IEEE Antennas and Propagation Magazine*, vol. 40, no. 2, pp. 15-28, Apr. 1998.

[14] N. Costa, and S. Haykin, *Multiple-input multiple-output channel models: theory and practice*, 1st ed., New Jersey: John Wiley & Sons, 2010.

[15] W. Weichselberger, M. Herdin, H. Özcelik, and E. Bonek, "A stochastic MIMO channel model with joint correlation at both link ends," *IEEE Transactions on Wireless Communications*, vol. 5, no. 1, pp. 90-100, Jan. 2006.

[16] E. Bonek, H. Özcelik, M. Herdin, W. Weichselberger, and J. Wallace, "Deficiencies of a popular stochastic MIMO radio channel model," in *Proc. International Symposium on Wireless Personal Multimedia Communications*, Yokosuka, Japan, 2003.

[17] L. Wood, and W. S. Hodgkiss, "Understanding the Weichselberger model: A detailed investigation," in *Proc. IEEE Military Communications Conference*, San Diego, CA, 2008, pp. 1-7.

[18] N. Costa and S. Haykin, "A novel wideband MIMO channel model and experimental validation," *IEEE Transactions on Antennas and Propagation*, vol. 56, no. 2, pp. 550–562, Feb. 2008.

[19] A. Saleh and R. Valenzuela, "A statistical model for indoor multipath propagation," *IEEE Journal on Selected Areas in Communications*, vol. 5, no. 2, pp. 128–137, Feb. 1987.

[20] L. M. Correia, "The COST 273 MIMO channel model," in *Mobile broadband multimedia networks*, 1st ed., Oxford, U.K.: Academic Press, 2006, pp. 364-384.

[21] C. Oestges, "Multi-link propagation modeling for beyond next generation wireless," in *Proc. Loughborough Antennas and Propagation Conference 2011 (LAPC 2011)*, Loughborough, UK, 2011, pp. 1-8.

[22] J. Han and M. Kamber, *Data Mining, concepts, and techniques*, 1st ed., San Francisco: Morgan Kaufmann Publishers, 2001.

[23] A. F. Molisch, H. Asplund, R. Heddergott, M. Steinbauer, and T. Zwick, "The COST 259 directional channel model – I. overview and methodology," *IEEE Transactions on Wireless Communications*, vol. 5, no. 12, pp. 3421–3433, Dec. 2006.

[24] H. Asplund, A. A. Glazunov, A. F. Molisch, K. I. Pedersen, and M. Steinbauer, "The COST 259 directional channel model – II. macrocells," *IEEE Transactions on Wireless Communications*, vol. 5, no. 12, pp. 3434–3450, Dec. 2006.

[25] J. Laurila et al., "Wideband 3-D measurements of mobile radio channel in urban environment," *IEEE Transactions on Antennas and Propagation*, vol. 50, no.2, pp. 233-243, Feb. 2002.

[26] S. Wyne et al., "A cluster-based analysis of outdoor-to-indoor office MIMO measurements at 5.2 GHz," in *Proc. IEEE Vehicular Technology Conference 2006 Fall*, Montreal, Canada, 2006, pp. 1-5.

[27] J. Salo, J. Salmi, N. Czink, and P. Vainikainen, "Automatic clustering of nonstationary MIMO channel parameter estimates," in *Proc. Information and Communications Technologies (ICT'05)*, Cape Town, South Africa, 2005.

[28] N. Czink et al., "Cluster characteristics in a MIMO indoor propagation environment," *IEEE Transactions on Wireless Communications*, vol. 6, no. 4, pp. 1465–1475, Apr. 2007.

[29] N. Czink et al. "A framework for automatic clustering of parametric MIMO channel data including path powers," in *Proc. IEEE Vehicular Technology Conference 2006 Fall*, Montreal, Canada, 2006, pp. 1-5.

[30] N. Czink, "The random-cluster model- a stochastic MIMO channel model for broadband wireless communication systems of the 3rd generation and beyond," Ph.D. dissertation, Technische Universität Wien, Vienna, Austria, Dec. 2007.

[31] M. Zhu, G. Eriksson and F. Tufvesson, "The COST 2100 channel model: parameterization and validation based on outdoor MIMO measurements at 300 MHz," *IEEE Transactions on Wireless Communications*, vol. 12, no. 2, pp. 888-897, Feb. 2013.

[32] H. Hofstetter, A. F. Molisch, and N. Czink, "A twin-cluster MIMO channel model," in *Proc. 1st European Conference on Antennas and Propagation (EuCAP) 2006*, Nice, France, 2006, pp. 1-8.

[33] N. Czink and C. Oestges, "The COST 273 channel model: three kinds of clusters," in *Proc. International Symposium on Spread Spectrum Techniques Applications*, Bologna, Italy, 2008, pp 282-286.

[34] N. Czink et al., "Cluster parameters for time-variant MIMO channel models," in *Proc. 2nd European Conference on Antennas and Propagation*, Edinburgh, U.K., 2007, pp.1-8.

[35] G. Eriksson, F. Tufvesson, and A. F. Molisch, "Propagation channel characteristics for peer-to-peer multiple antenna systems at 300 MHz," in *Proc. IEEE Global Communications Conference*, San Francisco, USA, 2006, pp. 1-6.

[36] J. Poutanen, K. Haneda, J. Salmi, V.-M. Kolmonen, and P. Vainikainen, "Modeling the evolution of number of clusters in indoor environments," in *Proc. 4th European Conference on Antennas and Propagation*, Barcelona, Spain, 2010, pp. 1-5.

[37] M. Zhu, K. Haneda, V.-M. Kolmonen and F. Tufvesson, "Parameter based clusters, physical clusters and cluster based channel modeling in sub-urban and urban scenarios," submitted to *IEEE transactions on Wireless Communications*, Jun. 2014.

[38] N. Czink, C. Mecklenbräuker, and G. D. Galdo, "A novel automatic cluster tracking algorithm,", in *Proc. IEEE International Symposium on Personal, Indoor and Mobile Radio Communications (PIMRC 06)*, Helsinki, Finland, 2006, pp. 1-5.

[39] N. Czink et al., "Tracking time-variant cluster parameters in MIMO channel measurements," in *Proc. China Communications Conference*, Shanghai, China, 2007, pp. 1147-1151.

[40] S. M. Kay, *Fundamentals of Statistical Signal Processing, Estimation Theory*, New Jersey: Prentice Hall, 1993.

[41] J. Poutanen et al., "Development of measurement-based ray tracer for multi-link double directional propagation parameters," in *Proc. 3rd European Conference on Antennas and Propagation*, Berlin, Germany, 2009, pp. 2622–2626.

[42] E. Olsson, "Analysis of radio wave propagation using 3D-maps and MIMO measurements", Msc. Thesis, Department of Electroscience, Lund University, Lund, June, 2004.

[43] M. Zhu, A. Singh, and F. Tufvesson, "Measurement based ray launching for analysis of outdoor propagation," in *Proc. 6th European Conference on Antennas and Propagation*, Prague, Czech Republic, 2012, pp. 3332-3336.

[44] B. H. Fleury, M. Tschudin, R. Heddergott, D. Dahlhaus, and K. Ingeman Pedersen, "Channel parameter estimation in mobile radio environments using the SAGE algorithm," *IEEE Journal on Selected Areas in Communications*, vol. 17, no. 3, pp. 434-450, Mar. 1999.

[45] J. Salmi, A. Richter, and V. Koivunen, "Detection and tracking of MIMO propagation path parameters using state-space approach" *IEEE Transactions on Signal Processing*, vol. 57, no. 4, pp. 1538-1550, Apr. 2009.

[46] J. Salmi, A. Richter, M. Enescu, P. Vainikainen, and V. Koivunen, "Propagation parameter tracking using variable state dimension Kalman Filter," in *Proc. IEEE Vehicular Technology Conference 2006 Spring*, vol. 6, Melbourne, Australia, 2006, pp. 2757-2761.

[47] J. Poutanen, K. Haneda, V.-M. Kolmonen, J. Salmi, and P. Vainikainen, "Parameterization of the COST2100 MIMO indoor channel model," in *Proc. 5th European Conference on Antennas and Propagation*, Rome, Italy, 2011, pp. 3606-3610.

[48] C. Gustafson, K. Haneda, S. Wyne, and F. Tufvesson, "On mm-wave multi-path clustering and channel modeling", *IEEE Transactions on Antennas and Propagation*, vol. 62, no. 3, pp. 1445-1455, Mar. 2014.

[49] K. Haneda, J. Poutanen, C. Oestges, F. Tufvesson, and P. Vainikainen, "Comparison of delay and angular spreads between channel measurements and the COST2100 channel model," in *Proc. Loughborough Antennas and Propagation Conference*, Loughborough, UK, 2010, pp. 477-480 .

[50] D. S. Baum et al., IST-WINNER D5.4. (2005). *Final report on link and system level channel models.* [Online]. Available: http://www.ist-winner.org.

[51] N. Jaldén, P. Zetterberg, B. Ottersten, and L. Garcia, "Inter- and intra site correlations of large-scale parameters from macrocellular measurements at 1800 MHz," *EURASIP Journal on Wireless Communications and Networking*, vol. 2007, article ID 25757, Jul. 2007.

[52] M. Zhu, F. Tufvesson, and J. Medbo, "Correlation properties of large scale parameters for 2.66 GHz multi-site macro cell measurements," in *Proc. IEEE 73rd Vehicular Technology Conference*, Budapest, Hungary, 2011, pp. 1-5.

[53] J. Poutanen, K. Haneda, J. Salmi, V.-M. Kolmonen, and P. Vainikainen, "Analysis of correlated shadow fading in dual-link indoor radio wave propagation," *IEEE Antennas and Wireless Propagation Letters*, vol. 8, pp. 1190–1193, Nov. 2009.

[54] R. Fraile, J. Gozalvez, O. Lazaro, J. Monserrat, and N. Cardona, "Effect of a two dimensional shadowing model on system level performance evaluation," in *COST 273* TD(04)190, 2004.

[55] R. Fraile, J. Monserrat, N. Cardona, and J. Nasreddine, "Impact of shadowing modelling on TD-CDMA system-level simulations," in *Proc. International Symposium on Wireless Communication Systems (ISWCS)*, Valencia, Spain, 2006, pp. 535-539.

[56] J. Poutanen et al., "Multi-link MIMO channel modeling using geometry-based approach," *IEEE Transactions on Antennas Propagation*, vol. 60, no. 2, pp. 587-596, Feb. 2012.

[57] L. Liu et al., "The COST 2100 MIMO channel model," *IEEE Wireless Communications*, vol. 19, no. 6, pp. 92-99, Dec. 2012.

[58] M. Gudmundson, "Correlation model for shadow fading in mobile radio system," *IEEE Electronics Letters*, vol. 27, no. 23, pp. 2145-2146, Nov. 1991.

[59] H. W. Arnold, D. C. Cox, and R. R. Murray, "Macroscopic diversity performance measured in the 800-MHz portable radio communications environment," *IEEE Transactions on Antennas and Propagation*, vol. 32, no. 2, pp. 277–281, Feb. 1988.

[60] J. Weitzen and T. J. Lowe, "Measurement of angular and distance correlation properties of log-normal shadowing at 1900 MHz and its application to design of PCS systems," *IEEE Transactions on Vehicular Technology*, vol. 51, no. 2, pp. 265-273, Mar. 2002.

[61] A. Algans, K. Pedersen, and P. Morgensen, "Experimental analysis of the joint properties of azimuth spread, delay spread and shadowing fading," *IEEE Journal on Selected Areas in Communications*, vol. 20, no. 3, pp. 523-531, Apr. 2002.

[62] A. Mawira, "Models for the spatial correlation functions of the (log-) normal component of the variability of the VHF/UHF field strength in urban environment," in *Proc. International Symposium on Personal, Indoor and Mobile Radio Communications (PIMRC 92)*, Boston, USA, 1992, pp. 436–440.

[63] A. Hong et al. "Experimental evaluation of correlation properties of large scale parameters in indoor pico-cell environments," in *Proc. International Symposium on Wireless Communication Systems (ISWCS)*, Valencia, Spain, 2006, pp. 55-59.

[64] V. Graziano, "Propagation correlation at 900MHz," *IEEE Transactions on Vehicular Technology*, vol. 27, no.4, Nov. 1978.

[65] T. Klingenbrunn and P. Mogensen, "Modeling cross-correlated shadowing in network simulations," in *Proc. IEEE Vehicular Technology Conference*, Amsterdam, Netherlands, 1999, pp. 1407-1411.

[66] E. Perahia, D. C. Cox, and S. Ho, "Shadow fading cross correlation between basestations," in *Proc. IEEE Vehicular Technology Conference*, Rhodes, Greece, 2001, pp. 313-317.

[67] N. Jaldén, P. Zetterberg, B. Ottersten, A. Hong and R. Thoma, "Correlation properties of large scale fading based on indoor measurements," in *Proc. IEEE Wireless Communications and Networking Conference (WCNC)*, Kowloon, Hongkong, 2007, pp. 1894-1899,.

[68] V.-M. Kolmonen et al., "Measurement-based evaluation of interlink correlation for indoor multi-user MIMO channels," *IEEE Antennas and Wireless Propagation Letters*, vol. 9, pp. 311–314, Apr. 2010.

[69] J. Poutanen et al., "Significance of common scatterers in multi-link indoor radio wave propagation," in *Proc. 4th European Conference on Antennas and Propagation*, Barcelona, Spain, 2010, pp. 1–5.

[70] J. Poutanen, K. Haneda, J. Salmi, V.-M. Kolmonen, and P. Vainikainen, "Analysis of radio wave scattering processes for indoor MIMO channel models," in *Proc. IEEE International Symposium on Personal, Indoor and Mobile Radio Communications (PIMRC 09)*, Tokyo, Japan, 2009, pp. 102-106.

[71] M. Zhu, and F. Tufvesson, "Virtual multi-link propagation investigation of an outdoor scenario at 300 MHz," in *Proc. 7th European Conference on Antennas and Propagation*, Gothenburg, Sweden, 2013, pp. 687-691.

[72] J. J. Spilker, Jr., "GPS signal structure and performance characteristics," *Journal of the Institute of Navigation*, vol. 25, no. 2, pp. 121–146, Summer 1978.

[73] L. Kaplan, "Global node selection for localization in a distributed sensor network," *IEEE Transactions on Aerospace and Electronic Systems*, vol. 42, no. 1, pp. 113–135, Jan. 2006.

[74] S. Gezici et al., "Localization via ultra-wideband radios: a look at positioning aspects for future sensor networks," *IEEE Signal Processing Magazine*, vol. 22, no. 4, pp. 70–84, Jul. 2005.

[75] Real-Time Kinematic surveying training Guide, part number 33142-40, Revision D, Sep. 2003, [Online]. Available: http://gpstraining.com/downloads/MANUALS-QUICK%20GUIDES/RTKTrainingRevD.pdf.

[76] J. Zhou, and J. Shi, "RFID localization algorithms and applications—a review," *Journal of Intelligent Manufacturing*, vol. 20, no. 6, Dec. 2009, pp. 695-707

[77] C. Li, et al., "Mobile healthcare service system using RFID," in *Proc. IEEE International Conference on Networking, Sensing and Control*, vol. 2, 2004, pp. 1014–1019.

[78] P. V. Nikitin et al., "Phase based spatial identification of UHF RFID tags," in *Proc. IEEE RFID Conference*, Orlando, FL, Apr. 2010, pp. 102-109.

[79] X. Li, Y. Zhang and M. Amin, "Multifrequency-based range estimation of RFID tags," in *Proc. IEEE RFID Conference*, Orlando, FL, Apr. 2009, pp. 147-154.

[80] A. Richter, "Estimation of radio channel parameters: Models and algorithms," Ph.D. dissertation, Technischen Universität Ilmenau, Ilmenau, Germany, May 2005 [Online]. Available: www.db-thueringen.de

[81] X. Yin et al., "Tracking of time-variant radio propagation paths using particle filtering," in *Proc. IEEE International Conference on Communications (ICC'08)*, Beijing, China, 2008, pp. 920–924.

[82] P. Meissner, D. Arnitz, T. Gigl, and K. Witrisal, "Analysis of an indoor UWB channel for multipath-aided localization," in *Proc. IEEE International Conference on Ultra-Wideband*, Bologna, Italy, 2011, pp. 565–569.

[83] P. Meissner, C. Steiner, and K. Witrisal, "UWB positioning with virtual anchors and floor plan information," in *Proc. 7th Workshop on Positioning Navigation and Communication (WPNC)*, Dresden, Germany, 2010, pp. 150–156.

[84] Y. Kuang, K. Åström, and F. Tufvesson, "Single antenna anchor-free UWB positioning based on multipath propagation," in *Proc. IEEE International Conference on Communications (ICC'13)*, Budapest, Hungary, 2013, pp. 5814-5818.

[85] M. Zhu, J. Vieira, Y. Kuang, A. F. Molisch and F. Tufvesson, "Tracking and positioning using phase information of multi-path components from measured radio channels," to be submitted to *IEEE Wireless Communications Letters*.

Part II

Included Papers

Paper I

Measurement Based Ray Launching for Analysis of Outdoor Propagation

Clustering is a key concept of existing MIMO channel models, such as the COST 2100 model. Parameter based clustering has been studied for a while, but how parameter based clusters relate to the physical environment is not well known yet. A measurement based ray launching tool is developed and used for studying clustering and its relation to physical scatterers. By using estimated angles and delays of multi-path components as input to the ray launching tool, the physical scatterers along the propagation paths are visualized. After the physical scatterers are grouped, we notice that when the receiver moves, some physical scatterers continue to contribute to the channel response while others disappear and sometimes also later re-appear as represented by the cluster life time and common clusters in the COST 2100 model. Our measurement based ray launching tool shows significant advantages for further channel analysis and modeling.

1   Introduction

Ray launching and ray tracing are attractive tools for wireless propagation investigations since they can provide predictions of propagation characteristics with high accuracy. Varieties of ray launching and tracing algorithms have been developed [1][2], generally based on models of the same propagation mechanisms such as reflection, diffraction and transmission. In order to make even better channel characterization, a combination of channel measurement results and ray launching can give valuable insights. Measurement can provide additional information such as angle of arrival (AOA), angle of departure (AOD), delay and power of multi-path components (MPCs), which helps identifying the most likely propagation paths and reduces the complexity of calculations.

An indoor scenario is analyzed with a simple measurement based ray launching tool by Poutanen *et al.* in [3]. New concepts for multi-user MIMO channel modeling and analysis such as common clusters [4], single/multiple interactions with the environment have been studied with such a ray launching tool. The indoor investigation in [4] shows the advantage and necessity of a ray launching tool for multi-user channel modeling.

The objective of this work has been to develop a new ray launching tool for outdoor scenarios based on channel measurement results and three dimensional (3D) maps. With this ray launching tool we are aiming to visualize the most likely propagation paths according to the measured information. The visualized geometrical propagation paths can then be used for further channel analysis, such as clustering, finding common clusters and identifying interaction processes and so on. It should be noted that our purpose is not to provide a tool competing with sophisticated ray tracing tools in performance and accuracy but rather, to help interpreting and analyzing measurement results.

The paper is organized as follows. The modeling assumptions are studied in Section II. Section III explains the main approach of the ray launching tool. The development platform and parameter choice are discussed in Section IV. Ray launching results are shown and analyzed in Section V. Section VI gives a short conclusion of this work.

2   Modeling Assumptions

To visualize propagation paths, good models of objects in the environment are required. For outdoor scenarios, the most important objects are buildings and vegetation, which directly influence direction and power of propagation paths. Vehicles, lamp posts and street signs can also be of interest, but they are generally not available in commercial 3D maps, and are therefore excluded
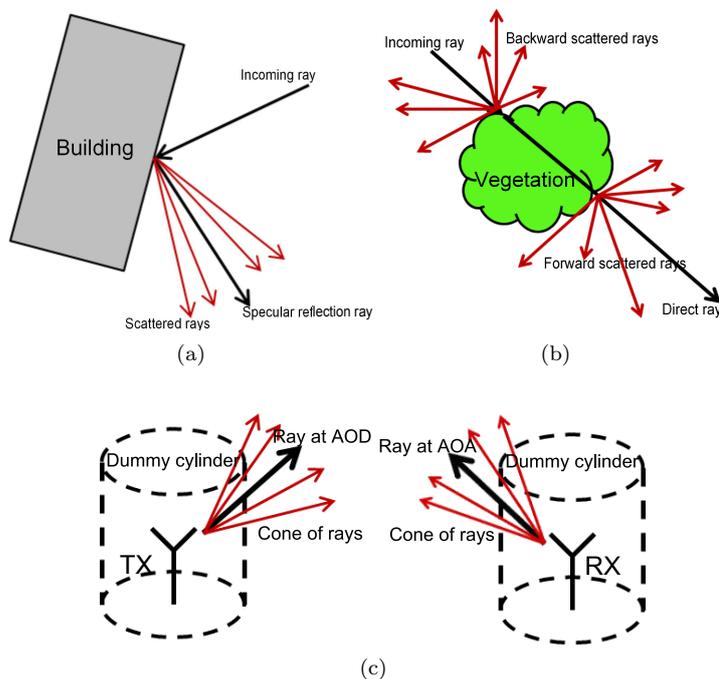
Figure 1: Object Models in 2-D projection: (a). Building reflection model, (b). Vegetation area scattering model, (c). Transmitter and receiver models.

in this paper.

2.1 Building Model

Building models are usually defined by reflection, transmission and diffraction properties [1]. The transmission through buildings is usually not considered for outdoor scenarios. The walls of buildings are often modeled as flat surfaces, however, real buildings are in general not totally flat. For example, in [5] a building model including windows has been discussed. Only one specular reflection is not enough to describe the building reflection process in general. Therefore a cone of scattered rays is launched around the specular reflection ray to represent rough wall reflections in our tool, see Fig. 1a. These scattered rays are generated by rotating the specular reflection ray in angles.

There are many models describing the diffraction around the edges or cor-

ners of buildings, such as Bullington's model, Epstein-Petersen model and so on [6]. To reduce the complexity of the building model, in our ray launching tool, rays are launched from both sides, and diffraction is only considered when rays from two sides can be matched though diffraction. Both single edge diffraction and diffraction from two parallel edges are taken into account.

2.2   Vegetation Model

Existing vegetation models generally focus on describing attenuation through a vegetation area. For example, in the ITU-R model [7], an attenuation factor based on frequency and distance is derived. Some research has been also carried out to give more advance vegetation models for ray-based propagation prediction tools. In [8], an expression for incoherent scattered field when rays are coming out from the vegetation areas is derived. However, these models do not fulfill the requirements in our ray launching tool design, since they usually only consider attenuation and forward scattering processes caused by the vegetation area. No modeling of the backward scattered rays from the vegetation area is given, and the vegetation scattering processes are not fully described .

In our tool, a slightly modified vegetation model is used, see Fig. 1b. The vegetation area is described by its size and shape as well as its height. When an incoming ray has an intersection point with an edge of the vegetation area, backward scattered rays with different azimuth and elevation angles are generated at this intersection point. At the same time, the incoming ray continues straight ahead until it reaches the other edge of the vegetation area. There, at the second intersection point, additional forward scattered rays are launched. Again, those scattered rays have varying azimuth and elevation angles around the direct ray. We try to cover the sphere around the vegetation area since the scattering of the vegetation area is quite complicated. It should be noted that this is a very simplified vegetation model, but good enough to fulfill its purpose here.

2.3   Transmitter and receiver model

The transmitter (TX) and receiver (RX) are represented by their orientation and location. In the 3D map, they are only single points, and dummy cylinders are introduced and centered at the coordinates of the TX and RX. The cylinder has 1 meters radius and a height of 2.8 meter above the ground. The rays passing through the cylinders do not change any properties and directions. The purpose of the dummy cylinder is to "capture" incoming rays in the matching process described below. To account for measurement and positioning inaccuracies, rays from TX and RX are launched in a cone centered
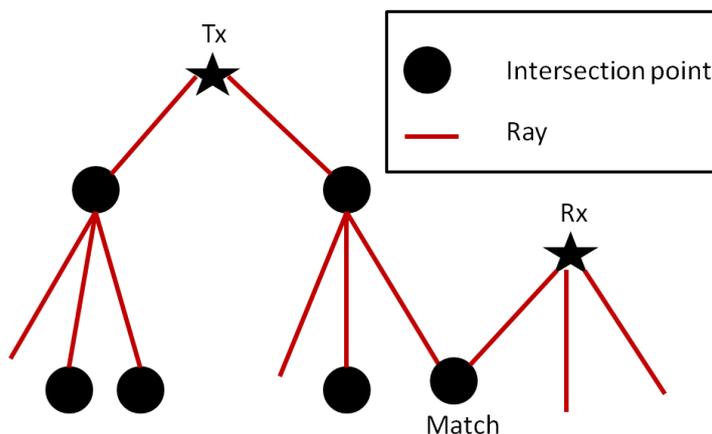
Figure 2: Structure of rays and intersection points.

around the measured AOA/AOD. Since it is a 3D ray launching tool, rays are also launched with slightly varying elevation angles, see Fig. 1c.

3   Measurement Based Ray Launching Approach

Two important concepts are used for the measurement based ray launching tool: intersection points and rays launched from these intersection points, see Fig. 2. The intersection points are where rays intersect with objects. Rays are launched at the intersection point according to the specific propagation mechanisms and they are characterized by their coordinates, propagation direction, power, traveling distance and the next intersection point. Rays, objects and intersection points are all processed in 3D.

Based on these two concepts, ray launching processes are implemented from both TX and RX sides to increase accuracy and efficiency, see Fig. 3. First, two points at TX and RX coordinates, respectively, are created. Dummy cylinders are placed around these two points respectively and cones of rays from these two points are launched according to the measured AOA/AOD as described in Sec. 2.3. Secondly, the tool processes all rays launched from the TX and RX points. For each ray, if there is an object at the propagation path, a next intersection point is determined. Otherwise, this ray continues propagating until it reaches the maximum traveling distance defined by the measured delay, including some extra margin (10%). The dummy cylinders around TX/RX are also taken into account and the corresponding intersection
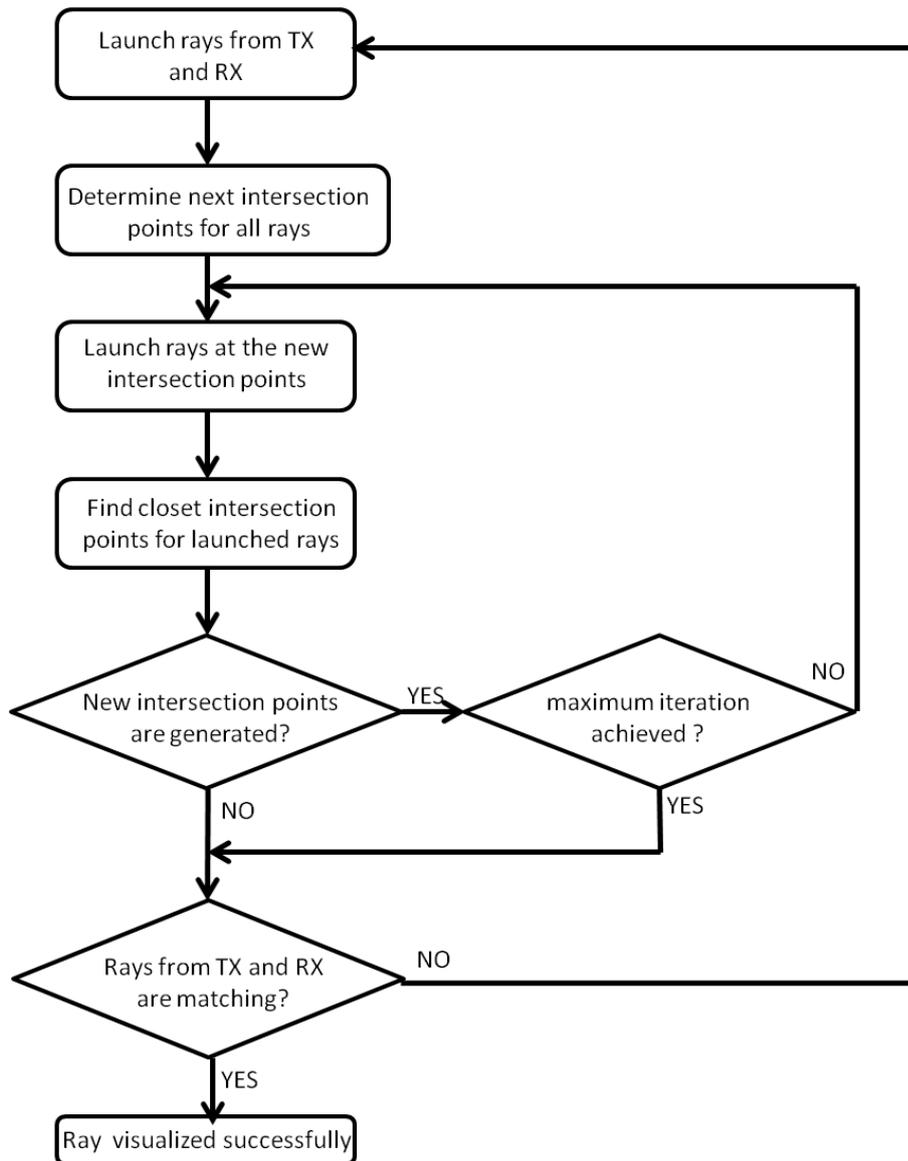
Figure 3: Float chart of the ray launching tool.

points are called dummy intersection points. Different objects change the propagation properties according to the building and vegetation models described above. New intersection points are determined until all the rays are processed. The tool continues launching new rays from these new intersection points and determining next intersection points again. It keeps generating rays and intersection points until either the number of reflection or scattering processes for the rays exceeds a certain limit or the traveling distances of rays are larger than the maximum traveling distance.

There is one important consideration when rays travel a long distance without any intersection points. Over a long distance, even a little angle inaccuracy at TX or RX side can lead to a large distance offset, which might lead to missed intersection points. To account for this, ray splitting is implemented, where a dummy intersection point is added at the position of ray splitting. Once the traveled distance of a ray exceeds a predefined ray splitting distance, a new cone of rays is released from this dummy point, centered around the propagation direction.

The last step of the algorithm is to check if rays launched from the TX and RX can be matched or not. Since rays are launched from two sides, they can only be matched at intersection points corresponding to physical objects or the dummy cylinders around TX/RX. Two parameters are checked: the measured delay for a certain MPC and the intersection angles of rays. In future versions, power will likely also be checked. The total traveling time from TX to RX has to be close to the measured delay.

$$|(D_{\text{TX}} + D_{\text{RX}})/c - \tau_{\text{MPC}}| < 0.1 * \tau_{\text{MPC}} \tag{1}$$

where D_{TX} is the distance from the TX to the matching point, D_{RX} is the distance from the RX to the matching point, τ_{MPC} is the delay for this particular MPC (from the measurement) and c is the speed of light. Similarly rays from TX and RX have to meet in a valid angle at the dummy cylinders. For example, the LOS ray departing from the TX should reach the RX with an angle matching the AOA of this MPC. After the matching processes there might be more than one candidate path for one particular measured MPC, the one who has shortest delay difference compared to the measured value is chosen as the final visualized propagation path.

Three matching scenarios are considered in this tool. 1) Matching at buildings. Reflection and diffraction are both investigated for the matching process at buildings. Rays can match through reflection when their intersection points with a building are on the same side and close to each other. Diffraction is more complicated, not only single edge diffraction but also multiple diffraction is considered. Rays can match when they are close to the same edge of a building or they intersect with two parallel edges. 2) For the matching at
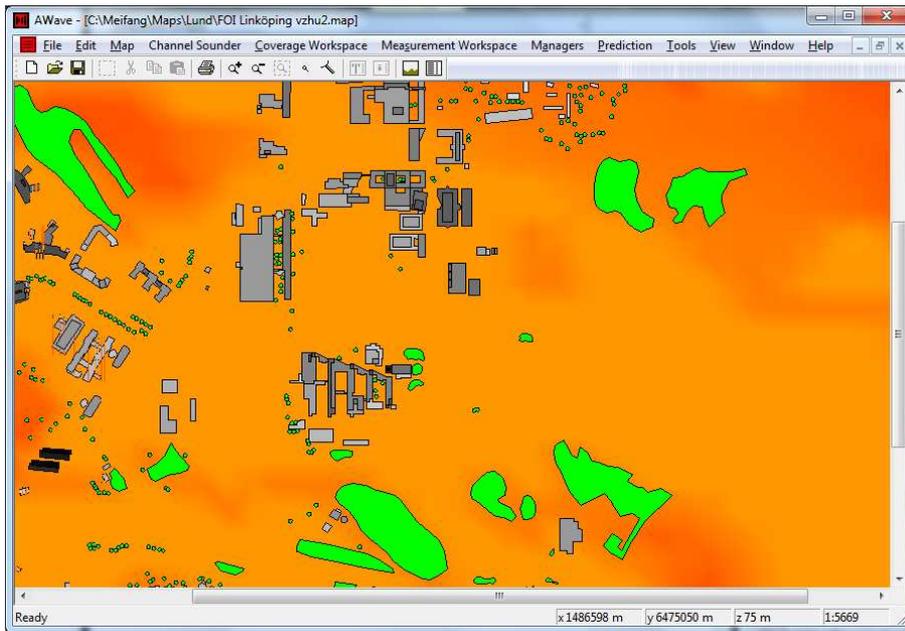
Figure 4: C++ application window showing the imported map.

a vegetation area, simple rules are applied. Rays can be matched when they intersect with the same vegetation area and the distance between the two intersection points is within the capture range. 3) Matching can occur when rays intersect with the cylinder around the TX or RX. As mentioned in previous paragraph, the angles are also checked here.

4   Development Platform and Parameters Setup

The ray launching tool is developed based on the C++ application built by E. Olsson [9] and A. Stranne. This application provides a graphical user interface (GUI), see Fig. 4, and we can easily import a 3D map. The map is shown by its 2D projection, elevation information is represented by color. The measurement results can also be handily imported into this application. With proper parameter setup, we are able to visualize the propagation path and intersection points on the map.

As we discussed in previous two sections, parameters such as number of scattered rays, width of the cone for ray launching and so on need to be ini-

Table 1: Parameters used.

Number of iterations from each side	3
Capture range [m]	10
Reflection coefficient	3
Path-loss exponent	4
Number of launched rays in Azimuth	4*2
Resolution of launched rays in Azimuth [deg]	2.0
Number of launched rays in Elevation	10*2
Resolution of launched rays in Elevation [deg]	2.0
Number of rays for ray splitting	3*2
Resolution for ray splitting [deg]	1.0
Number of scattered rays for vegetation	20
Resolution of scattered rays for vegetation [deg]	18
Number of reflected rays at buildings	4*2
Resolution of reflected rays at buildings [deg]	2.0
Maximum distance before ray splitting [m]	200
Maximum mismatch of angle [deg]	10
Maximum delay offset (of τ_{MPC})	10%

tialized. Those are given in the initialization window and the ray launching parameters can be changed according to user requirements. The parameters are listed in Table 1, the chosen values are set according to our analysis of measurements in [10], which are also used for the further analysis in next section. From the parameters, we can see the cone around the launched ray in azimuth direction is formed by 8 rays with 2.0 degree difference, so in total the width of launched cone is 14.0 degrees. Our measurement is in an outdoor scenario, which has lots of large buildings and vegetation areas. The capture range is set to 10 meter. The reflection coefficient is chosen as 3 [1]. The maximum distance controls the distance when rays start to split, 200 meter is chosen in this measured scenario. We also allow 10 degree mismatch when rays meet at the dummy cylinders. The maximum offset in delay is set to 10% for a valid match.
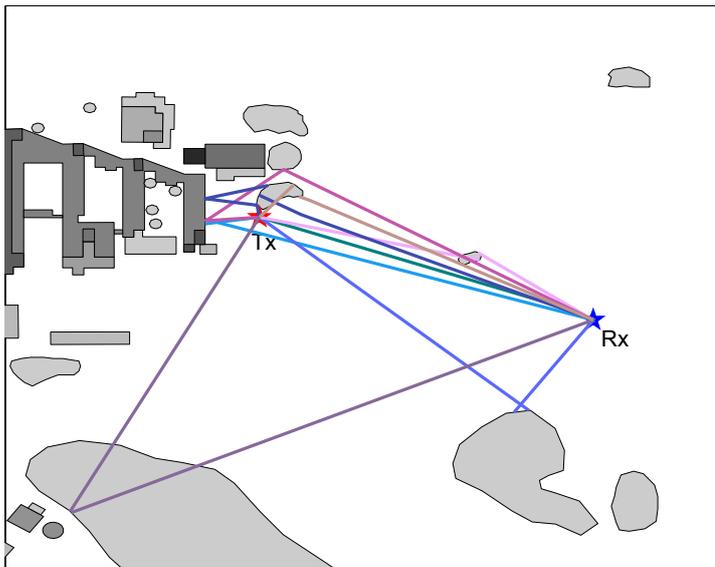
Figure 5: Visualized paths for several MPCs from one Rx position. Colors only present different MPCs.

5   Ray Launching Results

By using the parameters set in Table 1 and the measurement results in [10], ray launching results are analyzed and studied in this section.

In Fig. 5, the most likely paths are visualized for a particular RX position. These visualized MPCs have the strongest power among all MPCs at this RX position. It can be seen that there is a small angle mismatch at the TX side for the line-of-sight (LOS) MPC. The difference between the AOD and the propagation direction of ray is around 5 degrees. According to the estimated accuracy of the AOA/AOD and the TX and RX orientation, it is a reasonable difference, and rays can be matched. In addition, non-LOS (NLOS) MPCs are also visualized with several reflection and scattering processes that well reflect real propagation phenomena. It can also be noted that the rays going through the big vegetation area in the lower left side of the figure show a match at one side of the vegetation area, which is marked by yellow color in the figure. In fact, the ray from the TX can meet the RX ray in any place of the vegetation area. The visualized path is matched in the right vegetation area but maybe not at an accurate position. From a channel modeling point view, however, it
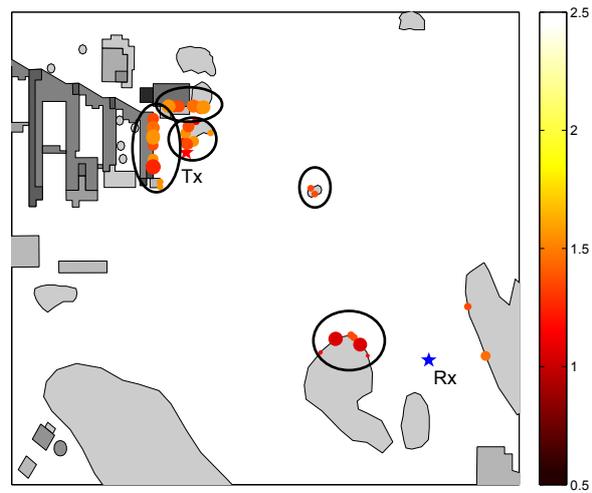
(a) LOS
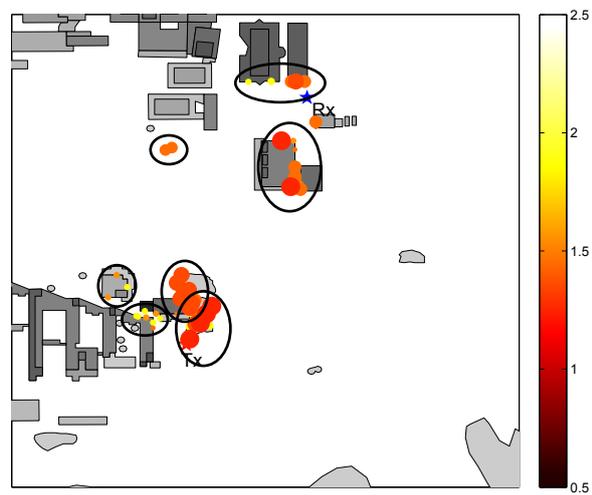
(b) NLOS

Figure 6: Scattering points for different RX positions in LOS and NLOS scenarios. Colors are used for different delays of MPCs, the size of markers represents the power of MPCs.
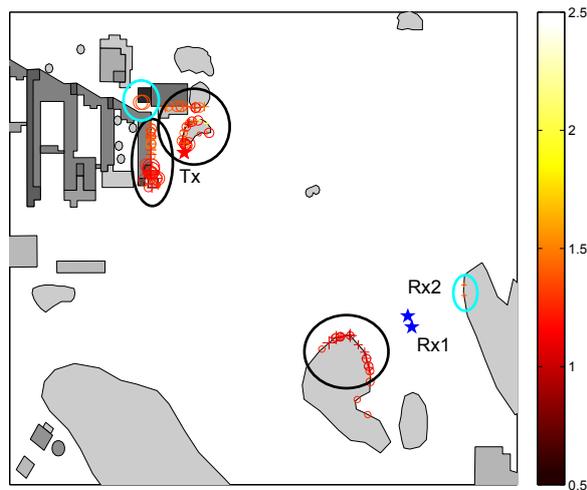
Figure 7: Visualized intersection points for two RX positions. Different markers are used for two RX positions, and the color represents the delay of MPCs, the size of markers represents the power of MPCs.

is good enough to obtain the physical scatterers and the propagation properties.

The intersection points for different RX positions are shown in Fig. 6, both for a LOS and a NLOS scenario. The physical intersection points are grouped together based on their physical positions and the power and delay of their MPCs. We can see in general, the NLOS scenarios show more intersections with physical scatters compared to the LOS scenarios. Clearly in this peer to peer scenario [10], the objects around the TX and RX are the most important scatterers.

In order to take a look at the time variant properties of clusters, we also show the intersection points for two RX positions separated around 10 meters (approximately 10 wavelengths), see Fig 7. When the RX is moved, some scatterers keep contributing to the channel response, which means that the cluster is active at different RX positions and has long cluster life time. In addition, one cluster near the TX side disappeared when moving to the new position and instead, a new cluster appears near the RX side. These results indicate possibilities for further usage of this measurement based ray launching tool, such as finding common clusters, extracting cluster life time *etc*.

In general, the tool is able to suggest the likely propagation paths for most measured MPCs, but some exceptions can be found. A maximum number of

iterations is set since in a real propagation scenario after several reflections, the power of ray highly decreases and it is not necessary to go to large number of iterations. In the peer-to-peer scenario here, the TX or RX might be surrounded by many objects. Rich reflection or scattering processes happen at these objects, and then the iteration limit can cause rays not to match. Larger number of iterations can also be considered in the future. At the same time, one MPC can have several matched candidates from the tool, and the best choice is still under discussion. In this work, the delay is chosen to be the most important criterion.

6   Conclusions

In this paper, we have described a new measurement based ray launching tool using 3D maps. Based on the delay and angular properties of the MPCs, the ray launching tool provides a good interpretation of propagation paths and shows the physical scatterers. This tool has a good GUI for analysis of measurement results analysis and provide a good understanding of physical propagation processes, e.g., multi-user MIMO channel modeling.

Acknowledgment

References

[1] G. E. Athanasiadou, and A. R. Nix, "A novel 3-D indoor ray-tracing propagation model: the path generator and evaluation of narrow-band and wide-band predictions", *IEEE Trans. Veh. Technol.*, vol. 49, No. 4, July, 2000.

[2] Z. Yun *et al.*, "A Ray-Tracing method based on the triangular grid approach and application to propagation prediction in urban environments", *IEEE Trans. Antenna Propagat.*, vol. 50, no. 5, May, 2002.

[3] J. Poutanen *et al.*, "Analysis of radio wave scattering processes for indoor MIMO channel models", in *IEEE PIMRC 2009*, pp. 102-106, Tokyo, Japan, Sept., 2009.

[4] J. Poutanen *et al.*, "Multi-link MIMO channel modeling using geometry-based approach", *to be published in IEEE Trans. Antenna Propagat.*, 2012.

[5] Z. Zhang *et al.*, "A ray-tracing approach for indoor/outdoor propagation through window structures", *IEEE Trans. Antenna Propagat.*, vol. 50, no. 5, May, 2002.

[6] A. F. Molish, "Propagation mechanisms", in *Wireless communications*, Wiley, 2006, pp. 52-64.

[7] Y. S. Meng, and Y. H. Lee, "Investigations of foliage effect on modern wireless communication systems: a review", *Progress In Electromagnetics Research*, vol. 105, pp. 313-332, 2010.

[8] Y. L. C. de Jong, and M. H. A. J. Herben, "A tree-scattering model for improved propagation prediction in urban microcells", *IEEE Trans. Veh. Technol.*, vol. 53, No. 2, March, 2004.

[9] E. Olsson, "Analysis of radio wave propagation using 3D-maps and MIMO measurements", MSC Thesis, Department of Electroscience, Lund University, Lund, June, 2004.

[10] G. Eriksson, F. Tufvesson and A. F. Molisch, "Propagation channel characteristics for peer-to-peer multiple antenna systems at 300 MHz," in *Proc. IEEE GLOBECOM 2006,* San Francisco, USA, Nov. 2006.

Paper II

Parameter Based Clusters, Physical Clusters and Cluster Based Channel Modeling in Sub-urban and Urban Scenarios

Cluster based channel modeling is an efficient way to describe correlation properties in multi-link multiple-input multiple-output (MIMO) systems. There are two kinds of clusters: 1) parameter based clusters are characterized with the parameters of multi-path components (MPCs); 2) physical clusters, which are determined based on the interactions with physical scatterers. The relation between parameter based clusters and physical scatterers is an open issue. In this work, geographical properties of parameter based clusters are analyzed both for urban and sub-urban scenarios with a measurement based ray launching tool. The analysis shows that single-bounce parameter based clusters can be related to groups of scatterers in the environment. However, multiple-bounce parameter based clusters cannot easily be related to such scatterers. To be able to characterize the multi-link MIMO channel properties, physical clusters, with a single scatterer or a group of scatterers, are introduced. The extracted physical clusters for the considered scenarios are studied. The cluster properties, i.e. the visibility region, delay spread and angular spread, are analyzed as well. The physical clusters are used to extract modeling parameters for the COST 2100 channel model. Finally, we also validate these parameters with respect to delay spread and singular value distribution using the MATLAB COST 2100 channel model implementation.

M. Zhu, K. Haneda, V.-M. Kolmonen, and F. Tufvesson,
"Parameter based clusters, physical clusters and cluster based channel modeling in sub-urban and urban scenarios."

1   Introduction

Cluster based modeling is a main concept in current channel models, such as the COST 2100 [1] and WINNER II channel models [2]. Conventionally, a cluster is defined as a group of multi-path components (MPCs) that have similar delay, angle of arrival (AOA) and angle of departure (AOD). Clustering algorithms have been developed to perform grouping of MPCs into clusters, examples include visual clustering, semi-automatic clustering and automatic clustering[3]. The clusters obtained from these approaches are called parameter based clusters since they are determined based on the characteristic parameters of each MPC. A parameter based cluster is usually characterized by its cluster lifetime, cluster angular spread, cluster delay spread, cluster shadowing factor etc., see e.g., [4, 5]. Parameter based clusters are usually not connected to scatterers and physical reality. By using a measurement based ray launching tool [6, 7], physical propagation processes of the parameter based clusters and their associated MPCs can be identified, which also offers the possibility to perform geographical clustering, i.e., to extract clusters having a close connection to physical reality. These extracted clusters are so called physical clusters, which is an important concept for multi-link MIMO channel models. For example, the multi-link extension in the COST 2100 channel model is implemented by modeling the correlation between two links with common clusters. The common clusters are based on the concept of shared physical scatterers between two links.

It is still an open issue how the physical clusters behave compared to the parameter based clusters and therefore we analyze this in more detail in this paper. To our best knowledge no such comparison has been done before. From the point view of physical clusters, we extract model parameters for the COST 2100 channel model for sub-urban and urban micro-cell scenarios. As such parameters are lacking in the literature, we also fill this gap of knowledge, which is a second important contribution of this paper. In addition, we also validate these parameters with the current COST 2100 channel model MATLAB implementation [8].

The paper is organized as follows: first, the considered two measurement campaigns are described in detail in section II. A brief introduction to the ray launching tool is given in section III. Section IV analyzes the properties of the parameter based clusters, for the two measurement campaigns. Clustering, based on physical properties of MPCs, is performed and the corresponding physical cluster properties are analyzed in Section V. Section VI discusses the COST 2100 channel model simulations with the physical cluster parameters. Finally, conclusions in section VII wrap up the paper.

2   Measurements and Data Processing

To make the study more general, two different measurement campaigns, conducted by two different institutions, were used for the analysis. One campaign is performed in a sub-urban scenario; the other is in an urban scenario.

2.1   Measurement Campaign I - Sub-urban

Sub-urban measurements were performed outdoors on the campus of Linköping University, Sweden, using the RUSK LUND MIMO channel sounder. The transmit antenna array (Tx) was placed 1.8 m above ground, at a static position and about 35 m from a large building. The receive antenna array (Rx) was mounted on a car with its lower ground plane approximately 2.1 m above the ground and was moving with a nearly constant speed. The measurements were carried out at a center frequency of 285 MHz, with a bandwidth of 20 MHz. Further details about the measurement campaign and the measurement principle can be found in [5], [9], [10]. The space-alternating generalized expectation-maximization (SAGE) [11] algorithm was used to estimate the parameters of the MPCs. The observed MPCs were characterized by their complex amplitude, delay, AOA and AOD, which all are used for the further cluster analysis.

2.2   Measurement Campaign II - Urban

Urban measurements were carried out in downtown Helsinki, Finland, using the TKK MIMO wideband channel sounder. A detailed description of the measurement equipment can be found in [12] and [13]. The transmitter was placed 10 m above ground, located on a crane 2 m in front of a building with 5-8 floors. The receiver was moved on the streets and the receive antenna was located around 1.6 m above ground. The center frequency is 5.3 GHz and the bandwidth is 120 MHz. More information about the measurement campaigns and principles are given in [14]. Further, the parameters of the MPCs were estimated by the improved SAGE algorithm as detailed in [15]. The relative delays, AOA, AOD and complex amplitudes of the MPCs were extracted from the measured impulse responses. By considering the geography of the measured area, the absolute delays are estimated from the observed relative delays. With these observed MPCs, further clustering analysis can be applied.

3   Ray Launching Tool

The used measurement based ray launching tool has been developed for visualizing the most likely MPCs with their AOA, AOD and delay in 3-dimensional

(3D) manner[7]. The measurement based ray launching tool supports ray re-
flection, diffraction, and scattering processes. It launches rays from the Tx
and Rx sides independently, according to the AOD and AOA of an MPC. The
launched rays can meet and interact with different objects such as buildings,
trees, and the corresponding reflection, diffraction or scattering process takes
places. To keep the complexity and processing time at a reasonable level, the
maximum number of bounces (interactions) is set to 5. To account for mea-
surement and positioning inaccuracies, rays from Tx and Rx are launched in a
cone centered around the estimated AOA/AOD for each MPC. Delay is then
used to determine the most likely one from the entire possible candidate MPCs.
Therefore, the interacting scatterers for an MPC along its propagating route
can be visualized and the number of interactions for a MPC can be determined
as well. A cluster is also characterized by its cluster AOA, cluster AOD and
cluster delay, and can thus be visualized in a similar manner as visualizing
MPCs.

For the considered urban and sub-urban scenarios, we first extract 3D maps
of the measured environments. For the sub-urban scenario, both buildings and
trees are considered while for the urban scenario, only buildings are taken into
account as trees are rare there. With the maps and the extracted AOA, AOD
and delay of MPCs, the most likely MPCs are visualized by the ray launching
tool. For parameter based clusters, the interacting properties of the associated
MPCs can be observed as well as the cluster centroids, which give detailed
insights of the geographical characteristics of the parameter based clusters. On
the other hand, MPCs can be associated to so-called physical clusters based on
their interaction with scatterers.

4   Parameter Based Clusters

Parameter based clusters are widely used for describing the characteristics of
MIMO channels. In this section, a brief summary of the parameter based clus-
tering algorithm and the cluster properties is given. By visualizing the clusters
and their associated MPCs, the geographical properties of the parameter based
clusters can be investigated. In addition, the properties of the interacting scat-
terers will be studied as well.

4.1   Clustering and Cluster Properties

There are a number of parameter based clustering algorithms used in the lit-
erature, for example, KPowerMeans, Hierarchical [17] and Gaussian-mixture
clustering. The KPowerMeans clustering algorithm has been extensively used

to extract clusters from the MPC parameter space. This algorithm performs clustering based on the values of the delay, AOD, AOA and power of each MPC from one measured snapshot. Each cluster is characterized by its centroid position, and described by its cluster delay, cluster power, cluster AOD, and cluster AOA, as well as by its intra-cluster spreads, including cluster delay spread, cluster AOD spread, and cluster AOA spread [4][5]. In this paper, the KPowerMeans algorithm is used to identify the parameter based clusters both for the sub-urban and urban scenarios.

A cluster is also characterized by the number of interactions; there are single-bounce and multiple-bounce clusters. For single-bounce clusters, only a single interaction with a scatterer during the wave propagation between Tx and Rx is modeled. The cluster delay determines the propagation distance between the Tx and Rx while the cluster AOA and AOD determine the possible position of the scatterer. A multiple-bounce cluster is modeled as a cluster that can be seen differently from the Tx and Rx side, respectively. Between the cluster seen from the TX and seen from the RX, a link propagation delay is modeled to describe high order interactions. The single- and multiple-bounce clusters are determined for the sub-urban and urban scenario with the same methodology detailed in [5].

4.2   Visualization of the Clusters and their Associated MPCs

The parameter based clusters are extracted based on the parameters of MPCs, but how they relate to the physical reality is not well understood. Therefore, the geographical properties of the parameter based clusters are studied with respect to the clusters and the associated MPCs in this section.

With the measurement based ray launching tool, the cluster centroids as well as the associated MPCs are visualized on the maps together with the interacting scatterers, see Fig. 1 and Fig. 2. In the figures, the buildings are represented with their regular shapes and the darker the higher. The trees are usually with irregular shapes and are only shown in sub-urban scenario. The ellipses represent the clusters, and the size of the ellipses is determined by the corresponding cluster delay spread and angular spread. Note that the parameters have been scaled so that the sizes of the ellipses do not correspond to the true distances in the map but they show relative relations. Different colors of the ellipses represent the cluster seen from the Tx or Rx side. The small circles and crosses represent the interacting points of the cluster centroids seen from the TX and RX sides, respectively. The color of the markers represents different delays of each MPC and the size of the markers represents the power of each MPC.
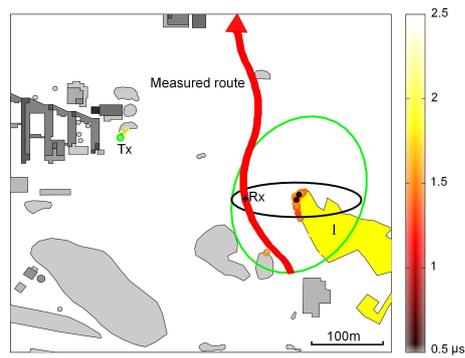
(a) Sub-urban
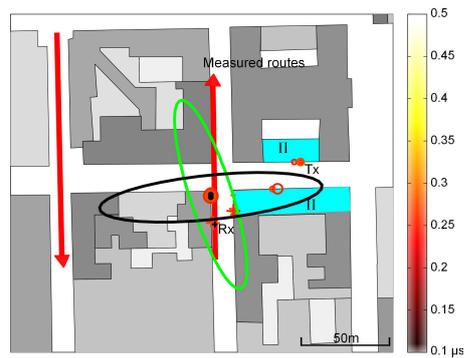
(b) Urban

Figure 1: A visualized parameter based single-bounce cluster and the associated
MPCs at a RX position in the sub-urban and urban scenarios.

Single-bounce Clusters

First, single-bounce parameter based clusters are investigated for both the sce-
narios, see Fig. 1. In the sub-urban scenario, the trees nearby the Rx (high-
lighted with yellow color, I) become the dominant interacting objects. It can
be noted that the MPCs with strong power (the ones with larger marker size)
usually interact with the same scatterer, and also this scatterer is usually the
one where the cluster centroid is placed at. In this sense, we can say that these
single-bounce parameter based clusters can be well reflected by the geographi-
cal properties of the scatterers, thus the physical reality. But when it comes to
the urban scenario, the situation becomes more complicated. First, there are
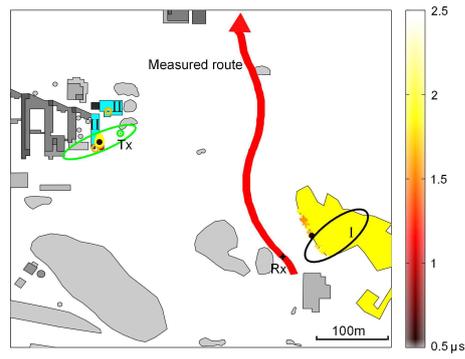
(a) Sub-urban
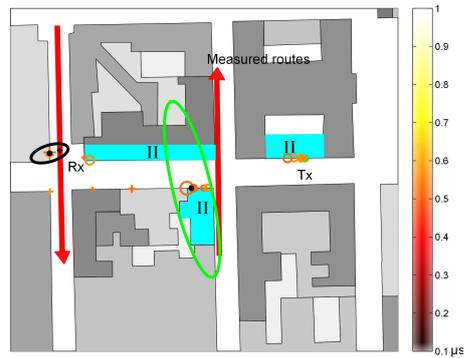
(b) Urban

Figure 2: A visualized parameter based multiple-bounce cluster and the associated MPCs at a RX position in the sub-urban and urban scenarios.

a few MPCs interacting with the same building where the cluster centroid is placed at. However, there are some MPCs from the same cluster interacting with other buildings, such as the ones at the opposite street (highlighted with cyan color, II). In this scenario, the MPCs interacting with buildings along the two sides of the street can have similar AOAs or AODs and reasonably equivalent delays, which consequentially cause these MPCs to be grouped into one cluster. However, generally speaking, single-bounce parameter based clusters have a high possibility to be reflected in the physical reality, except for some specific cases.

Multiple-bounce Clusters

Multiple-bounce clusters have been studied as well, see Fig. 2. The two cluster
centroids seen from the Tx and Rx side and the associated MPCs are visualized
on the map. When a dominant scatterer is near the Tx/Rx, MPCs associated
to such a cluster have a high possibility to interact with this dominant scatterer,
see the clusters at the Rx side in Fig. 2 (a) (highlighted with yellow color, I).
The cluster centroid is also placed at the same dominant scatterer, and can thus
be reflected in the physical reality. We also notice that the associated MPCs
of the cluster interact with multiple geographically separated scatterers, while
the cluster centroid only indicates interaction with a single dominant scatterer,
see the clusters at the Tx side in Fig. 2 (highlighted with cyan color, II).
These MPCs are grouped together according to their parameter space without
physical consideration, and in this case we cannot expect a close connection
with physical reality. It is seen that it is hard to relate multiple-bounce clusters
to the physical reality when we have rich scattering around the Tx/Rx, e.g.,
peer-to-peer communication, urban micro-cell.

4.3   Properties of Interacting Scatterers

We have seen that the associated MPCs of a parameter based cluster can
interact with several scatterers, distributed in a large or small, far or nearby
area, which can cause ambiguities when relating the parameter based clusters
to the physical reality. So we take a further step to investigate the properties
of these scatterers, to gain more insights of the relations between parameter
based clusters and the physical reality.

Distance Spread of Interacting Scatterers

First, the second order statistics of the distances from the Tx/Rx to the inter-
acting scatterers of the associated MPCs of a cluster is investigated. We call
this the distance spread of the cluster. Large distance spread indicates that
the MPCs associated to the cluster interact with a group of scatterers which
in turn are highly separated. A low distance spread means that, the scatterers
are less separated and MPCs often stem from a single scatterer. The distance
spread is here defined as

$$DS_{\mathrm{c}} = \sqrt{\frac{\sum_i^{N_c} P_i(d_i - \bar{d})^2}{\sum_i^{N_c} P_i}}, \tag{1}$$

where N_c is the number of MPCs associated to the cluster, d_i is the distance
from the Tx/Rx to the interacting point for each MPC, and P_i is the corre-

(a) Distance spread

(b) Angular spreads

(c) Number of scatterers
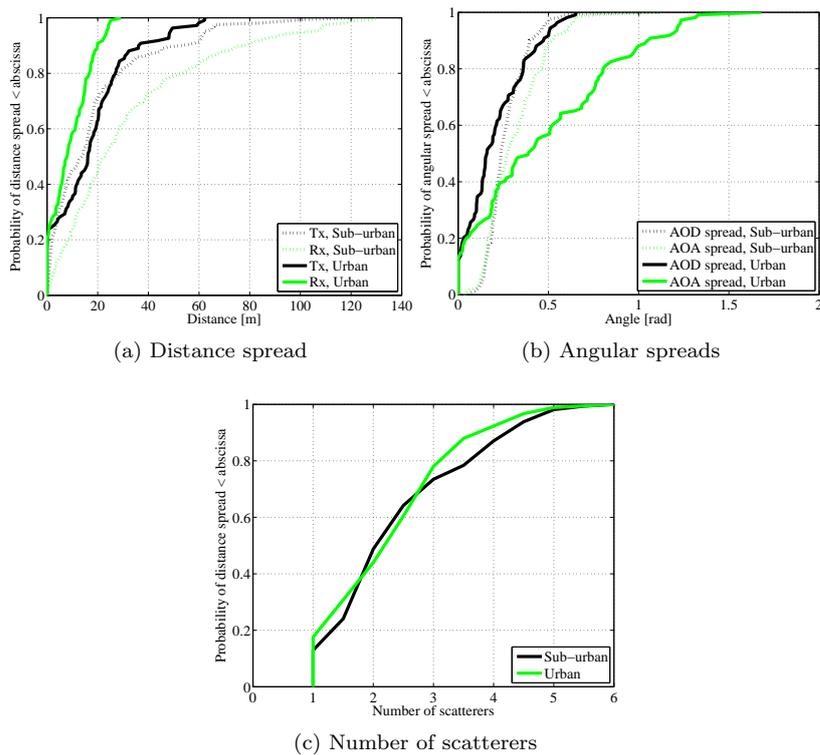
Figure 3: Properties of the interacting scatterers for the associated MPCs of a parameter based cluster: distance spread, angular spreads, number of scatterers.

sponding power. $\bar{d}$ is the power weighted mean distance, calculated as

$$\bar{d} = \frac{\sum_i^{N_c} P_i d_i}{\sum_i^{N_c} P_i}. \tag{2}$$

In Fig. 3, the distance spreads are evaluated. On average, distance spreads of 15 m and 20 m are observed at the Tx and Rx side in the sub-urban scenario and 10 m and 15 m in the urban scenario, respectively. It can be noted that the clusters usually have less than 50 m distance spread in the sub-urban scenario while in the urban scenario, it is typically less than 20 m. In general, the scatterers are distributed in a limited area. However, there are some clusters

with large distance spreads, such as the ones with more than 100 meter spreads
in the sub-urban scenario. In short, the scatterers contributing to a parameter
based cluster can either be reasonably concentrated or highly separated. In
current parameter based clustering methods, the geographical properties of
scatterers are not considered. Clustering in the delay domain does control
the total traveling time of an MPC, but not the distances between scatterers.
Especially in an outdoor scenario, the distances between scatterers and the
distances from the scatterers to Tx/Rx can be of different orders [16], which
can cause the loss of physical interpretation.

Angular Spread of Interacting Scatterers

The AOA and AOD of a cluster are basically determined by the positions of the
first and last interacting scatterers of the MPCs with respect to the TX and RX
locations. Moreover, the AOA and AOD spreads for a cluster also indicate the
geographical relations among interacting scatterers of the associated MPCs.
In Fig. 3 (b), it can be noted that the AOA and AOD spreads mostly have
small values, approximately 80% of the spreads are smaller than 23 degrees,
which means that the parameter based clustering algorithm limits the scatterers
to a narrow angle. However, the AOA spreads in the urban scenario have
significantly larger values. The reason is that MPCs, with AOAs determined
by scattering from a large wide wall, are grouped in a single cluster due to their
similarities in the delay and AOD domain. In general, for the angular domain,
the parameter based clusters have strong connections with the physical reality.

Number of Interacting Scatterers

An MPC will interact with one or several scatterers along its propagation route.
The number of interacting scatterers of a cluster is determined by the interact-
ing scatterers of its associated MPCs. Fig. 3 (c) shows the number of interacting
scatterers for the extracted clusters in sub-urban and urban scenarios. Only
around 15% of the clusters interact with a single scatterer, most of the clusters
interact with more than one scatterer. The reason is that in the measured sub-
urban and urban scenarios, the scatterers near the Tx/Rx can provide similar
propagation properties, and are grouped into one cluster. Such a single scat-
terer well explains the single-bounce clusters and has strong relation to the
physical reality, but with the increase of the number of scatterers, it becomes
more challenging to connect the parameter based clusters to the physical real-
ity. Especially, there are clusters that are interacting with a very large number
of scatterers, such as 5 or 6. It can be the scatterers that are closely located or
highly separated geographically but are concentrated in angular domain when

illuminated by the specific position of the TX and RX.

4.4   Summary

From the analysis above, we can conclude that parameter based clusters usually group the MPCs inside a narrow angle, as expected. The delay of the MPCs used in the clustering algorithm can only control the total traveling distance from the Tx to Rx, but cannot determine if the MPCs with similar delays arise from the same/close scatterer or not. The clusters can interact with one or several scatterers, and usually single-bounce clusters have a strong connection to physical reality but not necessarily the multiple-bounce clusters. We have to be aware that the parameter based clusters sometimes lose connection to the physical reality which can cause some bias for the parameter extraction for the COST 2100 channel model. Therefore, further analysis of physical clusters is required.

5   Physical Clusters

Generally speaking, a cluster is defined as follows [17]: a cluster is a collection of data objects that are similar to one another within the same cluster and are dissimilar to the objects in other clusters. From this general definition, a physical cluster can be defined as a group of scattering objects, which are close in the physical reality. In this section, we aim to group the scatterers into clusters according to their geographical properties. In the meantime, the properties of the extracted physical clusters are investigated as well.

5.1   Physical Clustering

In outdoor environments, it is often possible to identify dominant scatterers from a map, for example, the two large buildings around the Tx and the groups of trees around the Rx in the sub-urban scenario, or the buildings around the Rx and Tx in the urban scenario. These dominant scatterers contribute to the channel impulse response over a large area of Rx movements and determine the main properties of the channel. The proposed geographical scatterer grouping is based on these dominant scatterers. These physical scatterers usually have a power contribution to the channel for a long time, i.e., over many different channel snapshots, however, the power has variations. A scatterer can be a single physical cluster. On the other hand, a scatterer can be blocked for a while, but later be visible and contribute to the channel again. This means that the scatterer can give rise to two physical clusters with different cluster
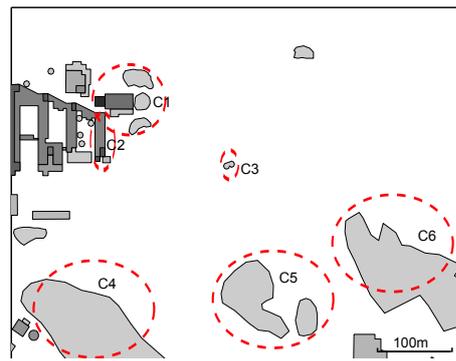
(a) Sub-urban
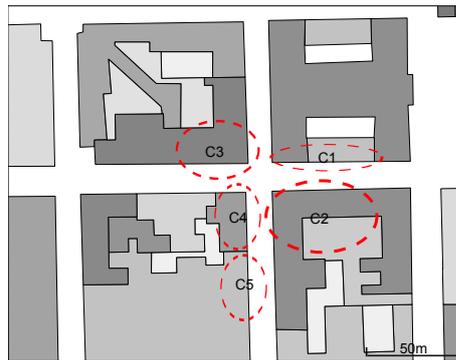
(b) Urban

Figure 4: The proposed grouping of scatterers based on geographical properties
for the sub-urban and urban scenarios.

properties. Also the scatterers who are geographically close to each other and
result in MPCs with thus similar parameters can be treated as a single scatterer.
In other words, the scatterer based physical clusters can be related to a single
scatterer or a group of scatterers and a scatterer can contribute to different
physical clusters based on how it is seen. When grouping scatterers, the most
important condition is the distance between scatterers. The distance between
scatterers should be sufficiently close, so that the Tx/Rx cannot distinguish
them. Here we define "close" as when the distance between scatterers is much
smaller than the distance to the Tx/Rx, more specifically one third of the
distance between Tx and Rx.

Fig. 4 shows an example of the extracted physical clusters for the sub-urban
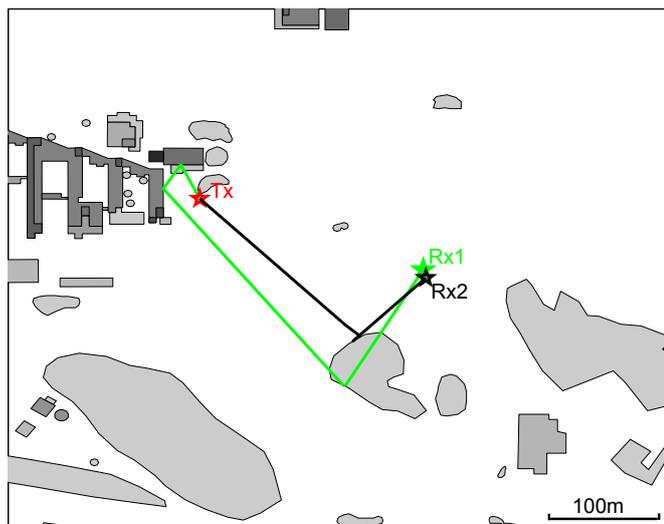
Figure 5: An example of physical single and multiple-bounce MPCs.

and urban scenarios. It can be noted that some dominant scatterers are treated as physical clusters alone, and some of the scatterers are grouped together as a single physical cluster. By visualizing the MPCs on top of the 3D maps, they can be associated to physical clusters. In addition, a physical cluster is also determined as single- or multiple-bounce cluster. It has to be noted that a physical cluster can be a single- or multiple-bounce cluster at the same time but with different cluster properties, see Fig. 5. It shows that MPCs can reach the different Rx positions by interacting with the same scatterer while they arise from different scatterers at the Tx side, and thus the MPC reaching Rx2 is associated to a single-bounce cluster while the other is associated to a multiple-bounce cluster.

5.2   Properties of Physical Clusters

To apply physical clusters to current cluster based models, the cluster properties have to be investigated. In this work, we discuss the cluster spreads, cluster visibility region, cluster power model and cluster cross-polarization discrimination in detail for the physical clusters. Other properties, i.e. number of MPCs inside a cluster, cluster selection factor, cluster shadowing etc., are parameterized in Table 3. Detailed extraction methodologies with respect to these parameters can be found in [5].

Table 1: Cluster properties of single-bounce physical clusters.

Sub-Urban					
Cluster	C1	C2	C4	C5	C6
Delay spread [μs]	0.11	0.05	0.12	0.06	0.15
AOD spread [deg]	21	12	10	4	4
AOA spread [deg]	3	3	6	12	17
VR [m]	173	164	97	182	172
Urban					
Cluster	C1	C2			
Delay spread [μs]	0.009	0.009			
AOD spread [deg]	5	4			
AOA spread [deg]	12	6			
VR [m]	68	79			

Cluster spreads

The physical clusters are also characterized by the associated MPCs. The corresponding cluster spreads are AOA spreads, AOD spreads and delay spreads, defined as [1]:

$$DS_{\mathrm{c}} = \sqrt{\frac{\sum_i^{N_c} P_i(\tau_i - \bar{\tau})^2}{\sum_i^{N_c} P_i}}, \tag{3}$$

$$AS_{\mathrm{c}} = \sqrt{\frac{\sum_i^{N_c} P_i(\mathrm{angle}(\exp(j \cdot (\varphi_i - \bar{\varphi}))))^2}{\sum_i^{N_c} P_i}} \tag{4}$$

where DS_{c} is cluster delay spread, AS_{c} is cluster angular spread, N_{c} is number of MPCs in each cluster and j is the imaginary unit. Furthermore, P_i is the power for the ith MPC, $\bar{\varphi}$ and $\bar{\tau}$ are power weighted means calculated as

$$\bar{\tau} = \frac{1}{\sum_i^{N_c} P_i} \sum_i^{N_c} P_i \tau_i \tag{5}$$

$$\bar{\varphi} = \mathrm{angle}(\sum_i^{N_c} P_i \exp(j \cdot \varphi_i)), \tag{6}$$

where τ_i is the delay and φ_i is the AOD/AOA of the ith MPC. Note that, the AOA/AOD discussed here is in azimuth plane.

Sub-Urban										
Cluster	(C1,C2)	(C1,C4)	(C1,C5)	(C1,C6)	(C2,C1)	(C2,C5)	(C2,C6)	(C4,C5)	(C5,C6)	(C6,C5)
Delay spread [μs]	0.08	0.07	0.12	0.16	0.05	0.12	0.14	0.06	0.10	0.18
AOD spread [deg]	21	8	23	12	18	17	10	4	3	5
AOA spread [deg]	5	3	20	13	3	18	4	7	14	12
VR [m]	164	19	163	115	154	95	144	77	134	47
Urban										
Cluster	(C1,C2)	(C1,C3)	(C1,C4)	(C2,C1)	(C2,C3)	(C2,C4)	(C4,C1)	(C4,C2)		
Delay spread [μs]	0.01	0.014	0.003	0.01	0.008	0.009	0.027	0.018		
AOD spread [deg]	9	14	10	4	4	7	1	1		
AOA spread [deg]	4	20	7	9	13	10	7	4		
VR [m]	103	73	30	63	62	10	24	79		

Table 2: Cluster properties of multiple-bounce physical clusters.

For the single-bounce physical clusters, the delay spread and angular
spreads have in general small values in the sub-urban and urban scenarios. It
is also true for the multiple-bounce clusters. From the cluster spread proper-
ties, it can be concluded that the physical clusters have a good control of delay,
and angular properties. Therefore, the size of the cluster is also in a limited
range.

Visibility Region and Transition Region

The visibility region is another important property of a cluster; it determines
the activity of the cluster. The visibility region of the physical cluster is also
studied here in detail, see Table 1 and Table 2. Here the visibility region
is defined as, along the RX moving route, the length of the route where the
physical cluster can be seen. It can be noted that physical clusters usually
have relatively long visibility regions which well reflect the fact that the nearby
scatterers are the main contributors to the channel. Together with the visibility
region, transition regions for the physical scatterers are extracted in the same
manner as in [5], and starts from the half of the maximum cluster power until
the cluster has disappeared. Due to the frequent fluctuations in the cluster
power, the estimated transition regions are subject to some uncertainty.

Cluster Power Model

The cluster power model is mainly characterized by the cluster power decay
factor and the cluster cut-off delay. The cluster power decay factor is a result of
linear regression analysis of the cluster power versus the cluster delay. For the
two considered scenarios, 14.5 and 248.3 dB/µs are observed. The significantly
large decay factor in the urban scenario is due to the lack of large distance
clusters, while the extracted clusters are within a small area. The cut-off delay
is recommended as the delay where cluster power has decreased 30 dB from
the maximum cluster power in the COST 2100 channel model. The power
of clusters with delays larger than the cut-off delay is modeled as constant.
From the measurements, cut-off delays of 2.5 and 0.29 µs are observed for the
sub-urban and urban scenarios, respectively.

Cluster Cross-polarization Discrimination

The cluster cross-polarization discrimination (XPD) characterizes the power
proportion from one polarization to another polarization. First, the XPD ratios
of the MPCs associated to one cluster are determined as:

$$XPD_{\mathrm{V}} = \frac{P_{\mathrm{VV}}}{P_{\mathrm{VH}}} \qquad (7)$$

Table 3: Channel model parameters extracted from the physical clusters.

Scenario	Sub-urban	Urban
Radius of visibility region:		
μ_R[m]	127	59
Radius of transition region:		
μ_T[m]	48	18
Number of far clusters:		
μ_{N_c}	6	5
Number of MPCs per cluster:		
μ_N	8	4
Cluster selection factor:		
$\mu_{K_{sel}}$	0.33	0.2
Cluster power decay factor:		
μ_{k_τ} [dB/µs]	14.5	248.3
Cluster cut-off delay:		
τ_{cutoff} [µs]	2.5	0.39
Radius of LOS visibility region:		
$\mu_{R_{LOS}}$ [m]	343	16
Radius of LOS transition region:		
$\mu_{T_{LOS}}$ [m]	93	11
LOS power factor:		
$\mu_{K_{LOS}}$ [dB]	-4.7	2.6
$\sigma_{K_{LOS}}$ [dB]	2.0	3.2
Cluster angular spreads:		
$\mu_{AS_c^{AOD}}$ [deg]	9.5	5.0
$\sigma_{AS_c^{AOD}}$ [dB]	3.0	4.3
$\mu_{AS_c^{AOA}}$ [deg]	8.1	7.5
$\sigma_{AS_c^{AOA}}$ [dB]	3.2	2.3
Cluster delay spread:		
μ_{DS_c} [µs]	0.08	0.01
σ_{DS_c} [dB]	2.5	2.7
Cluster shadowing:		
σ_{Sh_c} [dB]	5.2	13

and

$$XPD_H = \frac{P_{HH}}{P_{HV}}, \tag{8}$$

where P_{VH} is the power from the vertical polarization to the horizontal polarization and vice versa. The MPC XPD ratios are log-normally distributed over different clusters, with a mean μ_{XPD} and standard deviation σ_{XPD} for a cluster. Thus the cluster cross-polarizations are also log-normally distributed, with parameters $(m_{\mu_{XPD}}, S_{\mu_{XPD}})$ and $(m_{\sigma_{XPD}}, S_{\sigma_{XPD}})$. The extracted cluster cross-polarization parameters in the urban scenario are listed in Table 4. However, the cross-polarization parameters for the sub-urban scenario are not extracted due to the use of single-polarized antenna elements in the sub-urban measurements.

Table 4: Cluster Cross-polarization parameters extracted from the physical clusters.

Scenario	Urban
V-polarization:	
$m_{\mu_{\mathrm{XPD_V}}}$ [dB]	4.4
$S_{\mu_{\mathrm{XPD_V}}}$ [dB]	3.9
$m_{\sigma_{\mathrm{XPD_V}}}$ [dB]	3.8
$S_{\sigma_{\mathrm{XPD_V}}}$ [dB]	2.0
H-polarization:	
$m_{\mu_{\mathrm{XPD_H}}}$ [dB]	6.3
$S_{\mu_{\mathrm{XPD_H}}}$ [dB]	3.0
$m_{\sigma_{\mathrm{XPD_H}}}$ [dB]	3.9
$S_{\sigma_{\mathrm{XPD_H}}}$ [dB]	2.0

6 Channel Model Evaluation

The COST 2100 channel model is a geometry-based stochastic channel model (GSCM) for MIMO channel simulations [18]. It supports both single- and multiple-link MIMO channel accesses. The channel model is characterized by individual clusters, and corresponding visibility regions of the clusters. Therefore, in the MATLAB implementation of the COST 2100 channel model, the inputs to the model are based on the cluster parameters, i.e. cluster power decay factor, cluster visibility region and transition region. With a complete set of parameters, the channel model can give simulated propagation channels without effects of antennas. To include antenna effects, complex polarimetric radiation patterns of TX and RX antenna elements are needed.

First, we simulate channel realizations based on the COST 2100 channel model MATLAB implementation with the extracted parameters of physical clusters that are summarized in Table 3. A set of 100 simulation runs for both sub-urban and urban scenarios has been carried out. For the sub-urban scenario, the center frequency is set to 285 MHz and the channels are generated for a bandwidth of 20 MHz, while the frequency for the urban scenario is 5.3 GHz and the bandwidth is 120 MHz. These settings are identical to the measurements introduced in Section II. For both the scenarios, the BSs are placed at the center of the simulation area, and the MSs are moving along the pre-determined routes similar to the measurement routes. In total, 33200 and 50000 snapshots of propagation channels have been simulated for the sub-urban and urban scenarios, respectively, to provide enough statistics for the investigations.
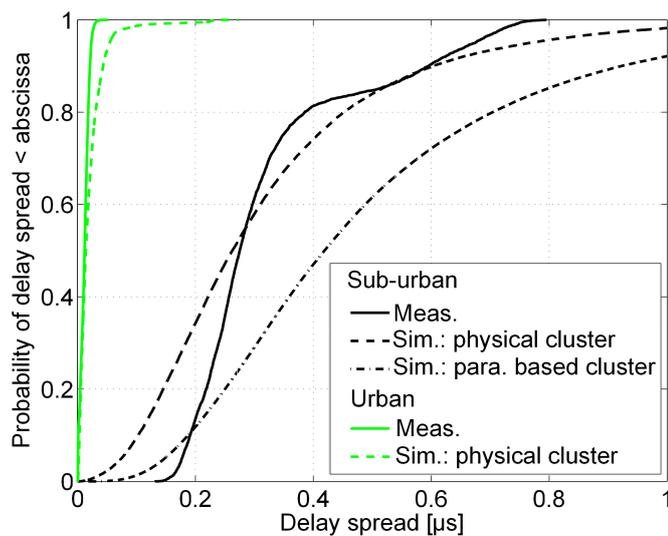
Figure 6: Delay spreads of the measured and simulated omni-directional antenna responses for the sub-urban scenario.

6.1   Delay Spread

We first compare simulated and measured channels concerning their respective delay spreads. For the sub-urban scenario, the comparison is performed for channel responses with an omni-directional antenna pattern in azimuth both at the TX and RX sides. Note that, when the measurements were carried out, a reference omni-directional antenna was set up at the RX side. Therefore, data connected from this single TX-RX pair can be used to evaluate the delay spread performance. The delay spreads are computed from the channel power delay profiles (PDPs) by using a noise threshold of 30 dB below the peak power in each PDP. All PDPs are truncated at 6 μs, and it can be assumed that no significant power will be received after this delay. The results are shown in Fig. 6, where the solid lines are cumulative distribution functions (CDFs) for the delay spreads extracted from the measured raw data and the others are CDFs for the delay spread from all simulation runs. It can be noted that the median delay spread is only 0.02 μs off between the simulations and measurements, which is a promising improvement compared to the parameter based cluster simulation performance [5]. However, significantly smaller and larger delay spreads still exist due to the limitations of the current channel model as pointed out in [5]. For the urban scenario, the delay spreads are
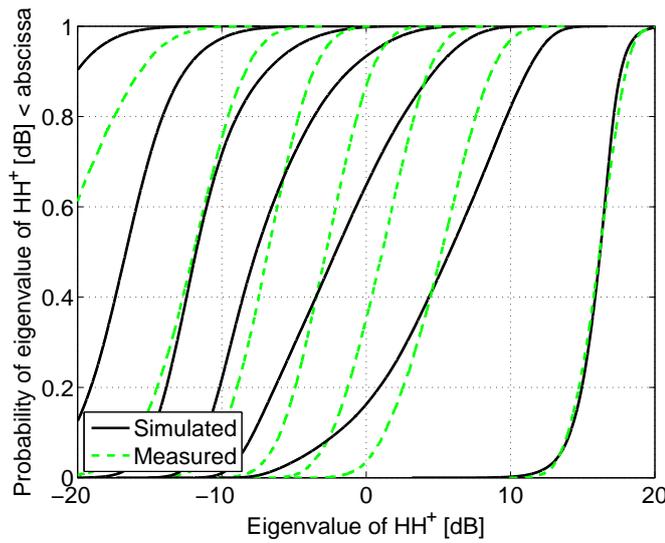
Figure 7: Distributions of ordered singular values of the measured and simulated channel impulse responses for the sub-urban scenario.

calculated based on the simulated and measured MPC parameters, see Fig. 6. It can be noted that the small delay spread values have been captured by the simulations, and up to 80%, the simulations and the measurements show a good agreement. However, the large delay spread is over estimated from the simulations that we think it is mainly due to the model limitations [5].

6.2   Singular Value Distribution

From a system perspective, the singular value distribution has been investigated as well. First, for the sub-urban scenario, 7-by-7 MIMO channel matrices have been simulated based on the COST 2100 channel model simulations and the Tx and Rx antenna radiation patterns. The patterns correspond to those of the measurement antennas. The singular values are derived from the normalized channel frequency response at an SNR of 20 dB. A good agreement between the measurements and simulations is obtained in the sub-urban scenario, especially for the first three dominant singular values, see Fig. 7. In the urban scenario, the same radiation patterns are also used for the comparison of the simulation and measurements. However, only a subset of measurement antenna feeds is considered in order to avoid too large MIMO channel matrix dimension. More
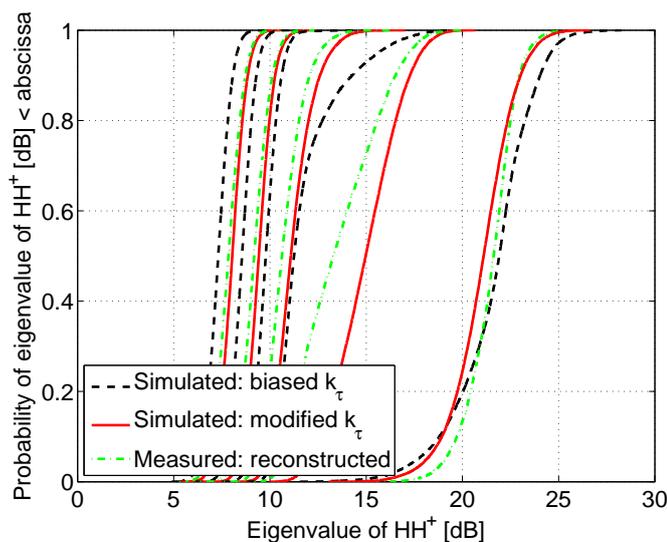
Figure 8: Distributions of ordered singular values of the measured and simulated channel impulse responses for the urban scenario with modified power decay factor.

specifically, a subset of RX spherical antenna elements that mainly receives the vertically polarized fields and the vertically polarized elements of the Tx planar antenna are used which leads to a MIMO channel of size 10-by-16. The distribution of the first five dominant singular values are investigated, see Fig. 8. It can be noted that the distributions of the second singular values show some differences between the simulations and measurements, which is mainly due to the extracted biased power decay factor. As mentioned before the extracted power decay factor is estimated from few realizations of large delay clusters, and therefore a modified power decay factor with value 24 dB/μs is applied. With the modified power decay factor, the simulated and measured channels give better agreements in singular value distribution, specifically speaking, less than 2 dB mismatch. In short, the channel characteristics with respect to singular value distribution show reasonable agreement between simulations and measurements when the physical clusters are used, therefore also the channel capacity can be well represented.

7   Conclusion

The cluster concept is widely used in current channel models, and the clusters help to reduce the modeling complexity. However, the cluster extraction is still an open topic. The parameter based clustering algorithms are based on the parameters of the MPCs. There is no common view of the relation between the parameter based clusters and physical reality. In this paper, we analyzed geographical properties of parameter based clusters with a ray launching tool. It has been seen that single-bounce parameter based clusters can well be reflected in the physical reality, but this is not necessarily the case for multiple-bounce clusters, which have more complicated behavior. Therefore, a simple geographical clustering method is proposed and we observed the corresponding physical clusters and their properties. A physical cluster can be seen for a long time. The frequent cluster deaths observed for the parameter based clusters are disappeared for physical clusters, which gives longer cluster visibility regions. Also, the physical clusters can be single- and multiple-bounce at the same time, which is not the case of parameter based clusters. The extracted parameters from the physical clusters have been applied to the COST 2100 channel model MATLAB implementation. In addition, the validation of these parameters is also performed with respect to the delay spread, and singular value distribution. We conclude that the physical clusters give better control of delay spread and the singular value distributions also give good agreement between the simulations and measurements.

In general, the physical clusters show promising results regarding the parameter extraction for the single-link COST 2100 channel model. The multi-link COST 2100 channel model is described by the concept of common clusters, which are interpreted based on the physical scatterers. Therefore, a more sophisticated physical clustering algorithm and physical cluster analysis are needed for the multi-link 2100 channel model development.

References

[1] R. Verdone and A. Zanella, "Radio channel modeling for 4G networks," in *Pervasive mobile and ambient wireless communications: COST Action 2100 (signals and communication technology)*, 1st ed., London: Springer, 2012, pp. 67-148.

[2] IST-4-027756 WINNER II D1.1.2 V1.2. (2008). *WINNER II Channel Models.* [Online]. Available: http://www.ist-winner.org.

[3] N. Czink, "The random-cluster model- a stochastic MIMO channel model for broadband wireless communication systems of the 3rd generation and beyond," Ph.D. dissertation, Technische Universität Wien, Vienna, Austria, Dec., 2007.

[4] N. Czink, R. Tian, S. Wyne, G. Eriksson, T. Zemen, J. Ylitalo, F. Tufvesson, and A. F. Molisch, "Cluster parameters for time-variant MIMO channel models," in *Proc. European Conf. on Antennas and Propagat.*, Edinburgh, UK, 2007, pp.1-8.

[5] M. Zhu, G. Eriksson and F. Tufvesson, "The COST model: parameterization and validation based on outdoor MIMO measurements at 300 MHz," in *IEEE Transactions on Wireless Communications*, vol. 12, no. 2, pp. 888-897, 2013.

[6] J. Poutanen, K. Haneda, L. Liu, C. Oestges, F. Tufvesson, and P. Vainikainen, "Multi-link MIMO channel modeling using geometry-based approach," in *IEEE Trans. Antennas Propagat.,* vol. 60, no. 2, pp. 587-596, Feb., 2012.

[7] M. Zhu, A. Singh, and F. Tufvesson, "Measurement based ray launching for analysis of outdoor propagation," in *Proc. European Conf. on Antennas and Propagat.*, Prague, Czech, 2012, pp. 3332-3336.

[8] L. Liu, and M. Zhu (2014), *COST2100 MIMO Channel Model MATLAB Implementation* (Version 2.2.5) [Source code]. Available: https://code.google.com/p/cost2100model/

[9] R. S. Thomä, D. Hampicke, A. Richter, G. Sommerkorn, and U. Trautwein, "MIMO vector channel sounder measurement for smart antenna system evaluation," *European Transactions on Telecommunications*, vol. 12, no. 5, pp. 427-438, Sep./Oct. 2001.

[10] RUSK channel sounder – Measurement principle. [Online]. Available: http://www.channelsounder.de/ruskchannelsounder.html.

[11] B. H. Fleury, M. Tschudin, R. Heddergott, D. Dahlhaus, and K. Ingeman Pedersen, "Channel parameter estimation in mobile radio environments using the SAGE algorithm," *IEEE J. Select. Areas Commun.,* vol. 17, no. 3, pp. 434-450, Mar. 1999.

[12] K. Kalliola, H. Laitinen, L. I. Vaskelainen, and P. Vainikainen, "Realtime 3-D spatial-temporal dual-polarized measurement of wideband radio channel at mobile station," *IEEE Trans. Instrum. Meas.*, vol. 49, pp. 439-448, Apr. 2000.

[13] V. M. Kolmonen, J. Kivinen, L. Vuokko, and P. Vainikainen, "5.3 GHz
MIMO radio channel sounder," *IEEE Trans. Instrum. Meas.*, vol. 55, pp.
1263-1269, Aug. 2006.

[14] L. Vuokko, V. M. Kolmonen, J. Salo, and P. Vainikainen, "Measurement
of large-scale cluster power characteristics for geometric channel models,"
IEEE Trans. Antennas Propagat., vol. 55, no. 11, Nov. 2007.

[15] B.H. Fleury, X. Yin, K.G. Rohbrandt, P. Jourdan, A. Stucki, "Perfor-
mance of a high-resolution scheme for joint estimation of delay and bidi-
rection dispersion in the radio channel," in *Proc. Veh. Technol. Conf.*,
Birmingham, AL, USA, 2002, pp. 522-526.

[16] J. C. Liberti, T. S. Rappaport, "A geometrically based model for line-of-
sight multipath radio channels," *IEEE 46th Vehicular Technology Con-
ference: Mobile Technology for the Human Race.*, Atlanta, GA, 1996, pp.
844 - 848.

[17] J. Han and M. Kamber, *Data Mining, concepts, and techniques*, 1st ed.,
San Francisco: Morgan Kaufmann Publishers, 2001.

[18] L. Liu, C. Oestges, J. Poutanen, K. Haneda, P. Vainikainen, F. Quitin, F.
Tufvesson, and P.D. Doncker, "The COST 2100 MIMO channel model,"
in *IEEE Wireless Commun.,* vol. 19, no. 6, pp. 92-99, Dec., 2012.

Paper III

The COST 2100 Channel Model: Parameterization and Validation Based on Outdoor MIMO Measurements at 300 MHz

The COST 2100 channel model is a geometry-based stochastic channel model (GSCM) for multiple-input multiple-output (MIMO) simulations. This paper presents parameterization and validation of the channel model for peer-to-peer communication in the 300 MHz band. Measurements were carried out in outdoor environments for both line-of-sight (LOS) and non line-of-sight (NLOS) scenarios. The COST 2100 channel model is characterized and parameterized based on clusters. The KpowerMeans algorithm and a Kalman filter are used for identifying and tracking clusters from measurements. General issues regarding the parameterization of the channel model are analyzed in detail. A full set of single-link parameters for the channel model is extracted from the measurements. These parameters are used as the input to the channel model validation processes, targeting delay spread, spatial correlation, and singular value distribution as well as antenna correlation. The validation results show good agreement for the spatial correlation and singular value distribution between the channel model simulations and the 300 MHz outdoor measurements. Our findings suggest that the model has potential for modeling 300 MHz channels in outdoor environments, although some modifications are needed for the distribution of cluster delay spreads and the size of cluster visibility regions.

1   Introduction

The channel model from COST 273 [1], and its successor COST 2100 [2] are
now available and can account for most of the important propagation processes
and effects that influence multiple-input multiple-output (MIMO) system per-
formance. The COST 2100 channel model is characterized by individual clus-
ters, i.e. group of multipath components (MPCs) showing similar properties
in delay, angle of arrival (AOA), angle of departure (AOD) and power, and
corresponding visibility regions of the clusters [2]. The model supports both
single-link and multiple-link MIMO channel access; the latter is achieved by us-
ing the concept of common clusters [3]. An overview of the COST 2100 channel
model is presented in [4], whereas a detailed description of the channel model
can be found in [2]. The parameterization of this generic model from measure-
ments is not yet complete and only a few environments have been studied. For
example, parameterization of the channel model has been performed for indoor
environments though some parameters are missing, such as cross-correlation co-
efficients for cluster spreads, and cluster shadowing [5]. Furthermore, there is a
lack of studies validating the COST 2100 channel model. One reason for this is
that there is no general methodology to evaluate the validity of channel models,
and the validation processes also depend on available measurement data and
the nature and usage of the particular channel model. In [6], validation of the
COST 2100 channel model, with respect to large-scale properties such as delay
spread and angular spread, has been carried out for an indoor environment
with good results. So far, studies on the COST 2100 channel model mostly
focus on indoor environments, but are missing for outdoor scenarios. For a
good generic model, different environments should be included and completely
parameterized. In addition, validation should be performed to determine the
accuracy and limitations of the channel model in those environments as well.

   In order to perform parameterization and validation of the COST 2100
channel model in outdoor scenarios, 300 MHz outdoor measurements were per-
formed and the collected data is used for further analysis in this paper. Fre-
quencies in the lower UHF range, as used for the measurements, are often used
for tactical communication. In addition, public cellular communication systems
are present at 450 MHz and 900 MHz, and TETRA, a cellular and peer-to-peer
system for first responders, operates at frequencies around 400 MHz. From a
scientific point of view, it is also of interest to characterize propagation condi-
tions at those frequencies as many common larger objects in the environments
(like vehicles, smaller buildings, and lamp-posts) have the size of a few wave-
lengths instead of tens to hundreds of wavelengths as for the standard cellular
frequencies. Hence, it is of significant interest to investigate and characterize
the channel properties and provide a basis for the usage of the COST 2100

channel model at lower frequencies.

The main contributions of this paper are:

- Cluster parameters and cluster time-variant properties are obtained from the 300 MHz measurements by using a joint clustering and tracking algorithm.

- Parameterization of the channel model for single-link outdoor MIMO communication at 300 MHz is conducted.

- Validation of the channel model is performed for the considered scenario by comparing simulated and measured delay spreads, spatial correlations, singular value distributions and antenna correlations.

The remainder of the paper is organized as follows: Sec. II describes the 300 MHz outdoor measurement campaign. Sec. III introduces the joint clustering and tracking algorithm for cluster extraction from the measurements. The parameterization for the COST 2100 single-link MIMO channel model in an outdoor scenario is performed in Sec. IV. Sec. V validates the single-link parameters for the channel model. Finally, the conclusions in Sec. VI complete the paper.

2   Measurement Campaign

The measurements were performed outdoors on the campus of Linköping University, Sweden using the RUSK Lund MIMO channel sounder [7], [8]; the measurement principle is described in [9], [10]. Identical antenna arrays were used for both the transmitter and the receiver. The antenna arrays are vertically polarized, 7-element uniform circular dipole arrays (UCDA), with one additional dipole element located at the center, in an elevated position [7], [11]. All 8 elements are sleeve dipoles and the center element, which has an omni-directional antenna response in azimuth, is located 0.78 m above the 7-element UCDA. The bandwidth of the antennas is 30 MHz, and the antenna gain for the UCDA is 8 dBi and 5 dBi for the omni-directional antenna. The 3 dB beam width of the lower antenna elements is 95 degrees in azimuth and 59 degrees in elevation. The transmit antenna array (Tx) was placed 1.8 m above ground, at a static position with coordinate (0, 0) and about 35 m from a large building. The receive antenna array (Rx) was mounted on a car with its lower ground plane approximately 2.1 m above the ground. The car was driven at a speed of around 8 m/s along the marked routes in Fig. 1, and the routes are labeled as 1 to 4. The minimum and maximum separation between the Tx and Rx are 197 m and 451 m, respectively. The measurements were carried out at a center
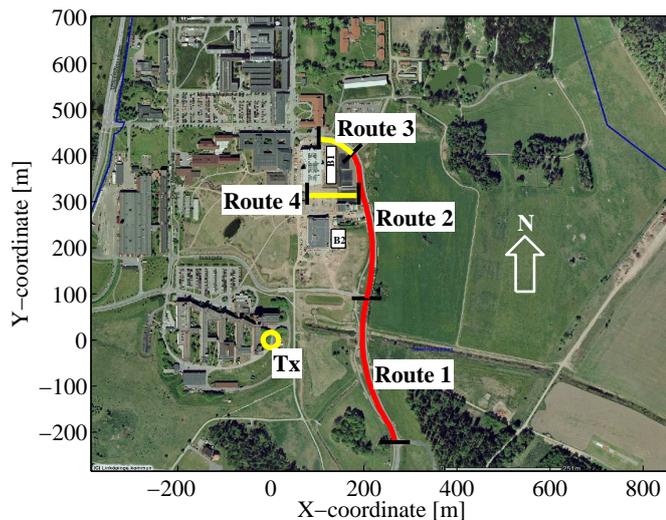
Figure 1: Overview of the measurements area at the campus of Linköping
University, Sweden. The transmitter with coordinate (0, 0) was placed near
the building, and the receiver was moved along the marked routes 1-4. B1 and
B2 represent two new buildings which were not present at the time the picture
was taken.

frequency of 285 MHz, with a bandwidth of 20 MHz, which is smaller than the
antenna bandwidth, and an output power of 43 dBm. The sounding signal is a
periodically repeated sequence with a length of 12.8 μs and the guard interval
between the repetitions is 12.8 μs. In the measurements, we used a wheel trigger
on the car to control the snapshot distance, which is approximately 0.97 m and
corresponding to 0.92 λ, where λ is the wavelength at the center frequency of
285 MHz.[1] This snapshot distance is also used in Sec. 4. At each trigger event,
one data block of 4 channel snapshots is recorded and averaged into a single
snapshot to increase the signal-to-noise ratio (SNR). The channel is assumed
to be approximately stationary over 4 consecutive snapshots, an assumption
that is verified. Due to practical constraints, all measurements were performed
using vertical polarization only. One should be aware of the limitations of the
parameter estimates from such a setup [12], and we have made every effort to
validate the directional estimates using 3-dimensional maps and photos of the

---

[1]Snapshots with distance 0.115 λ were actually measured, but every 8th snapshot is used
for further parameterization analysis.

environments.

By using the SAGE algorithm [13], MPCs with delay, AOA, AOD and complex amplitude were estimated from the measured transfer function matrices. From the analysis in [7], it can be seen that there are line-of-sight (LOS) conditions for most parts of routes 1 and 2, but occasionally with small obstacles blocking the LOS. Routes 3 and 4, on the other hand, are completely non line-of-sight (NLOS). In the following investigations, routes 1 and 2 are processed together and named group 1. This group is mostly LOS and partially obstructed LOS. Similarly, routes 3 and 4 are named group 2 and this group is completely NLOS.

3   Clustering and Tracking Method

Since the COST 2100 channel model is based on the concept of clusters, a joint clustering and tracking algorithm [14] is used to identify clusters and determine their time-variant properties from the measurements. The KpowerMeans clustering algorithm [15] is implemented to cluster each temporal snapshot of the channel, while a Kalman filter [16] is designed to track clusters from snapshot to snapshot. Previous research [17] has shown that the cluster time-variant behavior can be obtained with this joint algorithm.

MPCs extracted by the SAGE algorithm are used as the input to this joint clustering and tracking algorithm. In the first step, the KpowerMeans clustering algorithm performs clustering based on the values of the delay, AOD, AOA and power of each MPC from one measured snapshot. Each cluster is characterized by its centroid position, which is determined by cluster delay, cluster power, cluster AOD, and cluster AOA, as well as by its intra-cluster spreads, including cluster delay spread, cluster AOD spread, and cluster AOA spread. The identified clusters for a particular snapshot are known as current clusters. In the next step, a Kalman filter is applied to track the clusters over different snapshots. Based on the current clusters and clusters from the previous snapshot, the Kalman filter provides a prediction of the cluster centroids for the next snapshot and its state is also updated. If possible, the current clusters are associated with those from the previous snapshot and are then regarded as tracked clusters. Otherwise, untracked clusters in the previous snapshot are regarded as dead, and untracked clusters in the current snapshot are considered as new-born clusters. In this way, we could obtain the time-variant properties of clusters.

The number of MPCs extracted with the SAGE algorithm is 200 for each snapshot; MPCs with a power 30 dB lower than the peak power are discarded from further analysis. To ensure tracking stability, a sliding window with a

length of 2 snapshots is chosen [14]. A 1% cluster power threshold is set to
ensure that the identified clusters do not carry less than 1% of the total received
power. In addition, if the power of a tracked cluster never exceeds 2.5% of the
total received power somewhere during its lifetime, this tracked cluster is not
taken into account in the subsequent analysis. By considering the map of the
environments and in order to avoid cluster splitting, the maximum number of
clusters is chosen as 12, which is well above the extracted average number of
clusters, see the results in Sec. 4.2.

4 Channel Model Parameters

In this section, the methodologies for the parameterization are studied in de-
tail. Our goal is to extract the required parameters for the COST 2100 channel
model based on the 300 MHz outdoor measurements. All the extracted param-
eters are listed in Table 1.

4.1 Cluster Visibility Region and Transition Region

Cluster visibility regions are typically assigned to clusters in such a way that
when an Rx is inside a visibility region (VR), the cluster assigned to this
visibility region is active (contributes to the impulse response). The size of a
cluster visibility region is thus linked to the lifetime of a cluster: assuming a
stationary environment, the lifetime of a cluster is determined by the number
of snapshots over which the cluster is sequentially active. The product of the
cluster lifetime and the snapshot distance is called cluster life distance.

There is a general difficulty in extracting the size of cluster visibility regions
from a single measured route. For the measured route, the Rx does not always
go through the center of the cluster visibility regions. We propose a method for
finding the relation between the cluster visibility region radius and the mea-
sured cluster life distance as follows. Assume that the cluster visibility region
is a circle, and the radius of the circular visibility region R is deterministic.
Further assume that the measured route traverses the circular visibility regions
at a random (uniformly distributed) distance D from the respective centers of
the cluster visibility regions. Given this geometry, the length of an intersection
between a measured route and a cluster visibility region is

$$L = \begin{cases} 2\sqrt{R^2 - D^2} & 0 \leq D \leq R, \\ 0 & \text{otherwise.} \end{cases} \tag{1}$$

Now, the average cluster life distance is

$$\Gamma \triangleq E\left[L\right] = \int_0^R 2\sqrt{R^2 - x^2}\, f_D(x)\,\mathrm{d}x, \tag{2}$$

where $E[\cdot]$ denotes statistical expectation and $f_D(x)$ is the probability density function for D. By solving the integral in (2) for a uniformly distributed D, $0 \le D < R$, we obtain

$$\Gamma = \frac{\pi}{2}R, \tag{3}$$

where the factor $\frac{\pi}{2}$ is defined as compensation factor between the cluster visibility region radius R and the average cluster life distance Γ.

We group the measurements into two categories. The measured scenario of group 1, with routes 1 and 2, is categorized as a semi-rural environment where some scatterers have contributed to the impulse response for a long time, which leads to longer cluster life distances, and thus larger cluster visibility region radii. The measured scenario of group 2, with routes 3 and 4, on the other hand, is categorized as a sub-urban area. Scatterers can be blocked more often in this group, and thus smaller cluster visibility region radii are observed. Fig. 2 shows the distributions of the cluster visibility region radii for the two groups. Most of the visibility region radii are in the range of 10 to 100 m (approximately 10 to 100 λ). The average cluster visibility region radii for groups 1 and 2 are 32.8 and 24.5 m, respectively.

The cluster visibility region is modeled as a circle, where the cluster is active, with radius R. Centered in this circle is an effective area, a circle with radius r, where the cluster power exceeds a level of 6 dB below its maximum [18]. There is a smooth transition, from the border of the effective area to the border of the active area, taking place in the so-called cluster transition region. The size of the transition region is determined as $T = R - r$, and the extracted sizes of the transition regions are 16.8 m and 12.2 m for groups 1 and 2, respectively.[2]

4.2 Number of Clusters and Average MPCs per Cluster

There are two kinds of clusters in the channel model: local clusters and far clusters. Usually a local cluster occurs around the Rx. In our measurements, there is one active cluster which is visible along most of the snapshots for the two groups. At the same time, we notice that the distance between this cluster centroid and the Tx is larger than the distance from the cluster centroid to the Rx. In addition, often there is a larger cluster angular spread at the Rx

---

[2]r is extracted in a similar way to R.
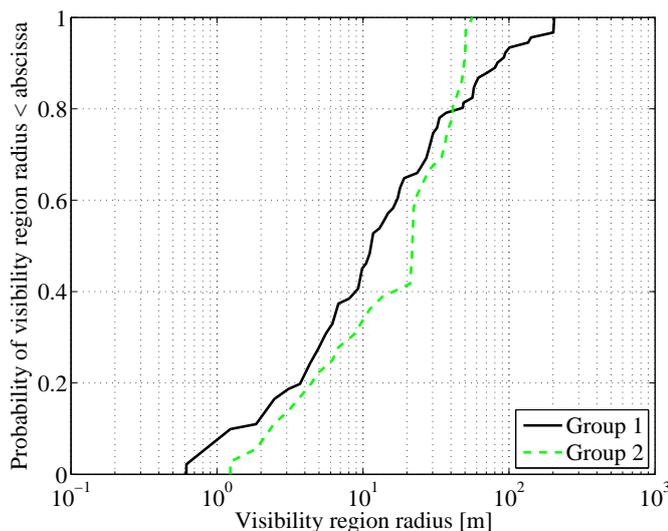
Figure 2: Distributions of the extracted cluster visibility region radii for the
two groups.

side, compared to the Tx side. These observations indicate that we observe an
Rx local cluster in the two measured groups. Far clusters are defined as any
clusters that are not local clusters. On average, approximately 6 far clusters
(N_c) are active for both groups 1 and 2.

Each cluster contains a few MPCs, and the average number of MPCs per
cluster (N_{MPC}) is extracted as the ratio between the total number of MPCs
and the number of clusters in each snapshot. There are approximately 27 and
48 MPCs per cluster for groups 1 and 2, respectively. For group 2, there are
generally more scatterers in the environment, which leads to a larger number of
MPCs per cluster, compared to group 1. Here, it should be noted that specular
components and dense multipath components [19] are not separated, and all
MPCs are considered as specular components.

4.3   Single-bounce and Multiple-bounce Clusters

Besides local clusters and far clusters, single-bounce and multiple-bounce clus-
ters are also distinguished in the channel model. Here, we suggest classifying
the clusters using their geometric properties. First, we take a look at the AOA
and AOD of a cluster and determine whether a ray from the Tx in the clus-
ter AOD direction and a ray from the Rx in the cluster AOA direction can

meet each other. If there is no valid intersecting point between the two rays, a multiple-bounce cluster is observed. With a valid intersecting point, we also analyze the total traveling time of these two rays. The traveling time from the Tx to the cluster centroid is τ_{Tx} and from the Rx to the cluster centroid is τ_{Rx}. Theoretically, the difference between the total traveling time of the two rays and the cluster delay τ_{delay} should be zero for a single-bounce cluster, but with the measured results, a threshold larger than zero has to be used. The threshold here is set as two times the cluster delay spread τ_{ds}, since we allow one delay spread offset from both the Tx and Rx sides. In other words, if a valid intersecting point between rays from the Tx and the Rx sides is obtained, and $|\tau_{\mathrm{Tx}} + \tau_{\mathrm{Rx}} - \tau_{\mathrm{delay}}| < 2\tau_{\mathrm{ds}}$ is satisfied, a single-bounce cluster is observed, otherwise it is classified as a multiple-bounce cluster. The relation between the number of single-bounce clusters N_{SB} and the number of multiple-bounce clusters N_{MB} is characterized by the cluster selection factor K_{sel},

$$K_{\mathrm{sel}} = \frac{N_{\mathrm{SB}}}{N_{\mathrm{MB}} + N_{\mathrm{SB}}}. \tag{4}$$

The extracted cluster selection factors are 0.1 and 0.2 for groups 1 and 2, respectively. We conjecture that these low K_{sel} factors are due to the fact that the measured scenario is peer-to-peer, where the Tx and Rx are only around 2 m above ground, and both surrounded by scatterers along most of the measured routes.

The concept of cluster link delay is introduced in conjunction with the multiple-bounce clusters. The cluster link delay τ_{link} is calculated as $|\tau_{\mathrm{Tx}} + \tau_{\mathrm{Rx}} - \tau_{\mathrm{delay}}|$. Hence, for a single-bounce cluster, there is no cluster link delay. The cluster link delay is modeled as an exponential distribution, with its mean and minimum value [2]. Since we use $2\tau_{\mathrm{ds}}$ as our threshold when distinguishing single/multiple-bounce clusters, the cluster link delay for multiple-bounce clusters never goes below $2\tau_{\mathrm{ds}}$. The extracted average cluster link delays are 0.9 and 1.1 μs with minimum values of 0.048 and 0.052 μs for groups 1 and 2, respectively.

4.4   LOS Parameters

The LOS component is extracted, based on the AOA, and AOD of the MPC with the strongest received power. In theory, the LOS component should have a matched pair of AOA and AOD and also the strongest power. However, due to uncertainties in vehicle positions and estimation errors of MPC parameters, there might be an offset in the measured AOA and AOD. Here, a maximum 10 degrees mismatch for the AOA and AOD is allowed. In other words, when

the mismatch between AOA and AOD of the MPC with the strongest power
is smaller than 10 degrees, this MPC is determined as a LOS component.

The size of the LOS visibility region is extracted based on the appearance of
the LOS component. When the power of the LOS component goes 6 dB below
the maximum LOS power during its lifetime, it enters the transition region
where it stays until it disappears. The transition region of the LOS component
is defined as the duration between the transition starting and ending points.
For group 1, the LOS component exists for almost the whole Rx traveling
route; 343 m is observed as the averaged LOS visibility region radius (R_{LOS})
and 93 m as the averaged LOS transition region radius (T_{LOS}). There is no
LOS component in group 2 so the sizes of LOS visibility and transition regions
are set to zero.

The relation between the power of the LOS component and the other MPCs
is denoted as LOS power factor [1],

$$K_{\text{LOS}} = \frac{P_{\text{LOS}}}{P_{\text{tot}} - P_{\text{LOS}}}, \tag{5}$$

where P_{LOS} is the power of the LOS component and P_{tot} is the total power for
MPCs. The observed mean K_{LOS} factor is -4.7 dB for group 1 with a variance
of 2.0 dB. In group 2, K_{LOS} is zero since it is a NLOS scenario.

4.5   Cluster Power Model

The cluster power P_{i_c} of the i_cth cluster, is modeled as [1]

$$\begin{aligned}
P_{i_c} = P_0 \max\{&\exp(-k_\tau(\tau_{i_c} - \tau_0)), \\
&\exp(-k_\tau(\tau_{\text{cutoff}} - \tau_0))\}.
\end{aligned} \tag{6}$$

Besides the peak cluster power P_0 factor, there are four more parameters in
this power model. Parameter k_τ is the power attenuation coefficient given in
unit of dB/μs, and is also called cluster power decay factor. τ_{i_c} is the cluster
delay while τ_0 is the delay of the LOS component. They are both in the unit
of μs. The last one is the cut-off delay τ_{cutoff}, with the unit of μs.

The cluster power decay factor is a result of linear regression analysis of
the cluster power versus the cluster delay. The slopes in Fig. 3 describe the
two power decay factors, which are 12.1 and 7.2 dB/μs for groups 1 and 2,
respectively. Moreover, it can be noted that the cluster power has residuals
from the regression lines. The residuals are referred as cluster shadowing com-
ponents, which will be discussed further in Sec. 4.7. The delay of the LOS
component is determined by the distance between the Tx and Rx. The cut-off
delay is determined as the delay where cluster power has decreased 30 dB from
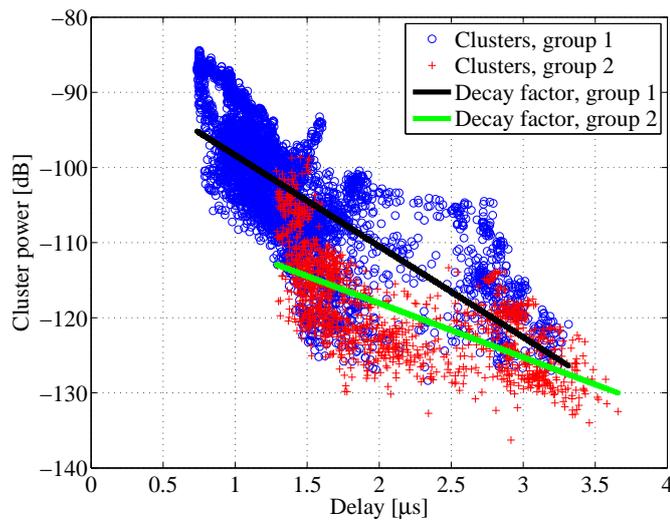
Figure 3: Cluster power decay factor. Scatter plots show the cluster power vs. the cluster delay. The reference level for the cluster power is the Tx power of 43 dBm. The power decay factors are 12.1 and 7.2 dB/µs for groups 1 and 2, respectively.

the maximum cluster power. The power of clusters with delays larger than the cut-off delay is modeled as constant, i.e., at a level 30 dB below the maximum cluster power. From the measurements, cut-off delays of 2.4 and 4.2 µs are observed for groups 1 and 2, respectively.

4.6   Cluster Spreads

Cluster spreads in delay, AOD and AOA determine the shapes of clusters, and are defined as [1]

$$DS_c = \sqrt{\frac{\sum_i^N P_i(\tau_i - \bar{\tau})^2}{\sum_i^N P_i}}, \tag{7}$$

$$AS_c = \sqrt{\frac{\sum_i^N P_i(\varphi_i - \bar{\varphi})^2}{\sum_i^N P_i}}, \tag{8}$$

where DS_c is the cluster delay spread, AS_c is the cluster angular spread and N
is the number of MPCs belonging to each cluster. P_i is the power for the ith
MPC, τ_i is the delay and φ_i is the AOD/AOA of the ith MPC. Furthermore,
$\bar{\varphi}$ and $\bar{\tau}$ are power weighted means calculated as

$$\bar{\tau} = \frac{\sum_i^N P_i \tau_i}{\sum_i^N P_i}, \tag{9}$$

$$\bar{\varphi} = \text{angle}(\sum_i^N P_i \exp(j \cdot \varphi_i)), \tag{10}$$

where j is the imaginary unit. The cluster spreads for a particular cluster are
computed from the set of MPCs that has been associated with that cluster. The
mean value and standard deviation of the extracted cluster spreads are listed
in Table 1, where AS_c^{AOD} defines the cluster angular spread at the Tx side and
AS_c^{AOA} is the cluster angular spread at the Rx side. It can be noted that the
average cluster delay and angular spreads are smaller in group 1 compared to
group 2. The reason is that in group 2, the rich scattering processes around
the Tx and Rx increase the spreads of the clusters. The MPCs from scatterers
near the Rx in group 2 can, for example, have really large angular spread but
are still grouped into one cluster.

4.7   Cluster Shadowing

Clusters experience large-scale fading in a similar way to that of MPCs. The
cluster shadowing is obtained during the process of estimating the cluster power
decay factor, see Sec. 4.5. When the cluster power decay factor is estimated, the
linear regression lines provide an expected cluster power for a certain cluster
delay. The cluster shadowing is defined as the residual between a cluster power
and its expected cluster power [20]. Note, however, that this shadowing is
not necessarily related to the physical effects of partial obstructions of clusters
by other objects. The observed standard deviations of the cluster shadowing
(σ_{Sh_c}) are 2.05 and 2.27 dB for groups 1 and 2, respectively.

4.8   Cross-correlation Coefficients

In order to jointly model cluster spreads and shadowing, the cross-correlation
coefficients of different pairs of the cluster spreads and shadowing are consid-
ered. We estimate the cross-correlation coefficient between a and b as

$$\rho(a,b) = \frac{\sum_k^M (a(k) - \bar{a})(b(k) - \bar{b})}{\sqrt{\sum_k^M (a(k) - \bar{a})^2 \sum_k^M (b(k) - \bar{b})^2}}, \tag{11}$$

Table 1: Extracted parameters from the 300 MHz measurements for the COST 2100 channel model.

Groups	Group 1	Group 2
Radius of visibility region: μ_R[m]	32.8	24.5
Radius of transition region: μ_T[m]	16.8	12.2
Number of far clusters: μ_{N_c}	6	6
Number of MPCs per cluster: $\mu_{N_{\mathrm{MPC}}}$	27	48
Cluster selection factor: $\mu_{K_{\mathrm{sel}}}$	0.1	0.2
Cluster power decay factor: μ_{k_τ}[dB/μs]	12.1	7.2
Cluster cut-off delay: τ_{cutoff}[μs]	2.4	4.2
Radius of LOS visibility region: $\mu_{R_{\mathrm{LOS}}}$[m]	343	0
Radius of LOS transition region: $\mu_{T_{\mathrm{LOS}}}$[m]	93	0
LOS power factor:		
$\mu_{K_{\mathrm{LOS}}}$[dB]	-4.7	0
$\sigma_{K_{\mathrm{LOS}}}$[dB]	2.0	0
Cluster angular spreads:		
$\mu_{AS_c^{\mathrm{AOD}}}$[deg]	14.6	18.6
$\sigma_{AS_c^{\mathrm{AOD}}}$[dB]	2.43	2.02
$\mu_{AS_c^{\mathrm{AOA}}}$[deg]	14.8	19.0
$\sigma_{AS_c^{\mathrm{AOA}}}$[dB]	2.68	2.03
Cluster delay spread:		
μ_{DS_c}[μs]	0.14	0.32
σ_{DS_c}[dB]	3.66	2.05
Cluster link delay:		
$\mu_{\tau_{\mathrm{link}}}$[$\mu$s]	0.85	1.02
$\min_{\tau_{\mathrm{link}}}$[$\mu$s]	0.048	0.052
Cluster shadowing: σ_{Sh_c}[dB]	2.05	2.27
Cross-correlation coefficients:		
$\rho(DS_c, AS_c^{\mathrm{AOD}})$	0.9	0.9
$\rho(DS_c, AS_c^{\mathrm{AOA}})$	0.9	0.9
$\rho(DS_c, Sh_c)$	0.0	-0.1
$\rho(AS_c^{\mathrm{AOD}}, Sh_c)$	0.0	0.1
$\rho(AS_c^{\mathrm{AOA}}, Sh_c)$	0.0	0.1
$\rho(AS_c^{\mathrm{AOD}}, AS_c^{\mathrm{AOA}})$	0.9	0.9

μ denotes expected value, σ denotes standard deviation and min denotes minimum value.

where $\bar{a}$ and $\bar{b}$ are the sample mean of the sets $\{a(k)\}$ and $\{b(k)\}$ with length M, respectively, and all the samples are in logarithmic scale [21]. The results for the extracted cross-correlation coefficients are shown in Table 1. A high correlation always exists between the delay spread and the angular spreads at both the Tx and Rx sides. Meanwhile, the cluster spreads exhibit low correlation with the cluster shadowing.

5   Channel Model Validation

The COST 2100 channel model with parameters from Table 1 is validated by comparing the channel properties of its output with the corresponding measured channel for the outdoor single MIMO link at 300 MHz in this section. Ideally, one should perform validation based on many independent measurements in similar but different environments, but due to the efforts involved in such a task, this is not practically possible. The comparison with the measurements is performed for the following four channel properties: 1) delay spread, 2) spatial correlation, 3) singular value distribution, and 4) antenna correlation.

5.1   Initial Considerations

The channel model has been implemented in MATLAB by Liu *et al.* [22], and this implementation provides a suitable framework for our validation. The input of this framework is based on both external and stochastic parameters. First, the external parameters include parameters such as frequency, and bandwidth. To be directly comparable with the measured data, the center frequency is set to 285 MHz and the channels are generated for a bandwidth of 20 MHz. The simulated area is defined as a cell with a radius of 500 m. Based on the cluster power decay factors derived in Sec. 4.5, we assume that clusters outside this radius will give a negligible contribution to channel responses. The Tx is placed in the cell center and the Rx is moving according to the measured routes. In order to evaluate the details of delay spreads and spatial correlations, channel snapshots are generated for every 0.115 λ movement of the Rx in the simulations. For each simulation run, this sampling distance gives us 5304 simulated snapshots corresponding to the group 1 measurements, and 1570 simulated snapshots corresponding to the group 2 measurements. Besides the external parameters, Table 1 summarizes all the stochastic parameters that are used as the input of the MATLAB framework. Evaluation, using a group of 100 simulation runs, is carried out for further validation, and for each such simulation run, we have simulated channel snapshots from a route similar to the measured one. This means that the number of channel snapshots used for
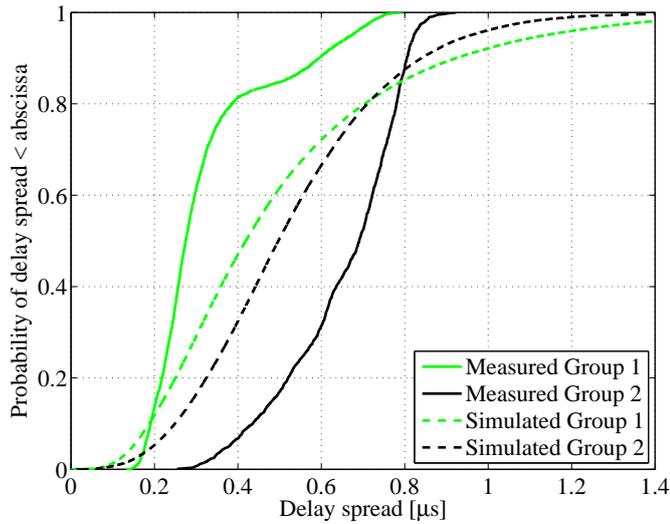
Figure 4: Delay spreads of the measured and simulated omni-direction antenna responses for groups 1 and 2.

validation exceeds 50,000 and 15,000 for groups 1 and 2, respectively, which gives us representative statistics. To verify the latter, another independent 100 simulation runs have been performed. By comparing the distributions of delay spreads, spatial correlation, and singular values, similar results were obtained, indicating that a group with 100 simulation runs is enough.

5.2   Delay Spread

Delay spread is the normalized second-order central moment of the power delay profile, and defined as [23]

$$S_\tau = \sqrt{\frac{\int_{-\infty}^{\infty} P_\tau \tau^2 d\tau}{\int_{-\infty}^{\infty} P_\tau d\tau} - \mu_\tau^2}, \tag{12}$$

where

$$\mu_\tau = \frac{\int_{-\infty}^{\infty} P_\tau \tau d\tau}{\int_{-\infty}^{\infty} P_\tau d\tau}, \tag{13}$$

τ is the delay and P_τ is the corresponding power arriving in the delay interval $[\tau, \tau + d\tau]$. The delay spread shows the frequency selectivity of the channel, and it
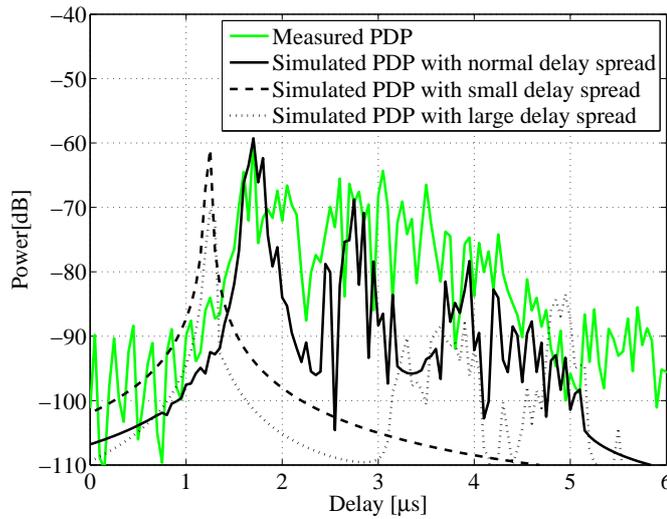
Figure 5: PDP examples. Measured PDP is extracted from a regular channel
under NLOS conditions. Simulated PDPs are for a well represented channel
under NLOS conditions and channels with very small and large delay spreads
under LOS conditions.

is a fundamental validation metric, affecting other validation metrics such as the
singular value distribution. We first compare simulated and measured channels
concerning their respective delay spreads. The comparison is performed for
channel responses with an omni-directional antenna pattern in azimuth. The
delay spreads are computed from the channel power delay profiles (PDPs) by
using a noise threshold of 30 dB below the peak power in each PDP. In addition,
all PDPs are truncated at 6 µs, and it can be assumed that no significant power
will be received after this 6 µs delay.

In Fig. 4, the dashed lines are cumulative distribution functions (CDFs) for
the delay spreads from all simulation runs, and the solid lines are CDFs for
the delay spreads extracted from the measured raw data. Group 1, which has
mostly LOS conditions, shows smaller delay spreads than group 2, which has
NLOS conditions. It can be noted that the CDFs for the simulated channels
start at smaller delay spreads than the corresponding CDFs for the measured
channels. Furthermore, the distributions for the simulated channels have tails
with significantly larger delay spreads than those which can be observed from
the two measured groups. It can also be noted that in the LOS scenario,
the simulated channels result in larger delay spreads, while in the NLOS sce-

nario, the simulated channels show smaller delay spreads for most of the time compared to the measurements. The delay spread differences of the medians between the simulations and measurements are 0.17 and -0.12 μs for groups 1 and 2, respectively. One should note that the measurement area, though we think it is representative for the intended scenarios and that there are differences in the propagation conditions within the area, might not show all possible channel variations when measuring at various places.

To understand the mechanisms behind the observed deviations between the simulated and measured delay spread distributions, we have investigated individual PDPs from simulations and measurements in detail. First, we show an example of a case in which the PDPs of simulated and measured channels agree well, see the two solid curves in Fig. 5. The PDPs indicate channels with rather dense multipath propagation. Next, the two dashed lines in Fig. 5 show examples of PDPs from simulated channels with delay spreads that deviate significantly from what have been observed in the measurements; one of the profiles leads to a very small delay spread, which is smaller than 0.2 μs and the other one causes a very large delay spread, which is larger than 1 μs. The profile leading to the small spread has contributions from only the LOS component and the local cluster, with no far clusters being present. Here, we find a limitation of the COST 2100 channel model when it is applied to outdoor scenarios. In reality, as the measurements indicate, it is not likely to have only one cluster active in an outdoor scenario in a built-up area with a few objects somewhere around Tx and/or Rx, but it can occur in the simulations. In the profile with the large delay spread, a large gap exists between the local cluster and the far clusters. This gap, which causes the delay spread to increase significantly, is observed only in the simulations. In reality, however, the PDP for such a scenario tends to be close to a continuous decay without large gaps. In the channel model, the radius of a cluster is generated according to a log-normal distribution, and thus some small radii exist. As a consequence, the MPCs belonging to the clusters with small radii are squeezed into a small delay region, which causes the gap in the PDP. In conclusion, a truncated log-normal distribution, which takes away the small cluster radii, can provide a better fit for the distribution of delay spreads in an outdoor scenario.

5.3   Spatial Correlation

Spatial correlation describes how the channel varies for a certain distance separation, and the normalized spatial correlation is evaluated for the channel envelope as [23]

$$\rho(\Delta d) = \frac{1}{N_d N_f} \sum_d \sum_f \frac{C(|H(d,f)|, |H(d+\Delta d, f)|)}{\sqrt{C(|H(d,f)|)C(|H(d+\Delta d, f)|)}}, \qquad (14)$$
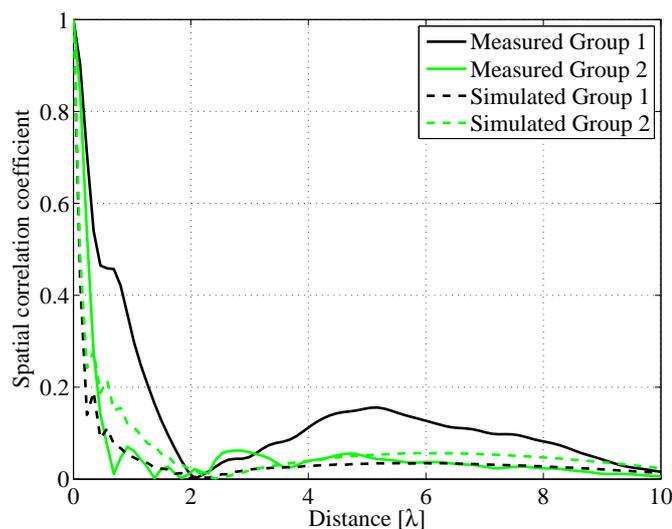
Figure 6: Spatial correlations of the envelope of the channels both in the measurements and simulations.

where f is the frequency, d is the distance of a certain snapshot, Δd is the distance difference between two snapshots, C means the covariance and $|H|$ represents the envelope of the channel, which is achieved from the omni-directional antenna element responses. We choose the envelope correlation since an oscillatory behavior of the averaged complex correlation is observed when the measured route is symmetric relative to the Tx, see routes 1 and 2 in Fig. 1. The symmetric property of the measured route is not representative, but a special case for this particular Tx-Rx arrangement. We investigate the envelope correlation properties for distance differences from 0 to 10 wavelengths. Data subsets with a size of 12 λ are used to maintain wide-sense stationarity (WSS) when evaluating the spatial correlation.

In Fig. 6, it can be noted that the match between the simulations and measurements is good for group 2, but not for group 1. The main deviations are in the region of low correlation, hence not so important. When the spatial correlation coefficient is around 0.5, the corresponding spatial distance differences between the simulations and measurements are only 0.2 and 0.1 λ for groups 1 and 2, respectively. The simulations have high correlation within a quarter of a wavelength, while the measurements show high correlation within half a wavelength. The spatial correlation is mostly determined by the distribution

Table 2: Comparison of mean and standard deviation of the singular values between the simulations and measurements.

Singular values (Ordered)	Group 1 (Sim./Mea.)		Group 2 (Sim./Mea.)	
	Mean [dB]	Std. [dB]	Mean [dB]	Std. [dB]
1	15.7/16.2	1.8/1.4	15.2/15.4	2.3/1.8
2	6.7/4.8	4.3/2.9	7.8/8.2	3.9/2.5
3	0.1/0.4	4.5/2.8	2.5/3.5	4.2/2.7
4	-5.3/-3.6	3.8/2.6	-2.2/-0.8	4.1/2.7

of the AOA spreads of the MPCs. In general, a large angular spread leads to a low spatial correlation. In measured group 1, the MPCs reach the Rx with a small angular spread since the scatterers are located close to the direction of the LOS component; the averaged measured AOA spread is around 39 degrees. As the Rx is moving, the channel is changing slowly. In measured group 2, more scatterers surround the Rx, and an AOA spread of 68 degrees is observed. Compared to group 1, this AOA spread is larger and leads to a lower spatial correlation. In the simulations, on the other hand, the clusters are placed uniformly in the cell; the AOA spread of the simulated MPCs is not controlled, so the two simulated spatial correlations are reduced compared to the values from the measurements. On the other hand, the size of the cluster visibility region also affects the spatial correlation; a longer visibility region radius gives a higher spatial correlation. As described in Sec. 4.1, some clusters have a really large visibility region radii, e.g. the local cluster, though many clusters have a short visibility region radii. An average cluster visibility region radius cannot reflect the real environment well, which in turn leads to the mismatch in the spatial correlation. The variations of the visibility region radius cannot be accurately described solely by an average value and a distribution function is therefore suggested for outdoor environments.

5.4   Singular Value Distribution

The capacity at a fixed mean SNR is strongly dependent on the singular value distribution. The singular value is extracted from the normalized channel frequency response by singular value decomposition. For the simulated channels, 7-by-7 channel transfer functions are generated for the two groups, based on the channel model and measured antenna calibration data. All singular values
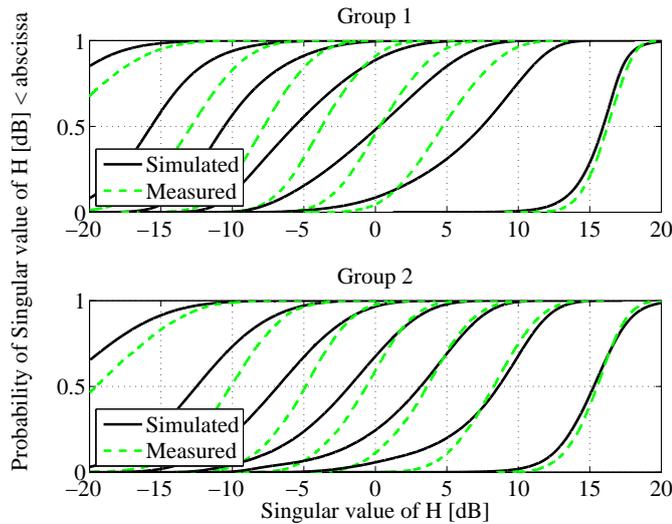
Figure 7: Distributions of ordered singular values of the measured and simulated channel impulse responses.

are evaluated at an SNR of 20 dB for both the simulations and measurements.

The channel model shows good agreement with the measurements in terms of the distributions of the singular values obtained from the channel matrices, and thus, in terms of channel capacity, see Fig. 7. The simulated dominant singular value has a mean of 15.7 dB and standard deviation (std.) of 1.8, while the measured one has a mean of 16.1 dB and a std. of 1.4 for group 1. The second largest singular value also matches well with the measured data in group 1. More numeric results are listed in Table 2. The fourth singular value is nearly 20 dB lower than the largest singular value in each group, and its contribution to the channel capacity is insignificant. It can thus be noted that the channel model provides a good model of the measured channel regarding channel capacity for outdoor measurements.

5.5   Antenna Correlation

Antenna correlation indicates the possible diversity and the richness of the multipath channel in the environment. The correlation coefficient between two

Table 3: Antenna correlations for one simulation run of the group 1 channels.

Tx side (Measured/Simulated)						
1/1	0.3/0.3	0.2/0.2	0.0/0.3	0.0/0.3	0.1/0.1	0.5/0.4
0.3/0.3	1/1	0.4/0.1	0.1/0.3	0.0/0.2	0.1/0.2	0.2/0.2
0.2/0.2	0.4/0.1	1/1	0.3/0.2	0.1/0.1	0.1/0.0	0.1/0.2
0.0/0.3	0.1/0.3	0.3/0.2	1/1	0.3/0.0	0.2/0.2	0.1/0.2
0.0/0.3	0.0/0.2	0.1/0.1	0.3/0.0	1/1	0.5/0.4	0.4/0.3
0.1/0.1	0.1/0.2	0.1/0.0	0.2/0.2	0.5/0.4	1/1	0.5/0.3
0.5/0.4	0.2/0.2	0.1/0.2	0.1/0.2	0.4/0.3	0.5/0.3	1/1
Rx side (Measured/Simulated)						
1/1	0.3/0.2	0.3/0.1	0.1/0.2	0.2/0.1	0.3/0.1	0.6/0.1
0.3/0.2	1/1	0.2/0.1	0.3/0.2	0.1/0.1	0.3/0.2	0.3/0.1
0.3/0.1	0.2/0.3	1/1	0.1/0.2	0.1/0.1	0.4/0.1	0.3/0.1
0.1/0.2	0.3/0.2	0.1/0.2	1/1	0.7/0.1	0.3/0.2	0.2/0.1
0.2/0.1	0.1/0.1	0.1/0.1	0.7/0.1	1/1	0.4/0.2	0.1/0.1
0.3/0.1	0.3/0.2	0.4/0.1	0.3/0.2	0.4/0.2	1/1	0.1/0.1
0.6/0.1	0.3/0.1	0.3/0.1	0.2/0.1	0.1/0.1	0.1/0.1	1/1

antennas is calculated according to

$$\rho_{12} = \frac{E\{H_1 H_2^*\}}{\sqrt{E\{H_1 H_1^*\} E\{H_2 H_2^*\}}}, \tag{15}$$

where H_1 and H_2 represent the channel response from two antennas, $E\{\cdot\}$ is the expectation operator over all the possible samples of H_1 and H_2, and $*$ represents the Hermitian transpose. The correlation coefficients for different antenna element offsets are extracted from the measured and simulated channel frequency responses by clockwise and counter-clockwise shifting of antenna elements. A sliding window of length 20 λ is used to ensure that we remain in a WSS region when evaluating the antenna correlation. Here, we only show the 7-element UCDA antenna correlation coefficients by using one simulation run over the area. Otherwise, over many simulation runs, the antenna correlation will finally become low due to the uniform cluster distribution in the channel model.

Table 3 summarizes the averaged absolute values of the complex correlation coefficients over different WSS regions for one simulation run of group 1 channels at both the Tx and Rx sides. The root-mean-square-errors (RMSE) between the measured and simulated antenna correlation are 0.1 and 0.2 for the Tx and Rx side, respectively. It can be noted that at the Tx side, better

agreement between the simulations and measurements is achieved compared to
the case at the Rx side. In the measurements, group 1 has a LOS component
and the AOA spread of the MPCs is only 39 degrees, which leads to the high
antenna correlation at the Rx side. In the simulations, however, the clusters
are placed uniformly in the cell which causes the large angular spread at the
Rx side, and leads to the lower Rx antenna correlation. Similarly, the RMSE of
antenna correlation at the Tx side is 0.3 while 0.1 at the Rx side for one simu-
lation run of the group 2 channels, which means larger differences are observed
at the Tx side. The measured angular spread at the Tx side is small, and most
of the MPCs stem from the trees and buildings in the upper north direction,
see Fig. 1, thus a high antenna correlation is observed from the measurements.
However, in the simulations, the uniformly distributed clusters decrease the
antenna correlation, which leads to the large RMSE at the Tx side. In general,
when the measured AOD or AOA are close to being uniformly distributed, a
good match is achieved with respect to the antenna correlation, but when the
angular spread is limited by the environment (the close building in our case)
the antenna correlation can be underestimated in the simulations.

6   Conclusion

The COST 2100 channel model framework is a good platform for realistic
MIMO simulations. Parameterization and validation of the channel model for
the scenarios of interest are necessary to get realistic and representative results.
In this paper, we parameterize and validate the channel model for outdoor envi-
ronments based on channel measurements at 300 MHz. Table 1 summarizes the
stochastic parameters of the outdoor MIMO measurements at 300 MHz. These
parameters provide a basis for the usage of the channel model in outdoor envi-
ronments. By applying the extracted parameters to the COST 2100 MATLAB
channel model, we perform validation by four means: delay spread, spatial
correlation, singular value distribution and antenna correlation. The spatial
correlation shows high similarity within a quarter of a wavelength between the
simulations and measurements. Similarly, the singular value distributions for
the three dominant eigenvalues also show good agreement. Regarding the de-
lay spreads, some mismatch occurs for the two investigated groups, one has
0.17 µs difference and the other has -0.12 µs difference for the delay spread dif-
ferences of the medians. Antenna correlation shows good agreement between
the simulations and measurements, when there are uniformly distributed scat-
terers around the antennas. Otherwise, there might be some mismatch. In
addition, the validation processes also provide a deep insight of the channel
model behavior for outdoor environments.

Table 4: Suggested modifications of the COST 2100 channel model for a 300 MHz outdoor scenario.

Parameters	In the model	Suggested modifications
Cluster delay spread	log-normal	truncated log-normal
Cluster visibility region	mean	mean and variance

In general, the COST 2100 channel model works well for representing the 300 MHz outdoor scenario, however, not all the properties show good agreement. We suggest that with the modifications of the distribution of cluster delay spreads, and cluster visibility regions in the channel model, see Table 4, better results can be obtained. The channel model also enables multi-link MIMO modeling, and studies related to multi-link will be carried out in the future.

Acknowledgments

References

[1] L. M. Correia, "The COST 273 MIMO channel model," in *Mobile broadband multimedia networks*, 1st ed., Jordan Hill, Oxford, U.K.: Academic Press, 2006, pp. 364-384.

[2] R. Verdone and A. Zanella, "Radio channel modeling for 4G networks," in *Pervasive mobile and ambient wireless communications: COST Action 2100 (signals and communication technology)*, 1st ed., London: Springer, 2012, pp. 67-148.

[3] J. Poutanen, F. Tufvesson, K. Haneda, V. Kolmonen and P. Vainikainen, "Multi-link MIMO channel modeling using geometry-based approach," *IEEE Trans. Antennas Propagat.*, vol. 60, no. 2, pp. 587-596, Feb. 2012.

[4] L. Liu, J. Poutanen, F. Quitin, K. Haneda, F. Tufvesson, P. De Doncker, P. Vainikainen and C. Oestges, "The COST 2100 MIMO channel model," *IEEE Wireless Commun...*, to be published.

[5] J. Poutanen, K. Haneda, L. Liu, C. Oestges, F. Tufvesson and P. Vainikainen, "Parameterization of the COST 2100 MIMO channel model in indoor scenarios," in *Proc. European Conf. on Antennas and Propagat.*, Rome, Italy, 2011, pp. 3603-3610.

[6] K. Haneda, J. Poutanen, L. Liu, C. Oestges, F. Tufvesson and P. Vainikainen, "Comparison of delay and angular spreads between channel measurements and the COST 2100 channel model," in *Proc. Loughborough Antennas and Propagat. Conf.*, Loughborough, U.K., 2010, pp. 477-480.

[7] G. Eriksson, F. Tufvesson, and A. F. Molisch, "Propagation channel characteristics for peer-to-peer multiple antenna systems at 300 MHz," in *Proc. IEEE Global Commun. Conf.*, San Francisco, USA, 2006, pp. 1-6.

[8] K. Wiklundh and G. Eriksson, "A study of the capacity for different element spacing on compact MIMO platforms," in *Proc. Personal, Indoor and Mobile Radio Commun.*, Cannes, France, 2008, pp. 1-5.

[9] R. S. Thomä, D. Hampicke, A. Richter, G. Sommerkorn and U. Trautwein, "MIMO vector channel sounder measurement for smart antenna system evaluation," *European Transactions on Telecommunications*, vol. 12, no. 5, pp. 427-438, Sep./Oct. 2001.

[10] RUSK channel sounder – Measurement principle. [Online]. Available: http://www.channelsounder.de/ruskchannelsounder.html.

[11] G. Eriksson, S. Linder, K. Wiklundh, P. Holm, P. Johansson, F. Tufvesson and A. Molisch, "Urban peer-to-peer MIMO channel measurements and analysis at 300 MHz," in *Proc. IEEE Military Commun. Conf.*, San Diego, CA, USA, 2008.

[12] M. Landmann, M. Käske and R. S. Thomä, "Impact of incomplete and inaccurate data models on high resolution parameter estimation in multidimensional channel sounding," *IEEE Trans. Antennas Propagat.*, vol. 60, no. 2, pp. 557-573, Feb. 2012.

[13] B. H. Fleury, M. Tschudin, R. Heddergott, D. Dahlhaus and K. Ingeman Pedersen, "Channel parameter estimation in mobile radio environments using the SAGE algorithm," *IEEE J. Select. Areas Commun.,* vol. 17, no. 3, pp. 434-450, Mar. 1999.

[14] N. Czink, R. Tian, S. Wyne, F. Tufvesson, J. P. Nuutinen, J. Ylitalo, E. Bonek and A. F. Molisch, "Tracking time-variant cluster parameters in MIMO channel measurements," in *Proc. China Commun. Conf.*, Shanghai, China, 2007, pp. 1147-1151.

[15] N. Czink, P. Cera, J. Salo, E. Bonek, J. Ylitalo and J. P. Nuutinen, "A framework for automatic clustering of parametric MIMO channel data including path powers," in *Proc. Veh. Technol. Conf.*, Montreal, Canada, 2006, pp. 1-5.

[16] S. M. Kay, "Kalman filters," in *Fundamentals of Statistical Signal Processing, Estimation Theory*, 1st ed., Upper Saddle River, NJ, USA: Prentice Hall, 1993, pp. 419-476.

[17] N. Czink, R. Tian, S. Wyne, G. Eriksson, T. Zemen, J. Ylitalo, F. Tufvesson and A. F. Molisch, "Cluster parameters for time-variant MIMO channel models," in *Proc. European Conf. on Antennas and Propagat.*, Edinburgh, U.K., 2007, pp.1-8.

[18] H. Asplund, A. A. Glazunov, A. F. Molisch, K. I. Pedersen and M. Steinbauer, "The COST 259 directional channel model-part II: macrocells," *IEEE Trans. Wireless Commun.*, vol. 5, no. 12, pp. 3434-3450, Dec. 2006.

[19] J. Poutanen, J. Salmi, K. Haneda, V. Kolmonen and P. Vainikainen, "Angular and shadowing characteristics of dense multipath components in indoor radio channels," *IEEE Trans. Antennas Propagat.*, vol. 59, no. 1, pp. 245-253, Jan. 2011.

[20] S. Wyne, A. F. Molisch, G. Eriksson, P. Almers, J. Karedal and F. Tufvesson, "Outdoor-to-indoor office MIMO measurements and analysis at 5.2 GHz," *IEEE Trans. Veh. Technol.*, vol 57, no. 3, pp. 1374-1386, May 2008.

[21] A. Algans, K. I. Pedersen and P. E. Mogensen, "Experimental analysis of joint statistical properties of azimuth spread, delay spread, and shadow fading," *IEEE J. Select. Areas Commun.*, vol. 20, no. 3, pp. 523-531, Apr. 2002.

[22] L. Liu, N. Czink and C. Oestges, "Implementing the COST273 MIMO channel model," in *Proc. NEWCOM-ACoRN Joint Workshop 2009*, Barcelona, Spain, 2009.

[23] A. F. Molisch, *Wireless Communications*, 2nd ed., Chichester, West Sussex, U.K.: Wiley, 2005.

Paper IV

Correlation Properties of Large Scale Parameters for 2.66 GHz Multi-site Macro Cell Measurements

Multi-site measurements for urban macro cells at 2.66 **GHz are performed with three base stations and one mobile station. The autocorrelation distance properties of large scale parameters for each link are analyzed, intra-site correlation of large scale parameters is also evaluated. By comparing these properties with the corresponding parameters from the COST 2100 and WINNER II models, we can see the measured autocorrelation distance of the shadow fading has similar properties as in the two models as well the autocorrelation distance of delay spread. The shadow fading and delay spread are negatively correlated in each link and match the two models well. In order to analyze the correlation properties of large scale parameters, we split up the routes into subsets, where it can be assumed that wide-sense stationarity (WSS) applies. Based on the WSS subsets, we can see that large scale parameters can be correlated, also when two BSs are far away from each other. In those cases the correlation of different links tends to be positively correlated when both base stations are in the same direction compared to the movement of the MS, otherwise the two links will be negatively correlated. We also can see that the cross-correlation between large scale parameters for different links usually have opposite signs.**

1 Introduction

In order to make realistic wireless channel models, lots of measurements are required so that parameters for channel models such as the COST 2100 [1], WINNER II [2] can be extracted. Among these parameters, there are so called large scale parameters describing the main characteristics of the environment, such as shadow fading, angular spread and delay spread. In the literature, many investigations of the shadow fading correlation in a single MIMO link can be found. In [3], the autocorrelation of shadow fading is modeled as an exponential function of the distance. The joint correlation properties of angular spread, delay spread and shadow fading is investigated in [4]. The two recent models also include all these correlation properties between the large scale parameters, but usually these parameters are studied for the single MIMO link. Due to the use of base station cooperation, the behavior of multi-site MIMO wireless channels become more and more interesting as well. Often it is assumed that there is no correlation between two links if the two links are far away from each other [5]. In [6] the cross-correlation of shadow fading for separate base stations is discussed and substantial correlation for closely located base station is found, but still not enough measurements are performed to form a generic model. In [7], it was found that the shadow fading can be correlated also for widely separated base stations in the indoor case. Recently, in [8] the cross-correlation properties for large scale parameters between different links in an outdoor scenario is studied from measured data, but there is no consideration about the wide-sense stationary region for the large scale parameters. If the large scale parameters in two non-WSS regions, then it is unfair to evaluate the correlation properties. Willink analyzed WSS regions based on the first and second moments of the data series for the MIMO radio channels [9]. There it can be seen that a homogeneous building has high possibility to get larger WSS regions. However, the parking lot between homogeneous buildings will interrupt the WSS regions.

In this paper, multi-site measurements with three base stations are analyzed where the three base stations are far away from each other. We propose a WSS region definition based on a map and the environments as well as the WSS time estimation and local scattering function. The correlation properties of large scale parameters are investigated both for each link and between different links in a urban macro scenario based on small WSS subsets. The autocorrelation distance and cross-correlation of each link are evaluated and compared with the corresponding values in the COST 2100 and WINNER II models. The correlation between different links provide a basis to model the cross-correlation in different links when base stations are separated.

This paper is organized as follows: In section II, a short introduction to the
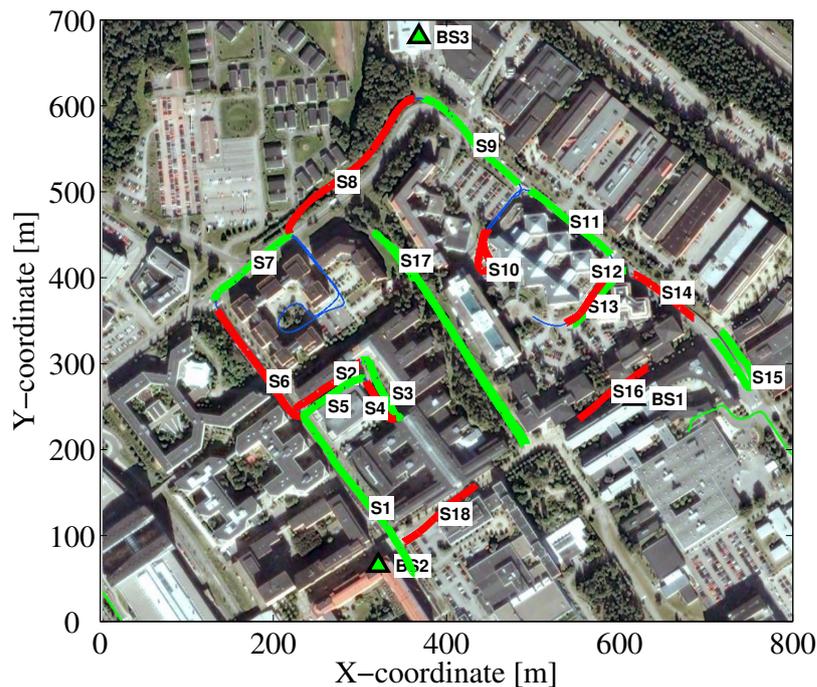
Figure 1: Subsets of measured routes.

measurement campaign and data processing are given. Large scale parameter estimation is discussed in section III. Section IV presents an analysis of the autocorrelation distance for the large scale parameters for each link. Section VI gives a deep analysis for the large scale parameters correlation properties when the routes are divided into small WSS subsets. Finally the conclusions are given in section VII.

2   Multi-site Measurement Campaign and Data Processing

2.1   Measurement Campaign

The measurements were performed in a urban macro cell environment in Kista, Stockholm, Sweden, see Fig. 1. Three base station (BS) sites with one antenna each are used, which are referred as BS1, BS2 and BS3 in the following. At

the mobile station (MS) side two dipole antennas and two loop antennas are
placed on the roof of a measurement van 30 cm from each other. The measured
center frequency is 2.66 GHz with a bandwidth of 20 MHz. The transmit
power of each BS is 0 dBm. The MS traveled along the routes in Fig. 1 and
the GPS positions of the MS were also recorded together with the channel
samples. Along the routes, the links between the BSs and MS experience line-
of-sight (LOS), obstructed line-of-sight (OLOS) and non line-of-sight (NLOS)
conditions. The routes are divided in to 18 small subsets which are called S_i.
The distance between BS1 and BS2 is approximately 354 m, 489 m between
BS1 and BS3, and 617 m between BS2 and BS3. A 4-by-3 MIMO channel
matrix over 432 frequency bins are obtained for each measured snapshot. The
links from the MS to each BSs are called link 1, link 2 and link 3 corresponding
to the index for each BS, respectively.

2.2   Data Processing

In order to extract the large scale parameters in a proper way, we consider
four rules when dividing the subsets for further analysis. First, the NLOS
and LOS scenarios have to be separated. Second if the environments are not
homogeneous we also need to separate the routes into small subsets. For BS2
as an example, S9 and S11 have to be separated, since S9 is in a large open
area without any building in the south west direction whereas S11 will be
shadowed a lot by a building. Third, if the traveling routes are orthogonal we
also need to split them, this applies e.g. to S1 and S2. Finally, the difference
in angle seen from the BS to the routes in a subset can not be too large. The
antenna gain have to be constant over the "sector" considered and the same
main propagation processes should be maintained.

At the same time, a WSS time is estimated according to the methodology
in [10]. The snapshot repetition time is $0.0053\mu s$, and the MS was moving
with velocity of $30km/h$ in average. The estimated WSS region are 75, 99 and
42 meters for three links respectively with the assumption that the correlation
threshold is 0.9. It can be generally said that the WSS region usually with
length around 100 meters which has a good agreement with subsets deviation.
When the traveling routes are orthogonal, a significant change of local scat-
tering function(LSF) will happen, see Fig.2, which well implies the deviation
of orthogonal routes. This change is applied for scenario change as well, Fig.3
show the LSF change from NLOS to LOS.
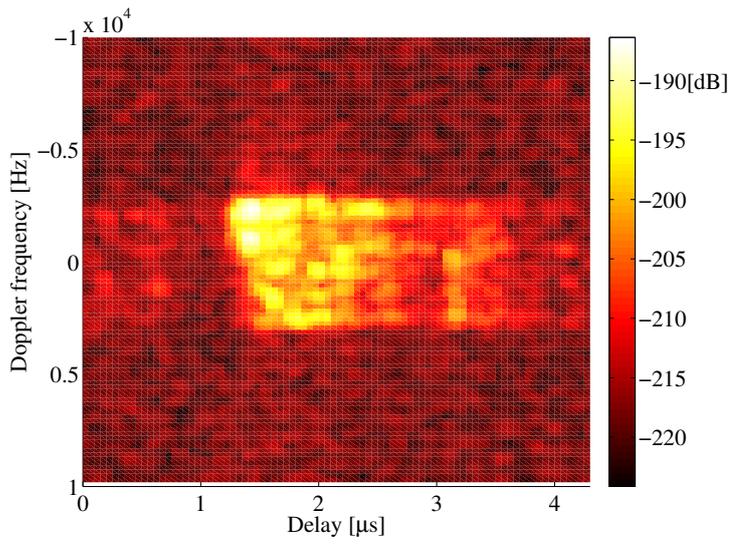
(a) Local scattering function from S2.
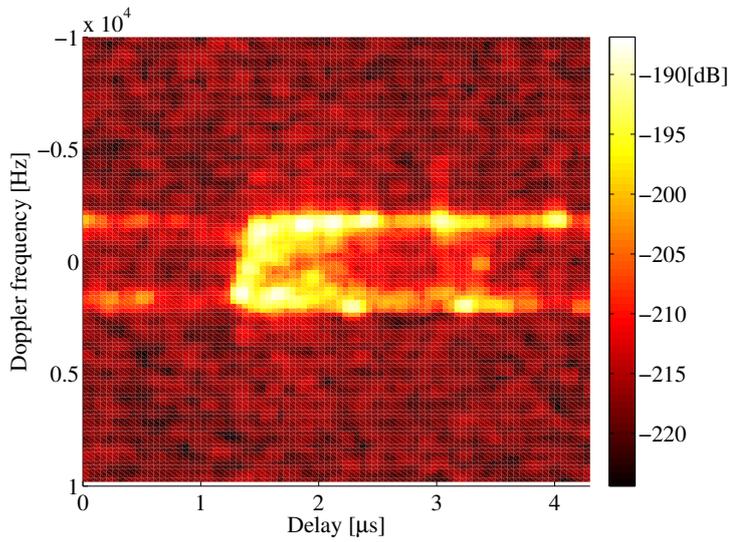
(b) Local scattering function from S3.

Figure 2: Comparison of local scattering function for orthogonal routes.
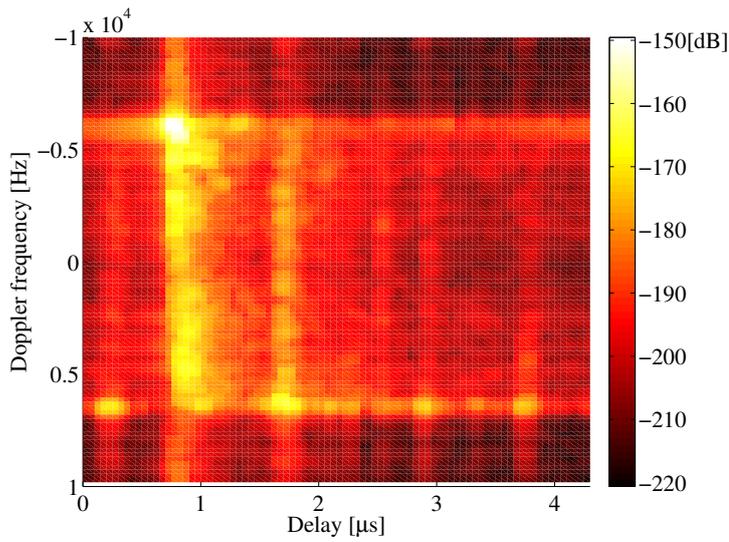
(a) Local scattering function for NLOS.
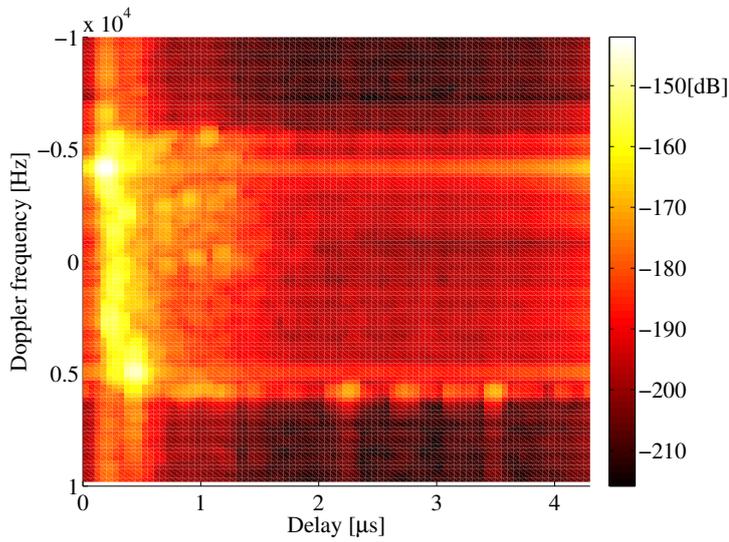
(b) Local scattering function for LOS.

Figure 3: Comparison of local scattering function for NLOS and LOS scenarios.

3   Large Scale Parameter Estimation

The most widely used large scale parameters for wireless channel modeling and analysis are shadow fading, angular spread, cross polarization discrimination and delay spread. In this work two parameters are investigated in detail, shadow fading and delay spread. The antenna arrangements do not allow a straightforward analysis of angular properties.

3.1   Shadow Fading

Shadow fading (SF) is the power fluctuation over a large area where the small scale variations are averaged out. Usually the small scale fading is removed by averaging the received power inside a 10λ window [11]. Then the averaged received power level can be modeled as

$$P(d) = P_0 - n * \log_{10}(\frac{d}{d_0}) + SF(d), \tag{1}$$

where d is the distance, n is the path-loss exponent and P_0 is a reference value at the distance d_0. To determine the shadow fading, a linear regression is performed and the deviation from the linear trend (in the log-domain) is determined.

In Table 1, the shadow fading for the subsets are listed. It can be seen that the path-loss exponents sometimes are negative, see S1 and S9 in link 2. One reason might be in the short route lengths here. The power varied a lot due to obstacles and the path-loss model parameter estimation becomes unreliable. Similarly, if the MS route is below the BS, when the MS and BS are quite close, the shadow might be shadowed by the building where the BS is placed.

3.2   RMS Delay Spread

The RMS delay spread (DS) is estimated based on the power delay profile (PDP) [11]. The PDP is extracted based on a quasi-stationarity time span, and a window with length 10λ is used in this work. The RMS delay spread is estimated in each time span according to:

$$S_\tau = \sqrt{\frac{\Sigma_{i=1}^{N_{bin}} P_h(\tau_i)\tau_i^2}{\Sigma_{i=1}^{N_{bin}} P_h(\tau_i)} - T_m^2}, \tag{2}$$

where

$$T_m = \frac{\Sigma_{i=1}^{N_{bin}} P_h(\tau_i)\tau_i}{\Sigma_{i=1}^{N_{bin}} P_h(\tau_i)} \tag{3}$$

Table 1: Subsets for each link with route length, path-loss exponent n, and
standard deviation of the shadow fading.

(a) Link 1

Subset	Length [m]	n	SF std	Scenario
S1,S3,S4,S6,S17	1145	3.83	4.78	NLOS
S2,S5,S7,S8,S12,S13	697	4.12	3.15	NLOS
S9	150	1.56	2.06	NLOS
S10	110	4.92	2.93	LOS
S11,S14,S15	357	0.23	3.14	NLOS
S16,S18	207	0.23	3.14	LOS

(b) Link 2

Subset	Length [m]	n	SF std	Scenario
S1	230	-0.59	3.34	LOS
S2,S5,S7,S8,S12,S13	697	2.82	4.51	NLOS
S3,S4,S17,S11,S14,S15	1164	3.30	3.63	NLOS
S6	159	4.58	3.35	NLOS
S9	150	-5.34	1,58	NLOS
S10	110	5.43	1.58	NLOS
S16,S18	207	0.03	2.25	LOS

(c) Link 3

Subset	Length [m]	n	SF std	Scenario
S1,S6,S3,S4,S17	1145	7.16	6.40	NLOS
S2,S5,S12,S13,S16,S18	566	8.76	5.73	NLOS
S7,S8	338	0.25	3.20	LOS
S9,S11	270	1.44	5.63	LOS
S10	110	11.06	4.24	LOS
S14,S15	288	6.00	5.32	NLOS

Table 2: Autocorrelation distances comparison.

	Link 1	Link 2	Link 3	COST 2100	WINNER II C2
SF [m] LOS/NLOS	35/56	50/185	90/86	100	45/50
DS [m] LOS/NLOS	28/62	45/40	80/90	100	40/40

and P_h is the PDP for each time span, N_{bin} is the number of delay bins and τ is the delay.

4   Autocorrelation Distances of Large Scale parameters

The large scale parameters do not change within a few wavelengths distance and when the MS is moving, the large scale parameters change slowly. The autocorrelation distance reflects how fast the large scale parameters are changing over the route. The autocorrelation distances of large scale parameters are quite important for channel models such as the COST 2100 and WINNER II models. In the WINNER II model, the autocorrelation distance is supported by measurements and is around 45/50 (LOS/NLOS) meters for the outdoor-to-outdoor scenario. In the COST 2100 model 100 meters is used. In this work, we estimate the autocorrelation distance for each link of the multi-site measurements according to the method in [8]. The autocorrelation distance is calculated by sorting the data into separate groups, with 40 meters between two adjacent groups. Then correlation coefficients are evaluated based on groups with different distances. The autocorrelation distance is defined as the distance when the correlation coefficient decreases to e^{-1}.

In Table 2, the autocorrelation distance are separated into LOS and NLOS. For link 1 and 2, the LOS routes is quite short, the autocorrelation might be underestimated. In link 3 the LOS connection is quite typical, and the value is nearly a good agreement with the COST 2100 model. In the NLOS scenario, all the autocorrelation distance somehow reflect the value in both of the two models, except for one extreme case in link 2.

5   Correlations of Large Scale Parameters

The lager scale parameters describe the wireless channel from different aspects, and they are usually correlated with each other [4]. When there are several

Table 3: Intra-site correlation for all subsets.

Subsets	SF-DS L1	SF-DS L2	SF-DS L3
1	-0.70	-0.71	-0.67
2	-0.50	-0.87	-0.90
3	0.07	-0.22	-0.53
4	-0.82	-0.77	-0.69
5	-0.58	-0.87	-0.91
6	-0.35	-0.77	-0.83
7	-0.66	-0.91	-0.60
8	-0.89	-0.78	-0.43
9	-0.83	-0.45	-0.61
10	-0.37	-0.34	-0.51
11	-0.83	-0.15	0.03
12	-0.26	-0.75	-0.92
13	0.07	-0.60	-0.93
14	-0.80	-0.93	-0.45
15	-0.79	-0.54	-0.68
16	-0.80	-0.28	-0.90
17	-0.81	-0.61	-0.90
18	-0.51	-0.43	-0.58

BSs in the measured environment, the multi-path components from BSs to MS
might have the same traveling route or at least some common traveling route.
It is of interest to investigate these dependencies as they should be included into
the wireless channel models. The large scale parameters in each link are usu-
ally correlated, which is called the intra-site correlation. The cross-correlation
of large scale parameters in different links is called inter-site correlation [8].
Next, we will investigate both intra-site correlation and inter-site correlation
for multi-site measurements in the measured urban macro cell.

Intra-site correlation

The intra-site correlation between shadow fading and delay spread at each link is extracted from the whole MS traveling route according to:

$$\rho\langle a,b \rangle = \frac{\sum_i^N (a(i) - \bar{a})(b(i) - \bar{b})}{\sqrt{\sum_i^N (a(i) - \bar{a})^2 \sum_j^N (b(j) - \bar{b})^2}}, \tag{4}$$

where $\bar{a}$ and $\bar{b}$ are the means of sample sets $\{a(i)\}$ and $\{b(i)\}$ with length N. The correlation coefficient is calculated in the log-domain as in [12] and the shadow fading is calculated based on the subsets in Table 1. The intra-site correlation is included both in the COST 2100 and WINNER II C2 model for the macro cell, with values -0.6 and -0.4 respectively. In Table 3, the correlation coefficient between shadow fading and delay spread for all small subsets are shown. Nearly all have negative values which means that when the shadow fading becomes larger, i.e. -0.87, there is usually a large delay spread. The mean values for all NLOS scenarios is -0.65 and -0.47 for LOS scenario, which more or less match to the COST 2100 and WINNER II models well.

Inter-site correlation

Until now there are not too many studies on the inter-site correlation, the main reason is the lack of multi-site measurements. It is usually assumed that there is no correlation between different links. However inter-site correlation exists and affects on system performance [13]. Here we also investigate the inter-site correlation for the urban macro cell.

The inter-site correlation is evaluated based on the same approach as we generated the groups of subsets, only inter-site correlation of subsets in homogeneous groups are analyzed, see Table 4. Generally the inter-site correlation and cross-correlation have opposite signs, e.g. see S2 and S5, which well reflect the negative intra-site correlation. It also can be seen that if the MS is placed in between two BSs, the link inter-correlation are higher, e.g. S2 and S5 for link 2 and 3.

One interesting thing is that the distance from the MS to BSs and distance of two BSs can't be used to determine the inter-site correlation. For example, S7 and S8 are far away from BS1 and BS2 and a quite small inter-site correlation is observed. S1 and S6 are also far away from BS1 and BS3, but instead a large shadow fading correlation is obtained for these two links. S2 and S5, they are highly correlated with respect to shadow fading and delay spread for link 1 and 3 which are far from the MS and far from each other.

Table 4: Inter-site correlation based on subsets.

(a) Inter-site correlation of Link 1 and 2

Subsets	SF-SF	DS-DS	SF-DS	DS-SF	Scenario
S2,S5	0.31	-0.26	-0.2	0.20	NLOS
S7,S8	0.16	0.05	0.08	-0.22	NLOS
S12,S13	0.48	-0.05	-0.25	0.21	NLOS
S3,S4	0.48	0.21	0.07	-0.51	NLOS
S6	-0.23	-0,39	-0.06	0.50	NLOS
S17	0.62	0.58	-0.43	-0.45	NLOS
S11,S14,S15	-0.11	-0.27	0.09	0.54	NLOS
S16,S18	-0.13	0.51	0.13	-0.03	LOS

(b) Inter-site correlation of Link 1 and 3

Subsets	SF-SF	DS-DS	SF-DS	DS-SF	Scenario
S1,S6	-0.4	-0.06	0.48	0.08	NLOS
S3,S4	0.60	0.05	-0.3	0.08	NLOS
S17	-0.5	-0.78	0.62	0.79	NLOS
S2,S5	0.82	0.26	-0.7	-0.24	NLOS
S12,S13	-0.49	-0.1	0.51	0.07	NLOS
S14,S15	-0.16	-0.19	0.10	0.38	NLOS
S10	-0.31	0.16	-0.06	0.16	LOS

(c) Inter-site correlation of Link 2 and 3

Subsets	SF-SF	DS-DS	SF-DS	DS-SF	Scenario
S3,S4	0.22	-0.04	-0.2	0.07	NLOS
S6	0.16	-0.36	0.13	0.23	NLOS
S17	-0.39	-0,69	0.56	0.71	NLOS
S2,S5	0.59	0.53	-0.63	-0.51	NLOS
S12,S13	-0.08	-0.36	0.16	0.31	NLOS
S14,S15	-0.14	-0.36	0.21	0.49	NLOS

Here, we analyze mainly the NLOS scenario since we do not have enough measurements for the LOS scenario. Only one inter-correlation is given for S16 and S18 in link 1 and 2 which are highly correlated in delay spread and the other for S10 in link 1 and 3 with high negative correlation in shadow fading.

S17 has high inter-site correlation for all links, since S17 is always between two links in our measurements. When we take a look at link 1 and 2, the MS is moving towards both BSs in S17, and then a positive correlation is obtained both shadow fading and delay spread. But for link 1 and 3, and with respect to link 2 and 3, the MS is always moving towards one BS and moving away to the other one, then a negative correlation is obtained. S2 and S5 also have the similar properties in link 1 and 3, high positive inter-site correlation is observed. In general, when the MS is between two BSs and also the main lobe of BSs face to the routes, then a high inter-site correlation often exist even if the BSs are far away from each other. If the MS is moving towards, or away from both BSs, positive inter-site correlations are obtained otherwise negative correlations are obtained.

6   Conclusions

In this paper, the properties of large scale parameters are analyzed and compared to the existing COST 2100 and WINNER II models. The autocorrelation distances for shadow fading and delay spreads more or less agree with the two models. The intra-site correlations from measurements have all negative values, and the average intra-site correlation have a good match with the two models. Another interesting observation is the inter-site correlation between multi-base stations. A study of the inter-site cross-correlation properties, especially for the shadow fading and delay spread, is presented. From the results, we can confirm that the inter-site correlation exists, even when the two links are far away from each other, with high or low correlation coefficients. Sometimes high correlation appeared for the different large scale parameters in different links. The shadow fading has shown negative cross-correlation between different links when the MS is moving towards one BS but away from the other BS. On the other hand, when MS is moving towards both BSs, the shadow fading is positively correlated. Similar behavior was shown for DS-DS inter-site correlations. The inter-site SF-DS cross-correlations have opposite sign since the corresponding intra-site correlations are also negative. It is quite important to include all these properties in wireless channel models. However, more multi-site measurements are needed to make a generic model for these properties and provide more realistic models.

References

[1] L. M. Correia, *Mobile broadband multimedia networks*, Academic press, 2006, pp. 378-383.

[2] IST-4-027756 WINNER II D1.1.2 V1.2. (2008). *WINNER II Channel Models.* [Online]. Available: http://www.ist-winner.org.

[3] M. Gudmundson, "Correlation model for shadow fading in mobile radio system," *IEEE Electron. Lett.*, vol. 27, no. 23, pp. 2145-2146,1991.

[4] A. Algans et al., "Experimental analysis of joint statistical properties of azimuth spread, delay spread, and shadow fading," *IEEE J. Select. Areas Commun.*, vol. 20, pp. 523-531, April, 2002.

[5] D. S. Baum et al., IST-WINNER D5.4. (2005). *Final report on link and system level channel models.* [Online]. Available: http://www.ist-winner.org.

[6] J. Weitzen and T. J. Lowe, "Measurement of angular and distance correlation properties of log-normal shadowing at 1900 MHz and its application to design of PCS system," *IEEE Trans. on Veh. Technol.*, vol.51, no.2, pp. 265-273, 2002.

[7] J. Poutanen, "Analysis of Correlated Shadow Fading in Dual-Link Indoor Radio Wave Propagation," in *COST meeting*, Wien, Austria, Sep., 2009.

[8] N. Jalden et al., "Inter- and intra site correlations of Large-Scale Parameters from Macrocellular Measurements at 1800 MHz," *EURASIP J. on Wireless Commun. and Networking*, vol. 2007, article ID 25757, July, 2007.

[9] T. J. Willink, "Wide-sense stationarity of mobile MIMO radio channels," *IEEE Trans. on Veh. Technol.*, vol.57, no.2, pp. 704-714, 2008.

[10] A. Paier et al., "Non-WSSUS vehicular channel characterization in highway and urban scenarios at 5.2 GHz using the local scattering function," in *Int. ITG Workshop on Smart Antennas (WSA)*, pp. 9-15, Feb., 2008.

[11] A. F. Molish, *Wireless communications*, Wiley, 2006, pp. 65-66.

[12] C. Schneider et al., "Large scale parameter for the WINNER II channel model at 2.53 GHz in urban macro cell," in *Proc. IEEE VTC Spring*, Taibei, May, 2010, pp. 1-5.

[13] N. Jalden, "Analysis and modelling of joint channel properties from multi-site, multi-antenna radio measurements", Ph.D. dissertation, School of Elect. Eng.,KTH, Stockholm, February, 2010.

Paper V

Virtual Multi-link Propagation Investigation of an Outdoor Scenario At 300 MHz

The COST 2100 channel model has introduced the concept of common clusters to model multi-link MIMO characteristics. In this paper, a ray launching tool is used to analyze multi-ink propagation properties in an outdoor scenario at 300 MHz. It is shown that in a multi-link propagation scenario there are shared scatterers among the different links, which reflects the physical existence of common clusters. The identification of common clusters in the measured outdoor scenario is discussed with respect to the shared scatterers and distances between the scatterers and multiple mobile stations (MSs). We observe that, as the MS separation distance is increasing, the number of common clusters is decreasing and the inter-link correlation is decreasing as well. Multi-link MIMO simulations are also performed using the COST 2100 channel model with extracted common cluster parameters. It is shown that the common clusters can represent multi-link properties well with respect to inter-link correlation and sum rate capacity.

1 Introduction

Current geometry-based MIMO channel models, such as COST 2100 [1] and
WINNER II [2], are all based on the concept of clusters. The COST 2100 chan-
nel model supports multi-link simulation by dropping multiple mobile stations
(MSs) and base stations (BSs) in the simulation area. When multiple MSs/BSs
are used, inter-link correlation can have significant effect on the system level
performance [3]. Hence, modeling of inter-link correlation is required. To be
well connected with the previous geometry-based stochastic channel models,
common clusters are introduced in the COST 2100 channel model to model
inter-link correlation. The significance of common clusters has been investi-
gated for indoor environments in [3] to quantify their power contributions to
each link. The common clusters have shown a certain level of significance, es-
pecially for the indoor corridor measurements, where, e.g., wave-guiding can
cause high significance of the common clusters. However, the method of iden-
tifying common clusters is not straightforward in outdoor environments. In
[3], criteria have been introduced for common cluster identification in indoor
environments. When these criteria are applied in an outdoor scenario, their
relevance and validity have to be considered.

In this paper, based on 300 MHz outdoor measurements and a ray launching
tool for outdoor environments, we investigate interacting scatterers for virtual
multi-links, and provide a simple method for identifying common clusters in
outdoor scenarios. The number of common clusters is extracted for both line-
of-sight (LOS) and non line-of-sight (NLOS) scenarios and the significance of
the common clusters is also studied for the considered scenarios. Furthermore,
the observed common cluster ratios are used with the COST 2100 channel
model framework to perform multi-link MIMO channel simulations. We vali-
date the common cluster modeling by means of inter-link correlation and sum
rate capacity.

The remainder of the paper is organized as follows: Sec. II describes the 300
MHz outdoor measurements and the ray launching tool. Sec. III introduces
the method for identifying common clusters in outdoor scenarios. Sec. IV
evaluates the number of common clusters, and significance of common clusters
based on the 300 MHz outdoor measurements. Sec. V validates the common
cluster modeling with the COST 2100 channel model simulations. Finally, the
conclusions in Sec. V complete the paper.
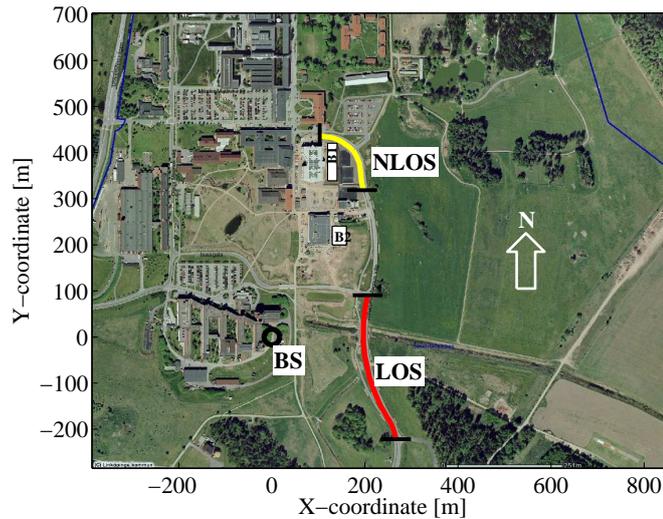
Figure 1: Overview of the measurement area at the campus of Linköping University, Sweden. The BS with coordinate (0, 0) was placed near the building, and the MS was moved along the marked routes with LOS and NLOS conditions. B1 and B2 represent two new buildings which were not present at the time the picture was taken.

2   Visual multi-link Measurements and the Ray Launching Tool

The measurements were performed outdoors on the campus of Linköping University, Sweden, using the RUSK Lund MIMO channel sounder [4]. Identical antenna arrays were used for both the transmitter and the receiver. The antenna arrays are vertically polarized, 7-element uniform circular dipole arrays (UCDA), with one additional dipole element located at the center, in an elevated position [4]. The transmit antenna array was placed 1.8 m above ground, at a static position with coordinate (0, 0) and about 35 m from a large building. The receive antenna array was mounted on a car with its lower ground plane approximately 2.1 m above the ground. The car was driven at a speed of around 8 m/s along the marked routes in Fig. 1. The measurements were carried out at a center frequency of 285 MHz, with a bandwidth of 20 MHz, and an output power of 43 dBm. Since the measured environment is nearly static, different positions of the measured routes can be used as virtual multi-

ple MS positions. LOS and NLOS virtual multi-link scenarios are assumed, see Fig. 1. From the measured transfer function matrices, the properties (delay, angle of arrival (AOA), angle of departure (AOD), and complex amplitude) of multiple-path components (MPCs) were obtained by means of the SAGE algorithm [5].

The used ray launching tool has been developed for visualizing the propagation path of a particular MPC with its AOA, AOD and delay [6]. Similarly, a cluster is characterized by its cluster AOA, cluster AOD and cluster delay, which can thus be visualized in a similar manner as visualizing MPCs. Therefore, the interacting scatterers for the clusters along the propagating paths can be visualized. With these interacting scatterers, the commonality of clusters can be decided based on their geometry properties, which will be further discussed in the next section.

3   Identification of Common Clusters

There are basically two difficulties when identifying common clusters. One is to identify clusters themselves, and the other is to determine the commonality of clusters. A detailed study about cluster extraction by the KpowerMeans algorithm has been carried out in [7]. It has been shown that the resulting clusters can represent the channel in a good manner and reflect the statistics of an environment to a reasonable level. The identified clusters from [7] are used as the basis for further common cluster identification.

With the ray launching tool, the interacting scatterers of the extracted clusters are visualized. If clusters from two links interact with the same scatterer at the BS side, these two clusters have the possibility to form a common cluster. This is, however, not a sufficient condition in outdoor scenarios since the same scatterer can lead to different propagation conditions depending on how the BS and MS see it. On the other hand, different scatterers can lead to similar propagation conditions. For example, a large building can be treated as separate scatterers when the clusters see different parts of the building, that are far away from each other (e.g., two opposite sides of a building). Similarly, when two scatterers are close to each other and also have similar distance to the BS, they can be treated as a single scatterer. In [3], the commonality of clusters has been determined in indoor scenarios by analyzing the distance and angle between them. This method works well in the indoor scenario since the scatterers are within in a small range and the angle limitation between two clusters is an efficient criterion. However, it is difficult to extend this method of identifying common clusters to outdoor scenarios directly since the angle condition in [3] becomes a bit vague. For short ranges, the angle can reflect distance differences

(a) Common when clusters overlap each other.

(b) Common when clusters are close enough.
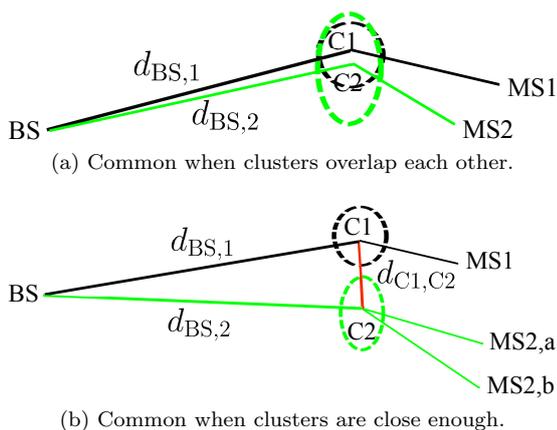
Figure 2: Concept of single interacting common clusters. Single interacting common clusters can have different associated MSs. The ellipses represent clusters.

efficiently, but for larger ranges, a small angle can be caused by scatterers with a large separation distance.

In order to achieve a clear identification of common clusters in outdoor scenarios, the positions of physical objects belonging to a possible common cluster are investigated. First single interacting clusters are studied, see Fig. 2. A typical common cluster is shown in Fig. 2 (a), where the clusters from two links overlap each other. It can also be noted that if the distance between two single interacting clusters is small compared to the distance from the BS to the cluster centroids, these two clusters can be treated as a common cluster since the BS cannot distinguish them, see Fig. 2 (b). At the MS side, no matter where the MS is placed, the commonality of the clusters is not affected. That is because the transmitted signal from the BS contributes to the received signal through the common clusters and gives similar properties in these two links, and there is some degree of correlation between the two links. There is also another type of clusters called multiple interacting clusters, it can be noted that the multiple interacting clusters can reach the MS side in different ways, see Fig. 3 (a) and (b). However, for identifying common clusters, we only consider if the two clusters have similar properties but not how they are seen from the MSs. Again, the commonality of two clusters also depends on the relation between the cluster centroid distance and the distances from the BS to the cluster centroids. With respect to the angle between the two clusters at the BS side, a small angle can be linked to physically highly separated clusters
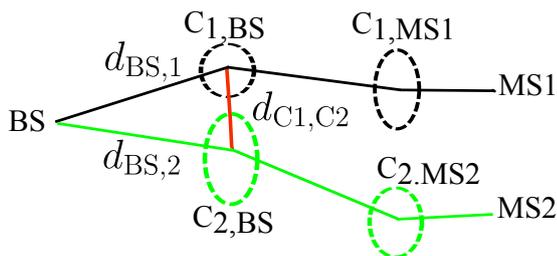
(a) Common when clusters at the receiver side are far
away from each other.
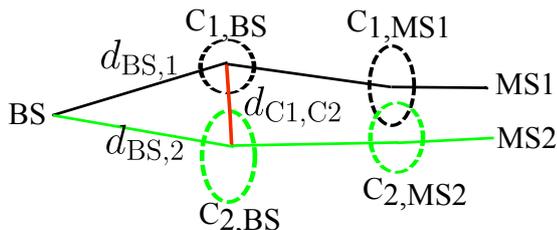
(b) Common when clusters at the receiver side have
overlapping areas.

Figure 3: Concept of multiple interacting common clusters. Multiple interacting cluster can be common no matter how the clusters are seen from the MS side. The ellipses represent clusters.

that are without commonality. The angle condition becomes less important in an outdoor scenario, and hence we focus on the physical distance between the clusters. Thus, we introduce a simple way for identifying common clusters as follows. Assume that the distance from the BS to cluster C1 and C2 are $d_{\mathrm{BS,C1}}$ and $d_{\mathrm{BS,C2}}$, respectively, and that the distance between two clusters is denoted $d_{\mathrm{C1,C2}}$. If the condition

$$\frac{d_{\mathrm{C1,C2}}}{\max(d_{\mathrm{BS,C1}}, d_{\mathrm{BS,C2}})} < \alpha \tag{1}$$

is satisfied, C1 and C2 are said to be a common cluster.

4 Common Cluster Evaluation

By using (1), the number of common clusters with different thresholds of $\alpha = 0.1$ and $\alpha = 0.2$ is evaluated both for the LOS and NLOS scenarios, see Fig. 4.
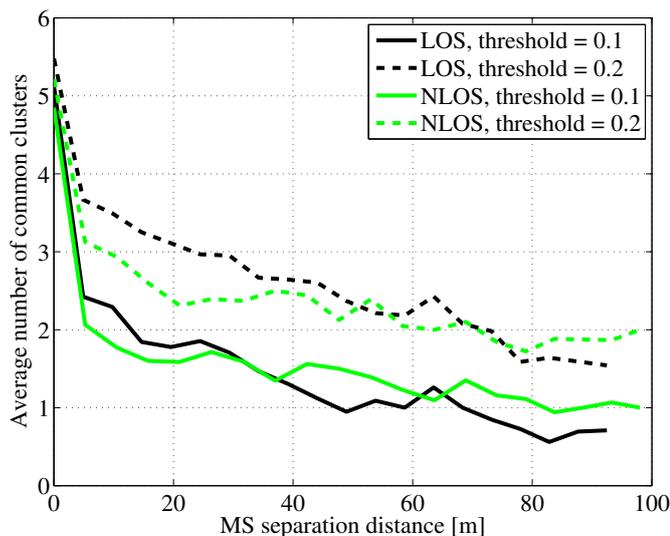
Figure 4: Average number of common clusters for different MS separation distances with different thresholds.

Generally, the extracted number of common clusters gives reasonable values for the considered scenarios. It can be noted that, as the MS separation distance is increasing, the number of common clusters is decreasing and only 1 common cluster is observed at a distance of around 100 meters for both the LOS and NLOS scenarios. At a distance of 20 m, approximately 3 and 2 common clusters are observed on the average for the two thresholds for the LOS scenario, while approximately 2 and 1 common clusters are observed in the NLOS scenario. The threshold influences the number of common clusters to some extent. For the distances between 0 to 5 m, a similar number of common clusters are obtained for the different thresholds. But as the MS separation distance is increasing, a difference of approximately one cluster is observed for different thresholds both for the LOS and NLOS scenarios. It is hard to determine the best threshold precisely, and based on our observations, a threshold of 0.2 is recommended for further analysis.

We also investigate the significance of common clusters, which shows the power contribution to each link from common clusters. The significance is defined as [3]

$$S_{\text{common}}^i = \frac{P_{\text{common}}^i}{P_{\text{tot}}^i} \tag{2}$$
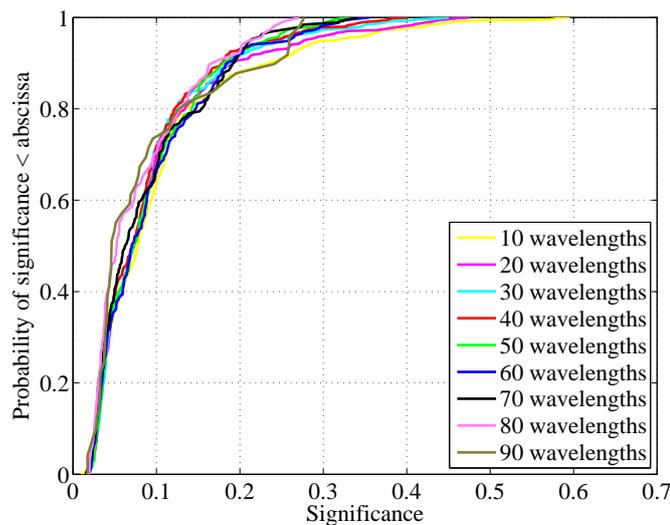
Figure 5: Example of significance of common cluster for different MS separation
distances, threshold = 0.2.

where P^i_{common} is the power for a common cluster in link i, and Pi_{tot} is the sum
of powers of link i. Here the cluster power is given by the total power of the
MPCs belonging to the cluster. The total power is given by the sum of powers
of all MPCs contributing to the link. For the LOS scenario with threshold 0.2,
approximately 10% significance is obtained in average, see Fig. 5. The reason
for this low value is that in the considered outdoor scenario, some clusters that
are not common can have strong power contribution and diminish the signifi-
cance of the common clusters, for example, the large building close to the BS.
When the MS separation distances are small, such as 10 or 20 wavelengths,
the common cluster can in a few cases have around 40% significance. In those
cases, there are some important scatterers that can be seen by the two links at
the same time, such as the trees close to the MS at the beginning of the LOS
route. For the NLOS scenario, the common clusters generally show low signifi-
cance due to the large open sub-urban scenario, approximately 8% significance
is observed in average.

5   Common Cluster Validation

The purpose of introducing common clusters is to model the multi-link MIMO properties. The effects of common clusters on system level characteristics are here analyzed with the COST 2100 MIMO channel model by means of inter-link correlation and sum rate capacity.

5.1   Simulation Considerations

To see the behavior of the COST 2100 channel model with the extracted common cluster ratio, we simulate multi-link MIMO channels with the COST 2100 MATLAB framework implemented by Liu *et al.* [8]. The input to this framework is based on both external parameters (e.g., frequency, bandwidth, scenarios) and stochastic parameters. To be directly comparable with the measured data, the center frequency is set to 285 MHz and the channels are generated for a bandwidth of 20 MHz. The simulated area is defined as a cell with a radius of 500 m, and we assume that clusters outside this cell will give a negligible contribution to channel responses [7]. The BS is placed in the cell center and the MS is moving according to the measured routes. Paper [7] summarizes the required stochastic parameters for the single-link simulations. In addition, common cluster ratios are extracted for different MS separation distances to fulfill the multi-link MIMO simulation requirements, see Table 1. Evaluation of 100 multi-link MIMO simulation runs is carried out for each common cluster ratio and its corresponding MS separation distance, and we have seen that these 100 simulation runs can provide enough statistics [7].

5.2   Inter-link Correlation

The inter-link correlation reflects the similarity between two links, and is defined as

$$\rho(\Delta d) = \frac{1}{N_d N_f} \sum_d \sum_f \frac{C(H(d,f), H(d+\Delta d, f))}{\sqrt{C(H(d,f))C(H(d+\Delta d, f))}}, \qquad (3)$$

where f is the frequency, d is the reference distance for one link, Δd is the separation distance between two links, C is the covariance and H represents the channel transfer function for the centered dipole antenna elements.

First, the measured inter-link correlation between two links and the common cluster ratios for the considered LOS scenario are investigated for different MS separation distances, see Table 1. It can be noted that the measured inter-link correlations and the common cluster ratios show a similar tendency as the MS separation distance is increasing, that is to say that the common clusters

Table 1: Common cluster ratios and inter-link correlations for different MS separation distances for the LOS scenario.

MS separation distance [m]							
5	10	15	20	25	30	35	40
Common cluster ratio							
0.52	0.50	0.46	0.44	0.42	0.42	0.38	0.38
Measured inter-link correlation							
0.61	0.45	0.43	0.35	0.32	0.29	0.26	0.25
Simulated inter-link correlation							
0.75	0.48	0.16	0.14	0.20	0.16	0.10	0.10

well capture the multi-link characteristics and thus seem to be an efficient modeling method for multi-link properties. Furthermore, the simulated inter-link correlations from the COST 2100 channel model for different MS separation distances are also investigated, see Table 1. Also, as the common cluster ratios are decreasing, the simulated inter-link correlations are decreasing in a similar manner, however, the simulated inter-link correlation decreases faster than the measured one after a distance of 20 m. One should note that the simulations provide a statistical evaluation for the considered scenario but do not reproduce the measured route. In short, the common clusters seem to represent the inter-link correlation and interference in a good manner.

5.3   Sum Rate Capacity

The multi-link channel capacity reflects the system level characteristics, and we investigate its behavior as well with the extracted multi-link parameters. The capacity with interference is expressed as [9]

$$C_{H_0,H_1} = \log_2 \left[\det \left(I_{N_R} + \frac{\rho}{N_T} H_0 H_0^H R_I^{-1} \right) \right], \tag{4}$$

and the instantaneous correlation matrix R_I is defined as

$$R_I = \eta_1 H_1 H_1^H + I_{N_R}, \tag{5}$$

where H_0 represents the channel of interest and H_1 represents the interfering channel. They are both the transfer functions for the UCDA elements. Further, ρ is the signal-to-noise ratio (SNR) and η is the interference-to-noise ratio
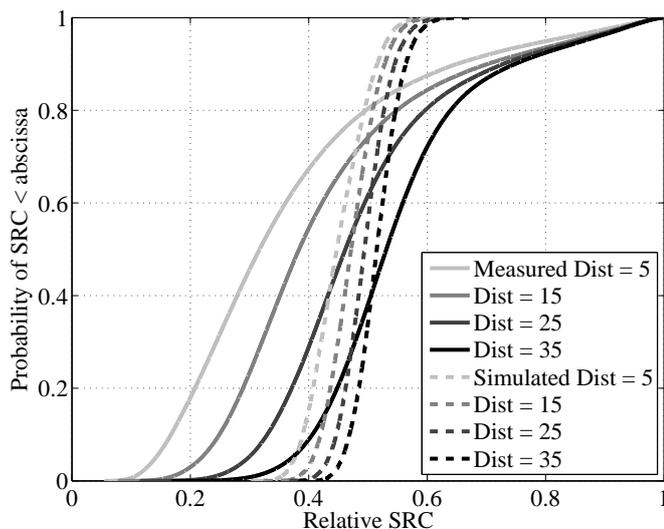
Figure 6: Relative sum rate capacity for different MS separation distances for the LOS scenario.

(INR), while N_T and N_R are the number of transmit and receive antennas, respectively. I_{N_R} is the identity matrix of size N_R. When the correlation matrix $R_I = I_{N_R}$, the corresponding capacity is in fact the single-link channel capacity, which is denoted C_{H_0}. The overall sum rate capacity (SRC) is thus defined as the average value of the instantaneous capacity over the frequency band. The relative sum rate capacity, has been used in [3], is given by the ratio between the sum rate dual-link capacity and the sum rate single-link capacity:

$$SRC = \frac{E\{C_{H_0,H_1}\} + E\{C_{H_1,H_0}\}}{E\{C_{H_0}\} + E\{C_{H_1}\}}. \tag{6}$$

We evaluate the relative SRC for the considered LOS scenario for different MS separation distances and common cluster ratios with 10 dB SNR and 10 dB INR, see Fig. 6. It can be noted that as the MS separation distance is decreasing [1], the sum rate capacity is decreasing. Both the simulations and measurements show this tendency, which indicates that the common clusters can capture the multi-link characteristics and well reflect the system level performance. However, it can be noted that the relative SRCs of the simulations

---

[1]In the published version of this paper, the word "increasing" was used, and it is corrected as "decreasing" in this thesis.

does not perfectly match with that of the measurements, the simulations cover
a larger span than the measurements. One should note that the considered LOS
scenario is from a single area measurement, and the simulations show the sta-
tistical characteristics for the measured scenario rather than reproducing it. In
addition, the statistical performance is more interesting since it can give more
insights of the multi-link properties for various, but similar, environments.

6   Conclusions

Common clusters have been introduced to describe the multi-link propagating
phenomena, but the definition and the method for identifying common clus-
ters have been open topics. In this paper, we introduce a simple and efficient
method to identify common clusters in outdoor scenarios with a ray launch-
ing tool. It has been shown that common clusters can represent the inter-link
correlation well. As the distance between two links is increasing, the number
of common clusters is decreasing, and the inter-link correlation is decreasing
as well. Moreover, the common clusters show a reasonable level of significance
with respect to the power contribution to each link for small MS separation
distances. However, less significance of common clusters is observed compared
to the indoor measurements due to the large open sub-urban scenario. The ex-
tracted common cluster ratios are used together with the COST 2100 channel
model and an initial analysis of the multi-link simulated channel is performed.
For the considered LOS scenario, the simulated inter-link correlation and sum
rate capacity are investigated. The inter-link correlation shows a decreasing
trend as the common cluster ratio is decreasing. Similarly, the SRC is also
decreasing as the common cluster ratio is increasing. It seems that the COST
2100 channel model can represent the inter-link correlation and sum rate ca-
pacity in a good manner, but more measurements and analysis are needed,
which will be performed in future work.

References

[1] R. Verdone and A. Zanella, "Radio channel modeling for 4G networks,"
    in *Pervasive mobile and ambient wireless communications: COST Action
    2100 (signals and communication technology)*, 1st ed., London: Springer,
    2012, pp. 67-148.

[2] IST-4-027756 WINNER II D1.1.2 V1.2. (2008). *WINNER II Channel Mod-
    els.* [Online]. Available: http://www.ist-winner.org.

[3] J. Poutanen, K. Haneda, L. Liu, C. Oestges, F. Tufvesson, and P. Vainikainen, "Multi-link MIMO channel modeling using geometry-based approach," in *IEEE Trans. Antennas Propagat.*, vol. 60, no. 2, pp. 587-596, Feb., 2012.

[4] G. Eriksson, F. Tufvesson, and A. F. Molisch, "Propagation channel characteristics for peer-to-peer multiple antenna systems at 300 MHz," in *Proc. IEEE Global Commun. Conf.*, San Francisco, USA, 2006, pp. 1-6.

[5] B. H. Fleury, M. Tschudin, R. Heddergott, D. Dahlhaus, and K. Ingeman Pedersen, "Channel parameter estimation in mobile radio environments using the SAGE algorithm," *IEEE J. Select. Areas Commun.,* vol. 17, pp. 434-450, Mar. 1999.

[6] M. Zhu, A. Singh and F. Tufvesson, "Measurement based ray launching for analysis of outdoor propagation," in *Proc. European Conf. on Antennas and Propagat.*, Prague, Czech, 2012, pp. 3332-3336.

[7] M. Zhu, G. Eriksson and F. Tufvesson, "The COST 2100 channel model: parameterization and validation based on outdoor MIMO measurements at 300 MHz," in *IEEE Trans. Wireless Commun.*, to be published.

[8] L. Liu, N. Czink, and C. Oestges, "Implementing the COST273 MIMO channel model," in *Proc. NEWCOM-ACoRN Joint Workshop*, Barcelona, Spain, 2009.

[9] V. Kolmonen, P. Almers, J. Salmi, J. Koivunen, K. Haneda, A. Richter, F. Tufvesson, A. F. Molisch and P. Vainikainen, "A dynamic dual-Link wideband MIMO channel sounder for 5.3 GHz," in *IEEE Trans. Instrum. Meas.*, vol. 59, no. 4, April 2010.

Paper VI

Tracking and Positioning Using Phase Information of Multi-path Components from Measured Radio Channels

High resolution radio based positioning and tracking is a key enabler for new or improved cellular services. In this work, we are aiming to track user movements with accuracy down to centimeters using standard cellular bandwidths of 20-40 MHz. The goal is achieved by using phase information of the multi-path components (MPCs) from the radio channels. First, an extended Kalman filter (EKF) is implemented to estimate and track the phase information of the MPCs. Each of the tracked MPCs can be viewed as a virtual transmitter with unknown position. By using a time difference of arrival (TDOA) positioning algorithm based on a structure-of-motion approach and translating the tracked phase information into propagation distances, the user movements can be estimated with a standard deviation of the error of 4.0 cm. It has been demonstrated that phase based positioning is a promising solution for movement tracking with extraordinary accuracy within cellular systems.

1   Introduction

Radio based positioning and tracking is a research area that has attracted a lot of attention during the past decades. The technology is often seen as a key enabler for new cellular services. Global Navigation Satellite Systems (GNSS) such as the Global Positioning Systems (GPS) is one of the most important technologies to provide location information around the globe through a constellation of at least 24 satellites [1]. However, the accuracy of GPS is usually limited and the GPS system even cannot work properly in shadowed areas, such as inside buildings, and beside tall buildings. Therefore, there has been extensive research in developing new positioning techniques to cover these areas and providing ubiquitous positioning solutions with accuracy down to meters or centimeters.

Ultra wideband (UWB) positioning is an attractive candidate due to the characteristics of the UWB signals, which allow centimeter accuracy in ranging [2]. Operating with GHz of bandwidth allows distances to be resolved within centimeter accuracy, mainly due to the fine delay resolution. However, bandwidth is itself an expensive resource. How to obtain the same accuracy as in UWB system but with a smaller bandwidth has emerged as a crucial problem for positioning.

To address the previous problem, let us take a step back and consider wireless propagation channel characteristics. Wireless channels are often described by a sum of multi-path components (MPCs), which carry information of propagation distances in terms of delay and phase. As long as the MPCs propagate in the space, the delay and phase are varying at the same time. Delay estimates, which are used in UWB system to estimate propagation distances, are usually limited by the bandwidth while the phase estimates are not dependent on the bandwidth. Generally speaking, a 2π rotation of the phase is corresponding to a propagation distance of one wavelength. Usually, cellular systems are operating at high frequency, e.g., GHz, so that the corresponding wavelengths are in units of centimeters. If frequent measurements are conducted during one wavelength movement, the position accuracy can get down to centimeters or even millimeters consequentially. Therefore, it becomes attractive to utilize phase information for high accuracy positioning within cellular systems.

Phase based positioning and tracking has previously been proposed for Radio Frequency Identification (RFID) systems, where the phase of the dominant LOS component is tracked and used for positioning or tracking purposes, see e.g. [3]. Phase information is also used in a related way to improve the performance of GNSS, through Real Time Kinematics (RTK) and differential phase measurements [4]. In this paper, we use the MPCs as virtual, but coherent, transmitters located at unknown positions for positioning and tracking pur-

poses. The relative propagation distance of each MPC is estimated from the tracked phase information, where an EKF algorithm is implemented and utilized. Relative movements are located with a structure-of-motion approach that previously has been successfully applied to UWB measurements for tracking [5]. To the authors' best knowledge, until now this phased based approach for tracking and positioning purpose has not been implemented before.

The paper is structured as follows. Phase estimation and tracking are discussed in section II, including the implementation of the EKF algorithm. Section III gives details of an indoor measurement campaign at 2.6 GHz and tracked phases of the MPCs from the measured channels are discussed. Section IV discusses the used positioning algorithm and presents the tracked movements. Finally, conclusions in section V wrap up this paper.

2 Phase Estimation and Tracking

Phase estimation and tracking is one of the most challenging parts for phase based positioning. EKF, which is based on a state-space description, is an ideal solution for this purpose. In the following subsections, the dynamic model and EKF implementation are discussed for estimation and tracking of the phases of MPCs.

2.1 Dynamic Model

To extract parameters, e.g., delay, angle-of-arrival (AOA), angle-of-departure (AOD) and phase, from the measurements, a double-directional channel model is employed, and thus the channel can be represented as [6]:

$$\mathbf{H}(f) = \sum_{l=1}^{L} \mathbf{G}_{\mathrm{Rx}}(\varphi_{\mathrm{Rx},l}, \theta_{\mathrm{Rx},l}) \begin{bmatrix} \gamma_{\mathrm{HH},l} & \gamma_{\mathrm{HV},l} \\ \gamma_{\mathrm{VV},l} & \gamma_{\mathrm{VH},l} \end{bmatrix} \mathbf{G}_{\mathrm{Tx}}(\varphi_{\mathrm{Tx},l}, \theta_{\mathrm{Tx},l}))^{\mathrm{T}} \mathrm{e}^{-j2\pi f \tau_l},$$

(1)

where $\mathbf{G}_{\mathrm{Rx}}$ and $\mathbf{G}_{\mathrm{Tx}}$ are the mappings of antenna responses at AOA $(\varphi_{\mathrm{Rx},l}, \theta_{\mathrm{Rx},l})$ and AOD $(\varphi_{\mathrm{Tx},l}, \theta_{\mathrm{Tx},l})$ of the lth path. τ_l is the delay of lth path and L is the number of MPCs. $\gamma_{\mathrm{HV},l}$ is the amplitude of the lth path in horizontal-to-vertical polarization and vice versa. The amplitude γ_l consists of magnitude and phase, and can be written as:

$$\gamma_l = \alpha \mathrm{e}^{-j\phi}.$$

(2)

The parameters of the propagation paths in the double directional channel model are comprised as

$$\boldsymbol{\mu} = [\ \boldsymbol{\tau}^{\mathrm{T}} \quad \boldsymbol{\varphi}_{\mathrm{Tx}}^{\mathrm{T}} \quad \boldsymbol{\theta}_{\mathrm{Tx}}^{\mathrm{T}} \quad \boldsymbol{\varphi}_{\mathrm{Rx}}^{\mathrm{T}} \quad \boldsymbol{\theta}_{\mathrm{Rx}}^{\mathrm{T}} \ ]^{\mathrm{T}}$$

(3)

and

$$\boldsymbol{\gamma} = \begin{bmatrix} \boldsymbol{\gamma}_{\mathrm{HH}}^{\mathrm{T}} & \boldsymbol{\gamma}_{\mathrm{HV}}^{\mathrm{T}} & \boldsymbol{\gamma}_{\mathrm{VV}}^{\mathrm{T}} & \boldsymbol{\gamma}_{\mathrm{VH}}^{\mathrm{T}} \end{bmatrix}^{\mathrm{T}}. \tag{4}$$

Note that, here only the specular propagation paths are considered, but not the diffuse multi-path components (DMCs), which act as interference for positioning purposes and are treated as noise in this work. So the channel observation at time k can be approximately as a superposition of specular paths and random noise:

$$\mathbf{y}_k = \mathbf{s}(\boldsymbol{\mu}_k, \boldsymbol{\gamma}_k) + \mathbf{w}_k, \tag{5}$$

where $\mathbf{s}$ is a nonlinear equation originating from the double directional channel model and $\mathbf{w}$ is the Gaussian white noise.

To form a dynamic model of the propagation parameters, it is assumed that the propagation parameters are correlated over subsequent measurement snapshots and, specifically, depending linearly on the distance traveled. There have been a number of linear dynamic models for tracking purposes. In this work, a constant velocity model is employed, and it has also previously been shown that this model can give proper tracking performance of propagation parameters [7]. The state vector of the parameters $\mathbf{x}$ at time k is given as

$$\mathbf{x}_k = \begin{bmatrix} \boldsymbol{\mu}^{\mathrm{T}} & \Delta\bar{\boldsymbol{\mu}}^{\mathrm{T}} & \boldsymbol{\alpha}^{\mathrm{T}} & \boldsymbol{\phi}^{\mathrm{T}} & \Delta\bar{\boldsymbol{\phi}}^{\mathrm{T}} \end{bmatrix}^{\mathrm{T}}, \tag{6}$$

where $\Delta\bar{\boldsymbol{\mu}}$ and $\Delta\bar{\boldsymbol{\phi}}$ are the corresponding velocities for their belonging parameters. Note that the magnitude parameters $\boldsymbol{\alpha}$ is the logarithmic of the absolute amplitude same as stated in [7]. The discrete-time state transition equation is then defined as:

$$\mathbf{x}_k = \mathbf{F}\mathbf{x}_{k-1} + \mathbf{v}_k, \tag{7}$$

where $\mathbf{F}$ is the state transition matrix, and $\mathbf{v}_k$ is the state noise following Gaussian distribution with covariance matrix $\mathbf{Q}$.

This model is optimized to track MPCs resulting from smooth movements. However, there can be non-smooth or even discontinuous behavior in some specific scenarios, e.g., at the corners of a square movement pattern. In such situations, this model can show performance degradation for tracking and even diverge. In that case, state noise with large variance is needed, such that the model allows more random deviations.

2.2 Extended Kalman Filter Design

An extended Kalman filter is implemented for the purpose of estimation and tracking of the phases of MPCs. The EKF structure is reviewed here for convenience, but the interested reader is referred to [7] for further details. The EKF algorithm consists of two steps, namely prediction and correction:

Prediction:

$$\hat{\mathbf{x}}_{(k|k-1)} = \mathbf{F}\hat{\mathbf{x}}_{(k-1|k-1)} \qquad (8)$$

$$\mathbf{P}_{(k|k-1)} = \mathbf{F}\mathbf{P}_{(k-1|k-1)}\mathbf{F}^T + \mathbf{Q} \qquad (9)$$

Correction:

$$\mathbf{P}_{(k|k)} = \left(\mathbf{P}_{(k|k)}^{-1} + \mathbf{J}(\hat{\mathbf{x}}_{(k|k-1)})\right)^{-1} \qquad (10)$$

$$\Delta\hat{\mathbf{x}}_k = \mathbf{P}_{(k|k)}\mathbf{q}(\mathbf{y}_k|\mathbf{x}_{k|k-1}) \qquad (11)$$

$$\hat{\mathbf{x}}_{(k|k)} = \hat{\mathbf{x}}_{(k|k-1)} + \Delta\hat{\mathbf{x}}_k. \qquad (12)$$

The prediction step gives the predictions based on the previous state and the transition matrix. The filter error covariance $\mathbf{P}_{(k|k)}$ is also estimated in a similar manner considering the influence of the noise. The correction step aims to decrease the errors by using the new observed samples to correct the prediction. In the correction step, the first and the second order partial derivatives of the log-likelihood function of the measurement model are used, and these are defined as

$$\mathbf{q}(\mathbf{y}|\mathbf{x}) = 2 \cdot \Re\{\mathbf{D}(\mathbf{x})^H(\mathbf{y} - \mathbf{s}(\mathbf{x}))\}, \qquad (13)$$

and

$$\mathbf{J}(\mathbf{x}) = 2 \cdot \Re\{\mathbf{D}(\mathbf{x})^H\mathbf{D}(\mathbf{x})\}, \qquad (14)$$

respectively, where $\mathbf{D}(\mathbf{x})$ is the first-order partial derivatives with respect to the parameters $\mathbf{x}$ of the observation model $\mathbf{s}(\mathbf{x})$.

3   Experimental Investigation

Experimental tests are performed for the purpose of positioning with tracked phase of MPCs from measured radio channels. In this section, the measurement campaign is described in detail, followed by phase tracking for a circular and a square movements, where both a smooth and a discontinues behavior are experienced.

3.1   Channel Measurements

The measurements were conducted in a large open hall, using our RUSK LUND
channel sounder. 161 frequency points of a 40 MHz bandwidth channel were
measured with center frequency of 2.6 GHz. A Skycross SMT-2TO6MB-A
omni-directional antenna is mounted on a tripod on wheels 1.7 m above the
ground to represent a single-antenna user (MS). A cylindrical array acts as a
base station (BS), and the center of the cylindrical array is about 2.07 m above
the ground. The single antenna was moved manually along the predefined
movement patterns, which are a circle with radius 0.6 m and a square of side
length 1 m, until 5000 channel snapshots are harvested. We made sure that
the person moving the station influenced the measurements as little as possible
by remaining close to the floor to minimize body reflections, while at the same
time not to block the ground reflection. During the measurements, line-of-sight
(LOS) conditions are always fulfilled. The LOS distances are 12.6 m and 19.5
m for the circular and square movements, respectively.

3.2   Results and Discussions

Phases are expected to show sinusoidal shapes for the circular movement. Fig. 1
shows examples of the tracked phase of four MPCs in the vertical-to-vertical
polarization, where the sinusoidal patterns are clearly captured. It can be
crucial to note the maximum phase difference of each MPC is around 62 radians.
Consequently, it reflects the maximum distance change that is approximately
1.2 m, which also corresponds to the diameter of the circle. Note that, some of
the MPCs have phase differences slightly less than 62 radians. That is primarily
due to that these MPCs stem from scatterers, which are not in the same plane
as the single antenna MS. Thus, the scatterers see a slightly projected and
scaled copy of the circle, which leads to the projection of the phases of the
corresponding MPC.

Regarding square movement case, we note that at the corner of the square,
the movement follows a stop-and-go behavior since it was moved manually.
This movement is not considered as smooth. Thus, the tracking tolerance of
the filter was increased by defining a higher variance for the process noise to help
tracking this sharp change while staying with the same dynamic model. For
the square movement, an anti-symmetric pattern in phase is expected. Fig. 1
shows four tracked MPCs from the square movement measurements, where it
can be noted the anti-symmetric pattern is observed for each of the MPCs.
However, at the corner of the square, the phase does not show a sharp change
in slope. Instead, a smooth transition around the corners takes place. This is
a consequence of smoothing by the EKF. Also the maximum phase difference

(a) Circular movement   (b) Square movement
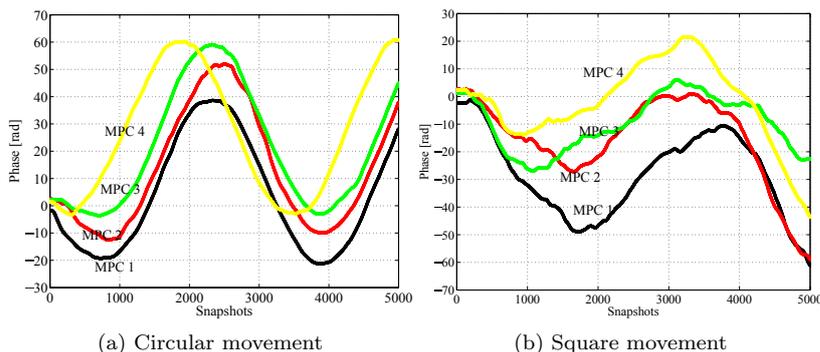
Figure 1: Tracked phases of a number of MPCs in circular and square movement measurements.

Table 1: Azimuth and elevation angle of the four MPCs both in circular and square movements at the base station side.

MPCs	Circular movement		Square movement	
	Azimuth [deg]	Elevation [deg]	Azimuth [deg]	Elevation [deg]
MPC 1	282	104	144	64
MPC 2	92	100	348	74
MPC 3	190	102	356	72
MPC 4	160	92	152	46

of an MPC is around 40 radians, which corresponds to a movement around 0.75 m. Compared to the predefined 1 m^2 square, the movement is somewhat scaled.

To have a thorough understanding of the projected phases, the elevation angles at the MS side are needed for each of the MPCs, which cannot easily be obtained straightforward due to the single antenna set up. However, it can be noted that the BS and MS are roughly in the same plane. If a single interaction is assumed, the elevation angles at the MS side can be estimated roughly. Table 1 lists the elevation angle at the BS side for the circular and square movements. It can be noted that the differences between the plane of the BS and the planes of the scatterers are approximately 10 degree at maximum for the circular movement. So the four MPCs can be either the LOS components or single reflections from the wall. Thus, the differences between

the plane of scatterers and the MS are also small as well as the projections of the
tracked phase for the circular movement. The MPCs of the square movement
are mostly from the ceiling, and at maximum an angle difference of 44 degrees
is observed between the scatterers and the plane of the BS. With the single
interaction assumption, the MS will see the scatterers from the ceiling with an
elevated angle, which causes large differences between the plane of scatterers
and the plane of MS. Therefore, the propagation distance of each MPC will be
scaled and projected.

4 Positioning

We are aiming for positioning based on relative movements in this work. There-
fore, a TDOA positioning algorithm based on the structure-of-motion problem
at hand is utilized. A detailed description of the algorithm can be found in [5].

The input to the TDOA positioning algorithm is the measured distance
matrix $\bar{\mathbf{D}}$, whose columns are MPCs and rows are estimated relative distances
for each channel snapshot. Therefore, the tracked phases are translated into
distance to form the matrix $\bar{\mathbf{D}}$. Specifically the distance for the lth MPC at
snapshot k is defined as

$$d_{l,k} = c\tau_{\mathrm{ref}} + \frac{(\phi_k - \phi_{\mathrm{ref}})}{2\pi}\lambda \tag{15}$$

where c is the speed of light, τ_{ref} is the selected reference delay, e.g., the
estimate delay of the first snapshot, ϕ_{ref} is the selected reference phase, ϕ_k is the
phase at snapshot k, and λ is the wavelength. By singular value decomposition
of $\bar{\mathrm{D}}$, the user movement can be estimated.

Fig. 2 shows the estimated movements together with the predefined moving
patterns. As stated before, the virtual transmitters and the MS are not in the
same plane. Therefore, the movements are slightly projected as well. For the
circular movement, it can be noted that the offset between the planned circular
movement and the tracked movement is 5 centimeters in maximum, and more
than 50% of the locations are within 2 centimeter offset. The overall standard
deviation of the circular movement is estimated as

$$\sigma = \sqrt{\frac{1}{n}\sum_{i=1}^{n}|r_{\mathrm{true},i} - r_{\mathrm{located},i}|^2}. \tag{16}$$

where $r_{\mathrm{true},i}$ is the true position, $r_{\mathrm{located},i}$ is the estimated position and n is
with a number of 3120. The standard deviation of the errors is approximately
4.0 cm. Note that the user movement is controlled manually, so the movements
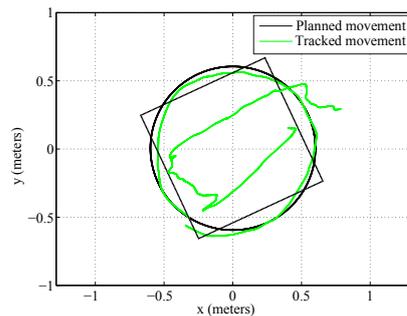
Figure 2: Positioning results for circular and square movements.

are most likely not a perfect circle, which can be part of the 4.0 cm offset as well. For the square movement, such comparison is not conducted due to the scaled tracked movement. Nonetheless, still it can be seen that the tracked square movement has a reasonably well projected track. If we assume the propagation environment is known, e.g. through floor plan information, we can actually compensate for the projection error as long as we are dealing with single reflections or interactions. However, for the proof of concept in this paper, this is out of scope of the investigation.

5   Conclusions

We have implemented EKF to perform phase tracking of MPCs for positioning purposes. With the tracked phase information, the relative distance changes of each MPC are observed. By using the structure-of-motion based TDOA positioning algorithm, relative movements have been tracked with accuracy down to centimeters. Our investigation has shown that with the 40 MHz bandwidth, the phase information of each MPCs can be properly estimated and tracked from the radio channels, which can be consequently translated into estimation of time-of-arrival. Therefore, positioning with accuracy down to centimeters is also possible with a limited bandwidth by using phase information. Overall, phase based positioning is a promising technique for tracking and localization purposes. This is the initial work in this area, investigations of different movement patterns, e.g., 3D movements, and the initial positioning will perform as future work.

References

[1] J. J. Spilker, Jr., "GPS signal structure and performance characteristics," *Journal of the Institute of Navigation*, vol. 25, no. 2, pp. 121-146, Summer 1978.

[2] S. Gezici et al., "Localization via ultra-wideband radios: a look at positioning aspects for future sensor networks," *IEEE Signal Processing Magazine*, vol. 22, no. 4, pp. 70-84, Jul. 2005.

[3] P. V. Nikitin et al., "Phase based spatial identification of UHF RFID tags," in *Proc. IEEE RFID 2010*, Orlando, FL, Apr. 2010, pp. 102-109.

[4] Real-Time Kinematic surveying training Guide, part number 33142-40, Revision D, Sep. 2003, [Online]. Available: http://gpstraining.com/downloads/MANUALS-QUICK%20GUIDES/RTKTrainingRevD.pdf.

[5] Y. Kuang, K. Åström, and F. Tufvesson, "Single antenna anchor-free UWB positioning based on multipath propagation," in *Proc. IEEE Int. Conf. Communications (ICC'13)*, Budapest, Hungary, Jun. 2013, pp. 5814-5818.

[6] M. Steinbauer, A. F. Molisch, and E. Bonek, "The double-directional radio channel," *IEEE Antennas Propag. Mag.*, vol. 43, pp. 51-63, Aug. 2001.

[7] J. Salmi, A. Richter, and V. Koivunen, "Detection and tracking of MIMO propagation path parameters using state-space approach," *IEEE Transactions on Signal Processing*, vol. 57, no. 4, pp. 1538-1550, Apr. 2009.